A Practical Guide to Non Destructive Examination of Concrete

2004

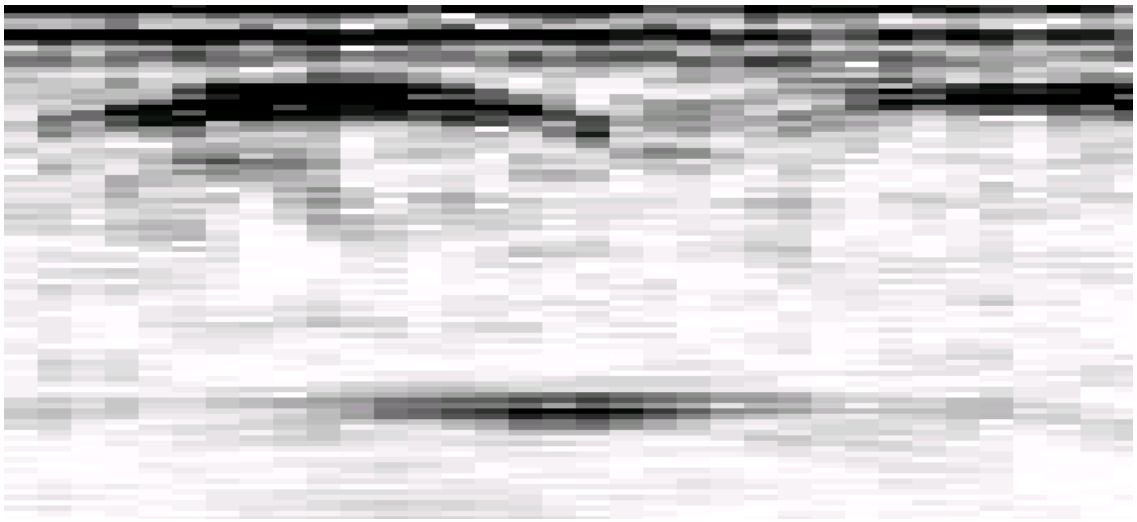

A Project sponsored by Nordic Innovation

Content

Aknowledgement

The support and financial assistance provided by Nordic Innovation Centre in making this work possible is gratefully aknowledged.

This is a *short* presentation of the capabilities of some NDT methods to a selection of typical problem cases encountered in civil engineering.
The opinions expressed here are those solely of the authors and are based on their personal experiences.

Project Partners	
Force Technology, Denmark	Peter Shaw, Jon Rasmussen, Torben Klit Pedersen Oskar Klinghoffer
Malå GeoScience, Sweden	Christer Gustavsson, Johan Friborg
Luleå Technical University, Sweden	Sten-Åke Elming
Vattenfall Utveckling, Sweden	Christian Bernstone
Danish Road Directorate	Erik Stoltzner
Norwegian Road Directorate	Ian Markey
NCC Teknik, Sweden	Per-Olof Björkqvist
Icelandic Building Research Institute	Gisli Gudmundsson

Written by P. Shaw, J. Rasmussen and T. K. Pedersen of Force Technology, Denmark
Editing contribution by N. Goodwin and G. Gudmundsson

Trial using laser to create surface waves in concrete

1.0 Introduction

This project was inspired by the need to know the actual capabilities of some non-destructive examination (NDE) techniques for use on concrete structures. A number of common problem types have been considered and the best available techniques chosen to investigate them. The process has involved construction of large and small mock-ups with well-defined details and idealised defects. Whether the artificial defects actually can reflect the true situation on site can be argued, but it is a necessary starting point when examining the techniques and describing the potential capabilities. Various examples of real structures and relevant problem types have been included.

The conditions on site are generally more difficult to deal with compared to a mock-up, as there are often many unknown factors such as the variability of concrete properties like quality, strength and moisture content. It is often not possible to accurately, predict NDE performance in the field or achieve the same results as in the laboratory. The performance on older structures is often poor due to a number of factors, including variability of concrete quality and other effects of poor workmanship and inadequate supervision at the construction stage. In addition, the condition of the concrete globally or through a thick section may have changed with time, and these conditions cannot always be predicted in an older structure. Although we can describe the capability of the techniques in specific conditions, this may change drastically on another site and will never be exactly the same at any two sites.

Modern concretes are usually of higher quality and lend themselves better to NDE. Since NDE performance improves with the quality of concrete then it could be argued that it is of more value to modern construction and will be of greater use in the future. If NDE is to be more widely accepted then it must be improved in many areas, but the best way to improved NDE must be better concrete.

To get the best out of non-destructive techniques requires a number of specialist skills, and these are often not found in one and the same person. The techniques themselves require a sound knowledge of wave motion physics and preferably an enthusiasm for sensor technology and data processing. These skills need the guidance of an experienced civil engineer who understands the problems in question and has a good all round knowledge of NDE. Many different techniques are needed to deal with the large variety of problems encountered. The all-round experience required may take several years to accumulate and NDE of concrete therefore remains a specialised area.

This presentation is intended for those who have a practical interest in knowing more about some common concrete problems and what to expect of the available techniques used to diagnose concrete. It is therefore focussed on the problems and not on making an exhaustive study of the techniques themselves. It is divided into 4 main chapters starting with a discussion about NDE and its use. The second chapter deals with the different kind of problem cases that are common. Chapter three gives an "easy" description of the different NDE techniques used throughout this project. The last chapter is devoted to describing how the techniques are applied to various problems, and being a practical work the favoured techniques are dealt with more fully. The appendix includes various examples of results from mock-up testing.

1.1 Why do we need NDE?

There are various situations in which NDE might be needed:

- Compliance testing
- Collection of specific data and parameters
- Condition assessment
- Damage assessment

Compliance testing is one of the most straightforward tasks, for example measurement of reinforcement cover, concrete thickness or the position of a pre-stressing cable. Modern techniques are capable of accurately describing these details. Compliance testing has never really been standard practice in civil engineering, at least not in the form of post construction checks using NDE. This is changing to some extent, as the awareness of concrete durability issues and structure lifetime increases. The checks made, may however be confined to measuring rebar cover thickness. If a new structure shows signs of distress, for example cracking, then compliance

checks are sometimes made of the internal structure including reinforcing details. It can be said that compliance includes quality, for example the presence or not of cracks, honeycombs and other irregularities that may ultimately affect the function and lifetime of a structure. This type of defect may be concealed to the eye yet be relatively easy to detect using NDE.

The other applications, mentioned above, have to be considered in their context of course, but they are usually more difficult to deal with using NDE alone. If information about concrete strength or other mechanical properties is required then NDE can be used to obtain a picture of how these might vary within the structure, which is useful when planning intrusive tests. Acoustic wave velocities can be used to calculate the dynamic elastic modulus, which in turn can be used to estimate the static elastic modulus. The same technique can provide a qualitative picture of the bond strength between layers of concrete and several hundred tests can easily be made in a day, which is of more value than a small number of random, mechanical tests. The internal geometry, including reinforcing details, can be accurately mapped using techniques such as covermeter, radar, and radiography. The covermeter is suitable for lightly reinforced structures when the cover thickness is small while radar can resolve two or three layers of reinforcing and at much greater depth.

Lifetime predictions require that the present condition of a structure first be established. Many structures including bridges and safety related buildings are required to meet new safety demands. At the same time, many of these structures are required to operate beyond their originally planned lifetimes. A number of serious incidents, such as the collapse of pre-stressed structures and leakages also point to the need for more information about our infrastructure. The means to obtain this information are available today.

Damage to a structure such as that caused by deterioration mechanisms like reinforcement corrosion, freezing and ASR are often, if not usually, coupled to weaknesses in the structure such as high permeability, i.e. construction-related defects and inappropriate detailing. To remedy damage, the cause and extent must be understood. The traditional methods of evaluating this type of damage are sometimes totally inadequate and misleading. New approaches are required that combine NDE with more flexible and imaginative mechanical tests.

NDE in civil engineering is often discussed as an isolated subject with focus on the tecniques and not so much their application in realistic situations. More focus should be placed on solving the problems at hand by combining NDE methods intelligently together with traditional methods of inspection and testing.

1.2 Choice of NDE methods

In this work, we have chosen to study a relatively small but important selection of problem cases and have chosen what we consider the best techniques for these. There is always a best technique for a specific job, if seen from a purely engineering perspective. The prevailing conditions, for example, accessibility, costs and time may force the choice of an alternative technique, although this will invariably be at the cost of quality, e.g. accuracy and reliability. A common failing is to stubbornly apply a single favoured technique to a wide variety of problem types, giving priority to promoting a technique rather than solving the problem in the best possible way. Our experience tells us that the choice of NDE methods or combinations thereof should be made on site, with some clear exceptions of course.

1.3 NDE as an alternative inspection method

Despite considerable research and expressed interest in non-destructive testing methods, they are rarely applied in practice. It is often argued that the methods are qualitative and of limited use to the structural engineer, that the results are ambiguous and not sufficiently qualified for this purpose. One reason may be the inability, or at least great difficulty in predicting how they will perform given the infinite variety of conditions on site. It has been said that more effort is put into finding reasons *why not* to use NDE than *how* to use it. NDE of concrete is not a trivial task and the difficulties have to be recognised. Considerable advances have however been made in recent years, which enable us to obtain vast amounts of useful information and a re-assessment of NDE is needed by the civil engineering community.

Much speculation has been made in recent years about the existing and potential capabilities of NDE with respect to specific types of problem. Little

data has however been available from actual laboratory or field tests to clarify these points, despite the relatively simple problem definitions. This has been the basis for our work.

1.4 What kind of concrete structures are considered?

This has been governed by the interests of the project partners and of course by practical considerations including method limitations. The type of concrete considered is typically 300 to 1500 mm thick, which could be a bridge slab or beam, slender dam wall or nuclear containment wall. The concrete is accessible from both sides, although much of the testing has here been carried-out from one side only. Pre-stressed structures have been given priority, as have wall structures around 1000 mm thick bearing in mind the interests of the nuclear industry.

Mock-ups for acoustic and radar measurements have been made using normal structural concrete with maximum aggregate size 25-32 mm. Two large mock-ups, B1 and B2 have been constructed (see Appendix for details of mock-ups) as well as several smaller ones for radiographic tests.

Fieldwork has included six bridges, two dams and a nuclear containment wall. In addition, many site investigations including bridges, nuclear containments, tunnels, piles, floor slabs etc out-with this projects have contributed to the accumulation of data and experience.

1.5 Problem cases considered

The original primary objectives have been to establish the capability to detect voids in concrete and voids in pre-stressed cable ducts embedded in concrete. A list of end-user requirements with respect to task priorities are summarised in Table 1.1 below. A more detailed list of end-user priorities is given in the Appendix.

Of the 17 items (objectives) listed, in the original questionairre, the detection of voids and mapping of concrete homogeneity were considered most important, as well as the detection and sizing of cracks perpendicular to and parallel with the concrete surface.

These priorities are obviously based on the individual requirements of the end-user in this project and do not entirely reflect the importance in a more general sense. For example, dam structures in the Nordic countries are rarely in corrosive environments or are they pre-stressed, so these subjects are not a priority for this particular owner. On the other hand cracking and progressive deterioration of concrete is. The number of problem cases and variety of conditions is really so great that it is not possible to treat them all in depth or come up with a universal solution. A small number of problem cases have been investigated in a way that we hope will allow an evaluation to be made of potential capabilities under various conditions.

The measurement of concrete thickness is sometimes regarded (within the NDT community) as a simple problem and perhaps not worthy of deeper study. We have found, however, that it can be very difficult in practice and have therefore devoted some time to this fundamental problem as it has a bearing on many other objectives, e.g. measurement of depth (to reinforcement and voids) and concrete quality.

Concrete cracking was a high priority although too difficult a problem to treat in this work. Some simple tools using ultrasonic wave velocity have previously been established to determine the depth of ideal surface-opening cracks in simple geometries. This is rarely the case in real life, however, as cracks are often a complicated network, closely spaced and not necessarily perpendicular to the concrete surface. No models have been studied of this particular damage case although some fieldwork has included cracked concrete.

Mapping reinforcement and cable ducts was given quite low priority by the end users. However, it is not possible to investigate the condition of either of these if we cannot locate them. In addition, the internal geometry (mainly reinforcing) of concrete has a significant bearing on the performance of NDE techniques, so from the inspector's perspective it must be given priority. Like measurement of concrete thickness, re-bar mapping is a fundamental task that is a necessary part of the investigative process.

Application and purpose	Comment	Ranking (%)
Detection of voids & in-homogeneity, typically to locate construction flaws	Quantify void detection threshold in thick sections (size of void and depth)	41.8%
	Detect voids > 20mm in grouted tendon ducts	41.8%
Detection and sizing (depth, width, length) of cracks normal to the surface	Improve variable performance statistics associated with depth measurement of surface cracks.	41.8%
Detection of delamination (cracking parallel with concrete surface)	Improve variable performance statistics for detecting large laminar flaws at > 10mm depth and larger than 100mm in any direction	39%
Measurement of concrete thickness to obtain as-built details	Measure concrete thickness with single-sided access with sensitivity of ± 5% section thickness.	37.8%
Mapping/sizing of steel reinforcement and tendons to establish as-built details	Enhanced resolution to measure reinforcement diameter with sensitivity of ± 10%	20.0%
	Resolve multiple layers of reinforcement, identifying individual bars at spacing <150mm and depths >30mm and measure bar diameter with sensitivity of ± 10%	20.0%

Table 1.1: Ranking of end-user priorities. Voids and cracks have high priority while re-bar mapping has low priority.

1.6 Which non-destructive testing techniques have been considered?

Radiographic, electromagnetic and acoustic methods have been used extensively in this work. The methods and their principles are described in greater detail in Chapter 3. Some of the methods were quite well tried at the outset, while others were relatively new - at least in terms of concrete inspection, and some were welcome additions to the original plan. The most significant new technologies that have benefited this work are the A 1220 Ultrasonic Pulse Echo unit from Spectrum, Russia and the Computed Radiography system from Agfa Strukturix. In addition, considerable improvements were made in radar antenna design quite early on in our work (ref. Malå GeoScience and Luleå Technical University).

There are of course other methods that have not been included and which may have performed better than the chosen ones in specific situations. There are also other designs of similar equipment available on the market, which may be better or poorer than those chosen. The package of techniques chosen is however a fairly representative one.

Acoustic methods

- Ultrasonic Pulse Echo U.P.E
- Impact Echo I.E.
- Spectral Analysis of Surface Waves S.A.S.W.
- Ultrasonic Pulse Velocity U.P.V. (Limited)

Radiographic methods

Source: Betatron 7.5 PXB accelerator, Iridium or Cobalt isotopes

"Receiver" Computed Radiography,
(H.E.C.R. is referred to in this report and means High Energy Computed Radiography).

Electromagnetic methods

- Ground Penetrating radar with antennae frequencies 500 MHz to 1 GHz.
- Covermeter

Equipment Suppliers

A1220 U.P.E. and UK1441 from Spectrum, Russia

Betatron from JME Ltd, UK

Impact Echo and SASW system from Olson Instruments, USA

Radar from Malå GeoScience, Sweden

Computed Radiography system from Agfa Strukturix, Belgium

Pundit from CNS Farnell Limited, England

Covermeter from Protovale Oxford Ltd, England

2.0 Typical problem cases

In Table 2.1 below there are examples of structure types and problem cases identified/provided by the end-users in this project. These can be compared with some typical examples of NDE investigations shown in the Appendix Table 3 (a)-(c), which have been made over a 10 year period out-with this project.

From Table 2.1 it can be seen that much of the work has involved mapping reinforcement and cable ducts, quality of cable duct grouting and measuring the depth of concrete deterioration.

Structure	Objective	Motivation	Result	Method
Bridge beam (350mm)	Post tensioned cables - duct fill - condition	Cracking and leaching visible (structural damage, corrosion risk?)	Void inside cable ducts. Wrong alignment of cable ducts. No corrosion.	H.E.C.R & radar
Bridge slab (1000mm)	Post-tensioned cable and duct fill condition	Extensive cracking through slab with leaching (corrosion risk?)	No voids in ducts	H.E.C.R
Bridge slab (1000mm)	Depth of s.o.* cracks	Visible on top surface (corrosion risk?)	Crack depth less than cover thickness	U.P.E. & covermeter
Bridge columns (900mm)	Depth of s.o.* cracks	Visible at surface (integrity?)	Crack depth limited (<100 mm)	U.P.V. & I.E.
Dam pillar (test depth < 200 mm)	Reinforcement position in relation to cracks and delamination	Visible cracks due to ASR freezing and movement (major structural weakness?)	Reinforcement mapped in relation to crack plane depth	Radar
Dam retaining wall (several m)	Depth of concrete deterioration from surface	Visible cracks due to thermal shrinkage and freezing (new or old, structural problem?)	Damage depth and concrete quality estimated	S.A.S.W & U.P.V

*s.o. : surface open (cracks)

Table 2.1: Examples of structures investigated as part of this project.

The types of task dealt with in the following chapters are:

1) Mapping the position of reinforcing and cable ducts
2) Measuring concrete thickness
3) Locating and sizing voids in concrete
4) Locating voids in pre/post-tensioned cable ducts
5) Measuring concrete quality and the depth of damaged concrete layers

2.1 Mapping the position of reinforcement and cable ducts in concrete

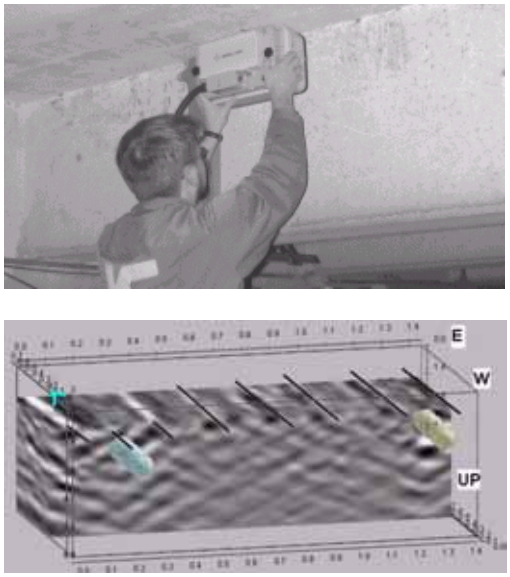

Fig. 2.1.1: The cable ducts and reinforcing in this bridge beam are being mapped using radar. Their position is being fixed prior to radiographic examination.

Mapping reinforcement and cable ducts is one of the more common types of investigation, usually made on older structures prior to cutting and drilling the concrete or when changing the loads. Covermeter, radar and radiography (in that order) provide increasing levels of detail about the reinforcing and cable ducts.

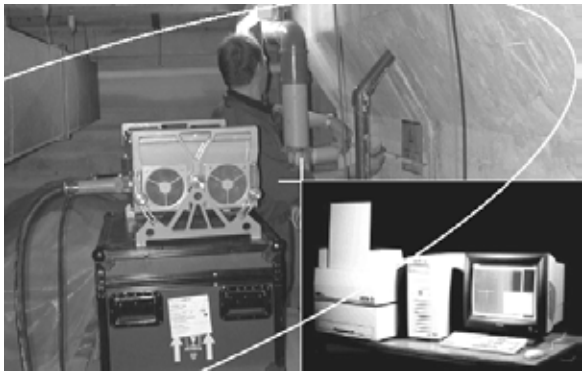

Fig. 2.1.2: The reinforcing details in this swimming pool are being examined with the Betatron and computed radiography (inset). The image plates were placed inside the pool in watertight bags.

Typical situations:

- Compliance check, when increasing loads or changing the structure
- When no reinforcing drawings are available
- To avoid damage when cutting and drilling
- When making condition surveys, e.g. cover depth to reinforcing
- For specific damage types, e.g. loss of rebar-section or voids in cable ducts where location must first be fixed
- To understand and plan other NDE testing, i.e. choose test points/lines and predict responses. This is normal when making a radar survey.

2.2 Measuring the thickness of concrete structures

Fig. 2.2.1: Tunnel with in-situ cast concrete liner (nominal thickness 600 mm). The thickness of the concrete is being measured using ultrasonic pulse echo.

Thickness measurement may seem like a simple task, but it can be extremely difficult to accurately determine concrete thickness with one-sided access to the structure. This is because wave velocities vary from structure to structure and may also in some cases vary considerably with depth. A good quality concrete not subject to extreme drying or damaged layers can however usually be quite accurately measured, i.e. if wave velocity/ depth variations are very small.

Measuring concrete thickness accurately is a fundamental and vital part of many site investigations.

Typical situations:

- Compliance check of structure after construction
- In connection with structural alterations
- In order to interpret other forms of measured data, e.g. acoustic wave velocities
- In connection with drilling operations on water-retaining structures or those with embedded steel liners
- To determine if the concrete is resting on solid material
- To locate foundations under slabs, e.g. when moving or installing heavy factory equipment
- To confirm the integrity of a structure by "visualising" the back wall echo

2.3 Locating and measuring voids and honeycombing in concrete

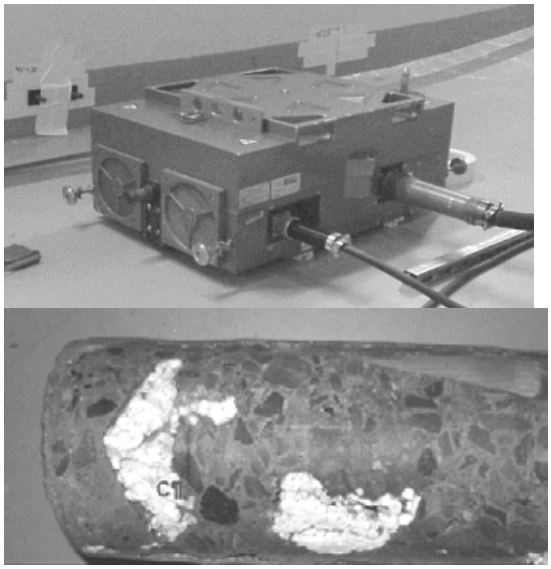

Fig. 2.3.1: The Betatron (top) in position for examination of a 1000 mm thick wall. The lower picture shows a core taken from the concrete revealing some cast-in refuse from construction (polystyrene foam and wood). These "voids" were detected using digital radiography.

Structures that are difficult to cast such as tunnel linings and pipe entries in walls are often checked as experience has shown that voids can occur and may remain hidden. A "void" may be the result of lack of fill, e.g. when filling or casting concrete or mortar up to an existing surface when there is a risk of entrapped air hindering fill. It may be due to the presence of building material and scrap in formwork during casting or poor vibration and compaction of concrete under pipes in a bridge deck. Voids may occur in pre-stressed cable duct fill due to leakage in duct joints or separation of material. Voids may take many shapes and sizes and are not necessarily air-filled. A "void" full of low-density material may constitute more of a problem than an air-filled void, as it may cause corrosion of embedded steel. Voids usually have some significance in terms of corrosion risk or leak-tightness. It is rare that a void just occurs in a mass of concrete, it is usually associated with a special building technique or detail. Therefore, their possible form and position can often be predicted, and knowing the expected shape, position and size of a void helps us to choose the correct method of investigation.

A void of several square metres may occur in the upper portion of a tunnel lining and this can result in both structural and leakage problems.

Small voids of only 10-20 mm can appear in pre-stressed cable ducts due to lack of fill and these can cause corrosion problems.

Voids can also occur under concrete slabs, e.g. due to erosion of filler material. This is not a "void in concrete" but a void in fill. However, it is a common type of problem that can be detected with NDE.

In some situations, there is no clear definition of the "void" under suspicion. For example, in newly constructed bridges problems can occur due to movement of formwork, settlement, lack of compaction, poor casting joints etc. The associated irregularities usually come under the common heading of "voids", although they may in fact be a combination of voids, honeycombing, tears, casting joints and cracks.

Typical situations:

- Post-construction quality checks, e.g. in water retaining structures
- If surface appearance suggests internal defects, e.g. if poor compaction of concrete can be suspected
- If voids can lead to other forms of deterioration such as corrosion to steel in the concrete, e.g. nuclear containment wall with a steel liner.

2.4 Locating voids in pre-stressed cable ducts

Fig. 2.4.1: A box-girder bridge in Norway. The pre-stressed cables in the beams are being examined using a Cobalt isotope and Betatron.

Fig. 2.4.2: The isotope in position on the inside (right) and image plates being fixed on the outside (left).

This is one of the most discussed topics in civil engineering inspection. The reason being that several collapses of this type of structure (Pre/post-tensioned) have occurred in the last 20 years and it is a recognised risk area. If voids occur in cable-ducts (in the case of mortar-injected ducts), then there is no protection against corrosion for the cable strands. The voids in a cable duct may be filled with air, water, sand or other injection material that constitute a corrosion risk. It may also be so that the cable duct has never been filled with mortar, so that apart from the risk of corrosion, there is also a structural

deficiency, as the cables are not bonded with the concrete.

Structural failure due to corrosion of strands in pre-stressed/post-tensioned structures can occur with little or no warning. Ordinary reinforced structures may suffer gradual and sometimes quite extreme deterioration although catastrophic failures are extremely rare.

Typical situations

- Quality control measure post-construction
- If surrounding concrete is cracked and porous and there is a risk of corrosion damage to embedded cables
- If voids are suspected or other evidence suggests they may exist
- Due to risk of corrosion of the cable strands
- For safety reasons

2.5 Measuring concrete quality and depth of damaged concrete layers

Fig. 2.5.1: A dam pillar in the north of Sweden. The concrete is suffering from freezing damage as well as ASR. Tests were made to find out how deep the cracks extended from the surface.

Concrete "quality" is a rather abstract term, but it is not uncommon to check new structures as a form of post-construction quality control – to see if it measures up to expectations. The uniformity of the concrete may be measured by the variation in wave velocity or, for example the density of a radiographic image. The mechanical properties of the concrete may be estimated on the basis of absolute values of wave velocities.

Concrete slabs and walls are rarely completely uniform with depth from the surface. In the case of older structures, the dominating mechanisms that cause variations with depth are drying (particularly thick structures indoors), and various forms of deterioration such as freezing, ASR and to some degree reinforcement corrosion.

In newly-constructed concrete, problems can occur at the surface and to some depth as a result of cracking (drying-shrinkage), separation of aggregates, tearing and cracking caused by moving formwork (for example slip-form) and early freezing.

Fire is a common problem and affects the concrete at the surface and to some depth depending on the intensity of the fire and exposure time.

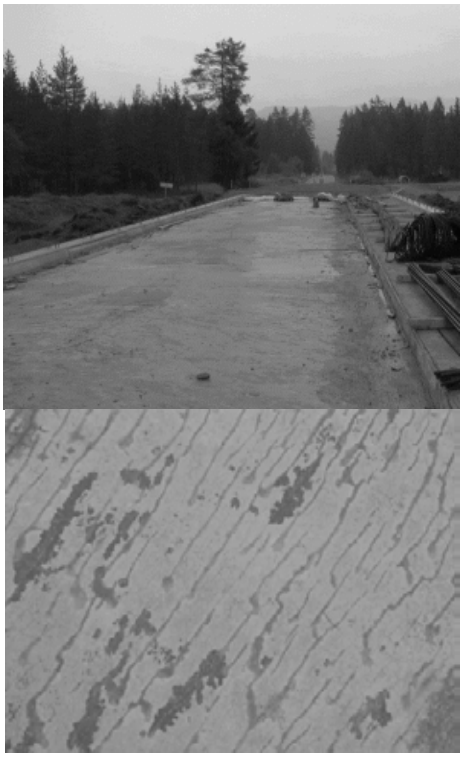

Fig. 2.5.2: A new bridge in Norway. Drying-shrinkage cracks appeared after casting the slab. The crack depths were found to be less than the cover thickness to reinforcing.

Typical situations

- To determine concrete quality and estimate mechanical properties for comparison with expected values as a post-construction check and as an evaluation of older structures
- To measure the depth of deteriorated layers, e.g. due to freezing, ASR or fire and evaluate the effect on bearing capacity
- To estimate the depth of surface-opening cracks
- To measure concrete thickness (wave speeds)

3.0 Non Destructive Examination (NDE), - The Methods – A Sixth, Seventh and Eighth Sense

3.1 Introduction

NDE methods are tools, which provide the concrete inspector with an additional three senses:

"Listening to concrete" - Acoustic methods to measure quality and detect defects, e.g. cracks and voids

"Feeling inside concrete" - Electromagnetic methods to detect metals, e.g. reinforcement bars

"Seeing through concrete" - Radiographic methods to detect variations in density, e.g. details of cable ducts and voids

The techniques enable us to "see" inside the concrete, and to describe details and measure properties that tell us about its condition. They are similar, if a bit cruder, to the instruments a doctor would use for medical examinations and similar to those used in traditional NDE.

Radiography should normally be reserved for point inspections, i.e. not for scanning, as the equipment is more cumbersome, and is relatively costly and slow. However, for many applications, e.g. mapping reinforcing and locating voids, it is the most capable of all NDE-techniques when we consider the amount of detail obtained and the relative ease in understanding the data it provides. It is arguably the only method that can be used in many difficult situations, e.g. for complicated geometries or where there are several interfaces (cables in a cast-in duct) through which the test must be made. Radiography provides less risk of ambiguity compared with other techniques.

Acoustic techniques and radar require only single-sided access as they transmit and receive information from the surface of the structure (those considered here). In this sense, they have an advantage over through transmission techniques such as radiography and wave transmission techniques (tomography). A slight disadvantage is the fact that the information is indirect, as we cannot always tell if the signals behave as we expect them to when propagating through the concrete. We thus refer, in acoustic technology, to "apparent" wave velocities. Also with radar care should be taken in interpreting images at face value alone as "ghost" images can be produced in some situations (see Fig. 3.6.5). Acoustic and radar data therefore require careful interpretation. Radiography is more direct in this sense as x-rays are not deflected around voids or rebars. One weakness with radiography is the fact that the entire volume of the concrete and reinforcing is projected onto a flat surface image, and the geometry of rebars and internal voids is thus in the form of a somewhat distorted image. The interpretation of a radiographic image is made easier by combining with radar, i.e. where information about rebars or ducts is required.

In some situations, only one method is required to obtain the required information with sufficient accuracy, speed and to an acceptable cost. Individual methods have limitations however, and in the following chapters, this will become clearer. The "investigative senses" can often be improved by combining methods, particularly if there is a danger of ambiguity. For example, radar may be used to measure reinforcement depth to provide perspective to a flat radiographic image. The *best* technique should be chosen for a given task and conditions, which means having access to several techniques. Each method has its advantages and disadvantages and these will be demonstrated below.

3.1.1 Acoustic methods – "Listening to concrete"

Acoustic methods such as ultrasonic pulse echo, impact echo and S.A.S.W. are based on the propagation and reflection of mechanical waves – in the cases considered on shear, compression and Rayleigh (surface) wave types respectively. They provide us with wave velocities which depend on strength properties and mass density, as well as images of reflecting interfaces, e.g. from voids and cracks. The waves are a form of mechanical energy and tell us about the mechanical properties of the concrete. An acoustic wave is sensitive to interfaces between concrete and lower density material, e.g. an air interface will prevent further propagation of waves and they will be reflected back to their point of origin. The difference in acoustic impedance (product of density and wave velocity) will determine the amount of energy reflected, which for a concrete: air interface is nearly 100%. This is why acoustic methods are suitable for detecting voids and cracks in concrete. They will also detect interfaces between steel and

concrete although the amount of energy reflected will be less (70%). The effectiveness in detecting interfaces is therefore dependant on the differences in density between the materials concerned. In the case of steel in concrete, part of the wave-energy continues through the steel and part is reflected. Acoustic methods are not significantly affected by the moisture content of the concrete but are affected by physical discontinuities, e.g. those caused by poor compaction and, in the case of higher frequency waves, by aggregate size.

The acoustic techniques considered in this work are as follows:

- Ultrasonic Pulse Echo (U.P.E.)
- Impact Echo (I.E.)
- Spectral Analysis of Surface Waves (S.A.S.W.)
- Ultrasonic wave velocity (U.P.V.)

3.1.2 Radiographic methods – "Seeing through concrete"

Radiographic methods, i.e. those based on røntgen and gamma radiation, which are both forms of electro-magnetic radiation, enable us to see through and describe the composition of reinforced concrete. The two forms of penetrating radiation considered here are the most common forms used in industrial radiography. Røntgen radiation is produced when electrons, accelerated to high energy levels, are forced to strike and de-cellerate against a metallic target thus producing photons or bundles of radiant energy. Gamma radiation is produced as a result of the instability and disintegration of the material nuclei of some materials (isotopes). This process causes energy emissions, or gamma radiation.

The amount of radiation that penetrates the object under investigation is measured using film or other detector (see below for description of computed radiography). This is dependant on the density of the material under investigation. A radiographic image is thus a projection of the volume of concrete that has been penetrated by the radiating beam, with image density that reflects the density of the object investigated. A void inside concrete will allow more radiation to penetrate while a re-bar will reduce the amount of penetrating radiation. The image produced will thus be darker in line with the projected void and lighter in line with the re-bar.

The technique is "direct" in the sense that a projected image is produced rather than reflected data. The latter requires processing and may have been "modified" in its passage (r.e. radar and ultrasonics). The images produced in a radiograph can have very high resolution enabling the inspector to recognise and describe the internal structure in great detail. The images are however projections of the total mass of reinforced concrete as a flat image with no immediate perspective of depth. This can however be overcome by making more than one image and/or combining with other techniques. Radiography requires access to both sides of the object under investigation.

The radiographic sources considered here are:

Medium energy sources: Cobalt (Co) and Iridium (IR) isotopes.

High-energy sources: Betatron 7.5 MeV

The imaging technique used was the Computed Radiography system (CR). Comparisons have been made with traditional industrial radiographic film (D7 and D8) as well as scintillator detectors.

3.1.3 Electromagnetic methods – "Feeling inside concrete"

The Ground Penetrating Radar (GPR) technique used and described in this work is a comparatively recent development (about 40 years). It was first used to study glaciers and later for geophysical studies, for which it is mainly used even today. High frequency antennae (500 – 3000 M Hz) have found use in civil engineering, specifically for mapping embedded steel reinforcing (main application) as well as thickness and condition assessment, e.g. moisture content/location of moist areas.

GPR is a high-resolution near-surface suveying tool. The antenna produces a short pulse of electromagnetic energy, which propagates into the concrete. The information received depends on the differences in the ability of the sub-surface material to promote or reject the energy. The reflected (rejected) part of the signal, the two-way travel time and the amplitude is recorded digitally.
In our investigations scans have been made with radar that are built up of measurements (time-

amplitude plots) each 2 or 4mm along a line. Several such lines can be combined to produce a data cube.

Steel in concrete produces strong wave reflections due to the difference in electro-magnetic impedance between the two materials. This is why radar is such a good tool for mapping reinforcement and pre-stressed cable ducts. It can also be used to detect voids, but not to the same effect.

The advantage of radar is that it is a high-resolution method of mapping reinforcing, in some cases two or even three layers of reinforcing to depths up to about 300mm. It does not require surface contact or a contact medium. It is not dependant on the magnitude (size and volume) of embedded steel, and this does not therefore affect depth measurement, for example cover thickness to re-bars. This is an advantage over the traditional covermeter. Radar is not affected by the size of aggregates. It is however strongly affected by the conductivity of the concrete.

3.1.4 Traditional /Manual methods

Tapping is an old and traditional way of checking concrete for shallow delaminations and is an effective starting point when investigating concrete. The method is however highly subjective and significant differences between surveys carried out by experienced inspectors are common. It requires only a small hammer and a good ear.

It goes without saying that no examination should be made without first making a visual inspection. This will tell us a little or a lot about the condition of the concrete and help in choosing the best NDE-method. It should be made within touching distance, e.g. concurrently with tapping.

3.2 Ultrasonic Pulse Echo

Instrument: A 1220 from Spectrum, Russia supplied by J.M.E. Ltd. UK

Fig. 3.2.1: The U.P.E. unit with transducer array on the right and small field computer on the left. This instrument is powered by four 1.5 V batteries, which normally are sufficient for at least two days of measurement. This unimposing instrument is probably the most advanced and usefull acoustic tool experienced by the authors.

Fig. 3.2.2: The transducer is pressed against the concrete and a measurement is completed and stored in a couple of seconds

U.P.E. is based on the propagation and reflection of mechanical waves. This particular instrument uses the shear wave component (as opposed to compression wave). The waves are generated at the concrete surface by an array of transducers that resonate horizontally. The transient* waves produced have a user selectable centre frequency in the range 33 to 250 kHz. The wave travel time through the concrete and back to the antenna is converted to distance, when the shear wave velocity is known. The shear wave velocity can be determined by measurement between two antennae along a line on the concrete surface or by measurement through concrete of known thickness. Alternatively, known compression or Rayleigh wave velocities can be converted to shear velocities. This is a dry-contact transducer and no surface preparation is needed.

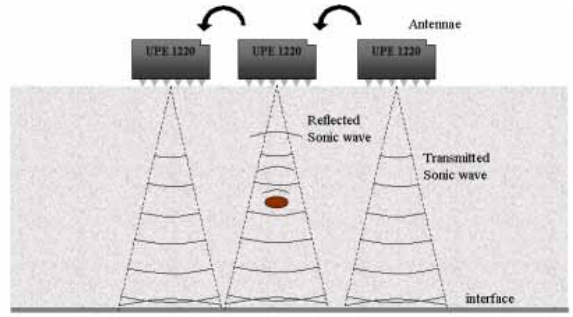

Fig. 3.2.3: A scan with U.P.E. is normally made, by moving the transducer array along the surface at pre-determined intervals. This is done from point to point rather than as a continual scan (compare with radar).

Fig. 3.2.4: Testing concrete "the comfortable way" using U.P.E. The equipment is surprisingly light and simple to use yet very capable for detailed testing of quite thick structures.

Reflecting interfaces, such as the backside of the

* Transient means that a short duration, broadband, impulse is used as opposed to a continuous single frequency source.

structure and internal voids, give rise to echoes, which are recognised by the antenna. The relatively strong echoes appear as large amplitude signals in the received data and can be distinguished from the multitude of smaller scattered reflections from the concrete grains.

3.2.1 Example

U.P.E.- Reflections from steel and air-filled voids in concrete

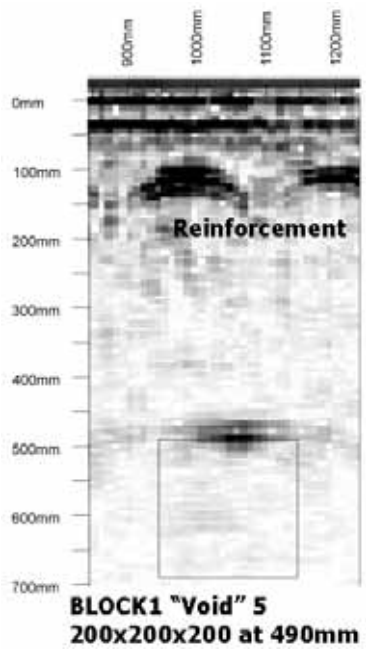

Fig. 3.2.5: Result of a scan across a reinforced concrete surface with a void at 500 mm. (Artificial void in Block 1 (see Appendix 1 for description of block)). The void at 500 mm can be easily seen as a dark surface (upper surface of void) as can strong reflections from the reinforcement. This B-scan was made over a length of 400 mm, with A-scan at 10 mm intervals. Frequency used: 70 KHz.

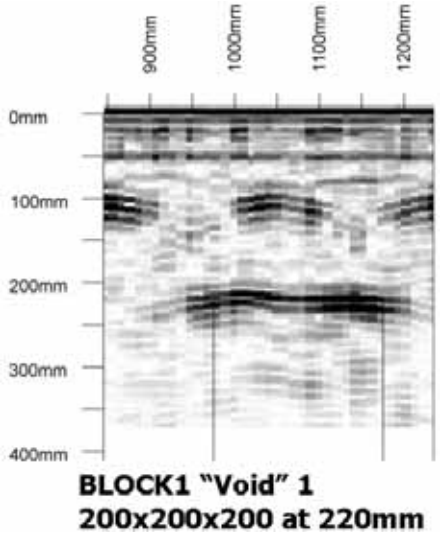

Fig. 3.2.6: Artificial void in Block 1. This void at 220 mm can be clearly seen and the size of the void (parallel with the surface) can be estimated. (The thin vertical lines indicate the void edges.)

In the figures above, we see the result of two measurement profiles (B-scans) using the U.P.E.-instrument on the surface of Block 1. A measurement has been made at 10 mm intervals across each void – the profiles cover a length of about 400 mm, i.e. 40 measurement points (A-scans.) The voids appear clearly as dark regions at depths of 490 mm and 220 mm. The approximate width of each void can be estimated, although the accuracy is better in the case of the void at 220 mm, as expected. It is not possible to distinguish voids from planar cracks. Reflections from the ϕ 16 mm reinforcement at about 80 mm from the surface cause hyperbolae, similar to what can be found in radar survey results (radargrams). As demonstrated here the U.P.E. technique will detect both higher and lower density material in concrete.

3.2.2: Example

U.P.E.-Reflections from the back-side of a structure

The thickness of a concrete structure can be visualized in the form of a contour map. This will reveal abnormal thickness variations as well as defects in the concrete, which prevent the transmitted waves from reaching the back-wall (the other side of a concrete wall or slab).

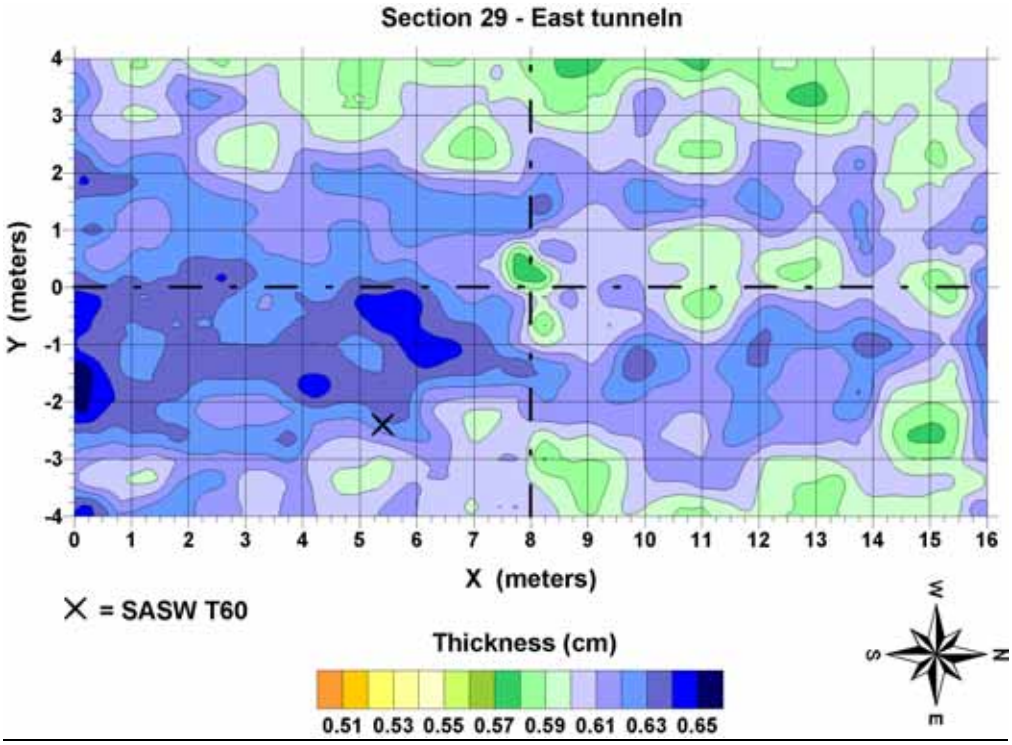

Fig. 3.2.7: Result of thickness mapping with the U.P.E.-instrument The depth/thickness of the concrete is contoured. The concrete in this case has a nominal thickness of 600 mm. The concrete is of high quality (K50) with crushed granite aggregates of max size 25 mm. The concrete is un-reinforced. The area shown in the C-scan above is 128 m^2. The concrete has been cast against a lower density membrane and it is at the interface between the membrane and the concrete that the reflections occur.

3.3 Impact Echo

Instrument: Supplied by Olson Instruments, U.S.A.

Fig. 3.3.1: The impact echo equipment including the field computer and various impactors and transducers (receivers).

By striking the concrete surface with a hammer or similar, compression waves are generated that propagate into the concrete and are reflected from the backside and propagate back to the surface of impact. The reflections back and forth between the surfaces will continue in the form of a standing wave with a frequency, **f** dependant on the velocity of the compression wave, $\mathbf{v_c}$ and thickness of the section, **d**:

$$f = \left(v_c \cdot \frac{1}{2d} \right)$$

The recorded signal is converted to the frequency domain using Fourier analysis (this means that a periodic signal can be described by Fourier decomposition as a Fourier series, i.e. as a sum of sinusoidal and cosinusoidal oscillations) with the result that we obtain frequencies corresponding to the depth of the reflecting interface. For a simple, homogenous slab of infinite size in the x- and y-directions, the only reflecting surface will be the backside and we will obtain a single dominant frequency in the frequency spectrum. The waves are generated by a single hammer strike - a transient impulse (as opposed to a shaker that can give a continuous signal.) The transient signal should preferably contain a broad spectrum of frequencies and thereby the frequency corresponding to the standing wave frequency. If a shaker was used it would be necessary to sweep over a broad range of frequencies to be sure that the standing wave frequency is included. The frequencies that do not correspond to the standing wave will rapidly dissipate and the recorded signal will be dominated by the frequency corresponding to the thickness.

The frequency content of the signal can be, varied by using small or large impactors. The former would contain frequencies that enable relatively small and shallow objects to be detected, e.g. a small void or near surface crack. The latter would be used to detect larger objects or measure slab thickness.

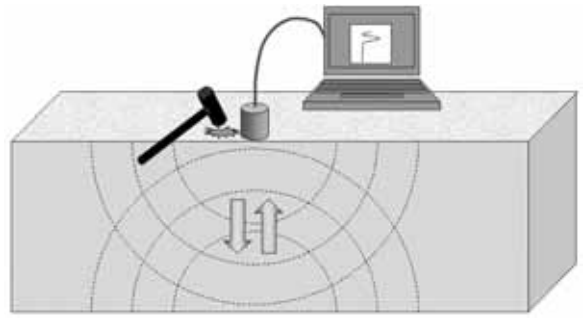

Fig. 3.3.2: The simple principle of Impact Echo measurement. A hammer is used to strike the concrete and create a compression wave, which propagates back and forth between the concrete surfaces. The concrete thickness or depth to a void is calculated from the frequency peak of the standing wave and the compression wave velocity of the concrete.

(Fourier analysis: An impact with an hammer will produce a mechanical wave that contains many different frequencies – the recorded signal from such a broad frequency signal can be treated mathematically so that each frequency component is extracted and the sum of these components form the initial broad signal. Thus, the transient signal is converted into a large number of single "shaker" frequencies.)

3.3.1 Example

Air void inside concrete block

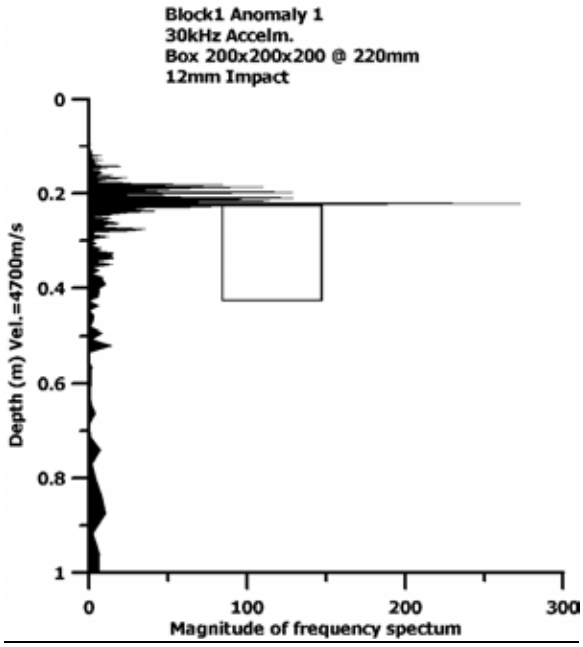

Fig. 3.3.3: Example of an Impact Echo test on a concrete slab (Block 1). The test was made above a 200 mm cubic void at a depth from the surface of 220 mm. The dominant echo is seen as a sharp high amplitude peak (the vertical scale has been converted to distance by using a compression wave velocity of 4700 m/s). Note that the back-wall echo from the bottom of the slab (803 mm) is missing, as the wave has been obstructed by the void. There are two things that tell us there may be a defect in the concrete – the dominant echo from something at 220 mm and the "missing" back-wall echo. It is however not possible to say if the "anomoly" is a void or a crack plane, i.e. it is not possible to characterise the anomoly.

3.4 Spectral Analysis of Surface Waves

Instrument: Supplied by Olson Instruments, U.S.A.

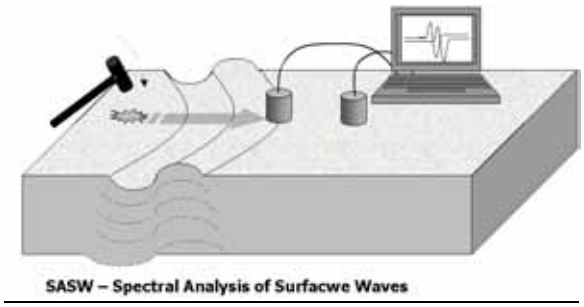

Fig. 3.4.1: Principle of SASW

As with Impact Echo, the mechanical energy (in this case the Rayleigh wave) is generated by striking the concrete surface with, a small hammer or similar impactor. The propagation of the Rayleigh (surface) waves can be measured at the surface and the velocity of each wavelength component calculated as the waves pass the two sensors on the surface. In this way, it is possible to create a diagram of Rayleigh wave velocity versus wavelength. Since the waves are influenced by material at depths proportional to wavelength (short wavelength: near-surface and long wavelength: far-surface) then we can create a diagram of the variation in wave velocity with depth - a so-called dispersion curve.

The equipment and testing set-up are very similar to that used for Impact Echo. The collection of SASW data and processing is however more lengthy. Two transducers are used with a maximum separation approximately equal to the thickness of the concrete under investigation. The use of two transducers in this way does of course restrict tests to sufficiently large and accessible surfaces.

According to our experience, this method is suitable for relatively large planar surfaces (access). Also the type of investigation is usually that of layered systems or material (ground, soil, concrete) variations with depth. The ability of the method to detect and describe relatively small defects/objects is not so good as Impact Echo or Ultrasonic Pulse Echo. It has the advantage that it can quite accurately measure thickness without the need for calibration, i.e. wave velocity calibration.

3.4.1 Example

SASW and cracks

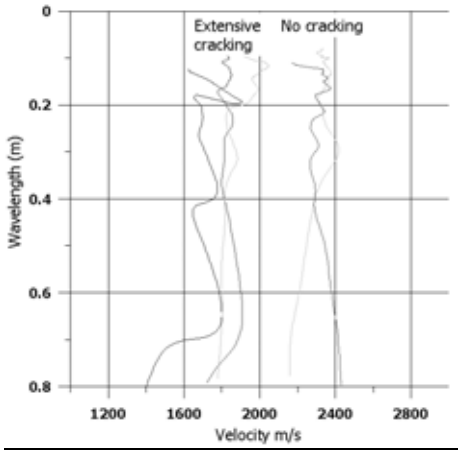

Fig. 3.4.2: Data collected with SASW. The dispersion curves are from a concrete wall with visible surface opening cracks.

In Fig. 3.4.2 the result of a SASW survey shows that the cracking in this particular concrete wall extends to some depth from the surface. Cracking was visible at the surface. The example shown is from a 800 mm thick wall. All of these measurements were made in the same region, although in both visibly cracked and uncracked concrete. The *apparent* wave velocity in sound concrete is approximately 2400 m/s and is uniform with depth. The corresponding velocity in cracked concrete is approximately 1800 m/s. The latter suggests clearly that the concrete is damaged, but retains some strength. (Experience has shown that an extremely damaged (cracked) concrete would have Rayleigh wave velocities around 1200 to1400 m/s see Fig. 4.6.5.5.)

3.4.1: Example

SASW and voids

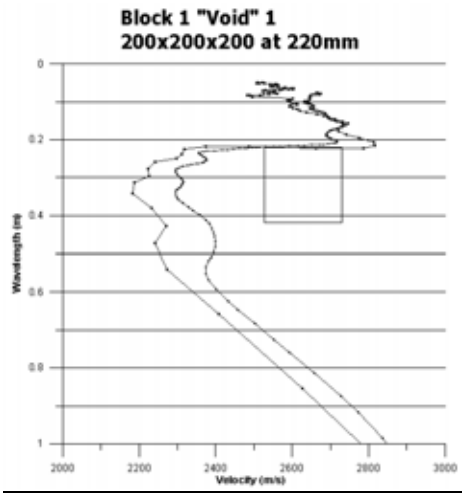

Fig. 3.4.3: SASW measurement clearly indicating the position of the void. In some circumstances, this technique can, be used to detect internal defects. The example shown is however one of the better examples that we have.

3.5 Radiographic techniques – "Seeing through concrete"

Radiography, or x-ray as it is commonly known, enables us to produce a 2-D image of the concrete and variations in the density, for example, those caused by reinforcing bars or voids. The technology used today enables us to produce extremely high-resolution digital images of reinforced concrete up to 1500 mm thick. The x-rays penetrate the concrete and are attenuated by the material to a degree that is dependant on the density and thickness of the object. The amount of radiation that penetrates the object will determine the brightness/contrast (darkness) of the image. A reinforced concrete structure will produce an image, which reflects the variations in density in the volume tested, so that rebars appear as lighter (less dense) images on a darker surface (providing that the concrete is homogeneous). If the concrete contains pores or voids then these will appear as darker spots/areas on the image.

Commonly used sources of radiation for industrial radiography are isotopes, for example, Ir (Iridium) and Co (Cobalt). These are permanent radiation sources, which decay with time depending on the half-life of the isotope. The Ir-isotope is used for concrete up to a maximum thickness of approximately 300 mm, while the Co-isotope can be used for thickness up to 600 mm. The quality of the images produced by isotopes is normally poorer than that obtained with an x-ray tube or accelerator. A high-energy radiation source, known as an accelerator, is needed to penetrate concrete more than 600 mm thick. These machines are portable and run off a normal 220V supply and are therefore applicable anywhere on site (see details of Betatron below). In our work isotopes have not been used for concrete thicker than 400 mm.

Common industrial x-ray tubes of energy 150 – 200 kV are not sufficiently powerful (low radiation dose and energy) to be of any use on concrete in most applications, i.e. >150 mm thick. There are however powerful, mobile accelerator units that can be used for concrete up to 1500 mm thick. This kind of equipment has been used in this work, namely the 7.5 MeV (7500 KeV) Betatron. Most of the examples from mock-up tests and on site inspections provided in this report were produced with the Betatron.

3.5.1: The imaging system - Computed Radiography – principles

A computed radiography system consists of an image plate, a scanner and erase unit, and a workstation for image processing, see below.

Fig. 3.5.1: On the left is the scanner with an inserted image plate and to the right a workstation.

An image plate is a flexible image sensor with many small crystals (grain size: about 5 µm) of photo-stimulable phosphor of barium fluorobromide. These contain a trace amount of bivalent europium (Eu), which is the luminescence centre (formulated as BaFBr: Eu^{2+}). The crystals are uniformly coated on a polyester support film. At certain locations, europium replaces barium ions in the space lattice and makes a bivalent ionic bond (Eu^{2+}) with halides.

The image plate is placed inside a cassette, and is first exposed, typically with x-rays or gamma rays. This makes the bivalent state (Eu^{2+}) into a trivalent one (Eu^{3+}). The number of ions excited in this way depends on the radiation dose at different locations on the image plate.

The image plate is then inserted into a scanner. A laser beam scans the image plate with a pre-selected scanning resolution. The reverse reaction of the europium ions from a trivalent to a bivalent state takes places with the result that an amount of light is emitted that is in proportion to the trapped energy. The emitted light is captured by a photo multiplier and converted into digital data by the system before it is sent to the workstation for post-processing.

After scanning the image plate, it is possible to erase the last of the latent image. This is done in

an erase unit with yellow light. It is then possible to re-use the image plate.

Computed radiography has some significant advantages compared to conventional film radiography on reinforced concrete, including:

- Imaging plates have a greater dynamic range compared to film
- Exposure time is as little as 5% of the equivalent exposure time required for to Agfa D7 film
- No need for chemicals and darkrooms
- Possibility for image processing such as contrast enhancement, latitude reduction, noise reduction, edge enhancement, zooming, spatial frequency control, measurement (size) etc.
- Easy archiving, distribution of images via Internet, e-mail or CD
- Imaging plates are more costly but can be re-used thousands of times

3.5.2 The 7.5 MeV Betatron

This is a mobile unit, which produces pulsed radiation with a peak energy of 7.5 MeV. The effect is a radiation dose rate of about 5 rads/hour at 1 metre distance in air. The unit consists of three parts – an accelerator head, a power supply unit and a control panel with combined weight 175 Kg. The separate units are connected by cables and run off a 220 V supply. The Betatron is a cyclic accelerator. The focus size of the equipment used is 0.3 x 1.2 mm, which is smaller than most industrial x-ray tubes.

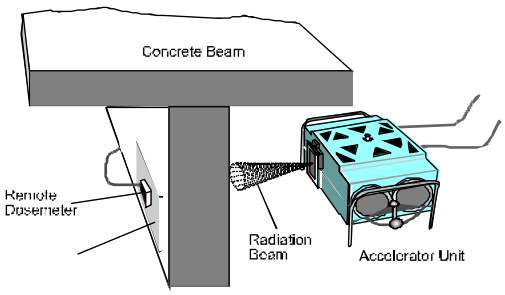

Fig. 3.5.2: Typical set up for radiography with the Betatron. The power and control units are separate (not shown in the picture). A 220 V, 15 A power supply is needed. The supply should be steady and not fluctuating, for example, due to the effects of welding or movement of heavy electrical machinery.

Fig. 3.5.3: The 7.5 MeV Betatron Source. In the phote we see the acceleraotr itself. The equipment is set up to x-ray a wall.

Fig. 3.5.4: A cobalt (Isotope) source "Collimator" with additional shielding from sand bags on each side

3.5.3 Procedure for determining optimum exposure parameters

In order to define the optimum procedure for an inspection using HECR on concrete a number of parameters have to be set:

1. The necessary energy level for the source
2. The choice of the right image plate
3. The choice of the right screens for the image plate
4. The necessary exposure times

All of the above parameters affect the signal to noise (S/N) ratio, which together with the contrast sensitivity determines the possibility of "detection". A high S/N ratio can be achieved with long exposure times using high resolution, image plates and thick lead screens. This of course increases the time and cost per exposure. Therefore, points 2, 3 and 4 have to be determined on the principle*: the image quality has to be good enough for safe interpretation of imperfections and nothing more.*

An example of how this cost effective image quality can be determined will be shown below. A test block was built with two cable ducts. Each cable duct has a diameter of 70mm and contains 12 x 12.5 mm "vsl" cables. Artificial voids were created with different widths* ranging from 30 mm to 70 mm.

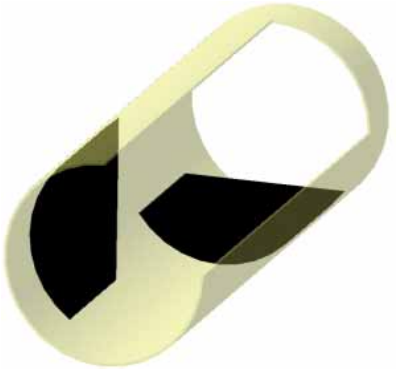

Fig. 3.5.5: View of artificial voids in a cable duct around a bundle of 12 cables. The voids were made with widths of 30 mm, 50 mm and 70 mm. The maximum thickness of these voids is 12mm.

These voids simulate lack of fill in cable ducts and the two void orientations made it possible to determine the contrast sensitivity as a function of void size in the direction of radiation (x-ray direction).

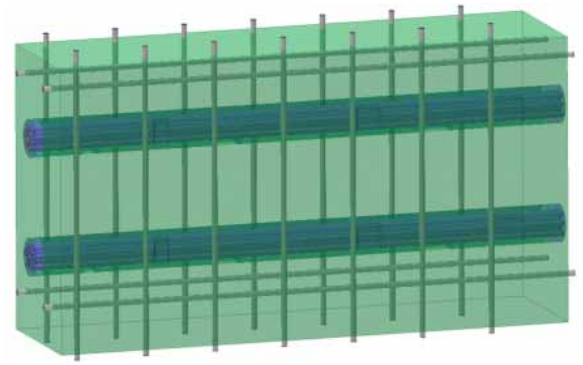

Fig. 3.5.6: Test block used to determine the required (adequate) image quality. The voids, as described above, have been placed inside the two cable ducts before filling the ducts with cement grout. In one case the voids are air-filled and in the other they are filled with water.

Fig. 3.5.7: Cable duct being prepared with air- and water-filled voids. The cable duct has a diameter of 70mm and contains 12 x 12.5 mm vsl cables. It is in other words a heavily reinforced and congested cable duct. The "voids" are placed on the outside of the cables. The duct was then cast in a 30 mm thick concrete beam.

An overview of images as a function of exposure

* The "width" is defined as the dimension along the longitudinal axis of the duct.

times, source energy, image plate quality and different front and back screens, is given below. All images were made using the 7,5 MeV Betatron.

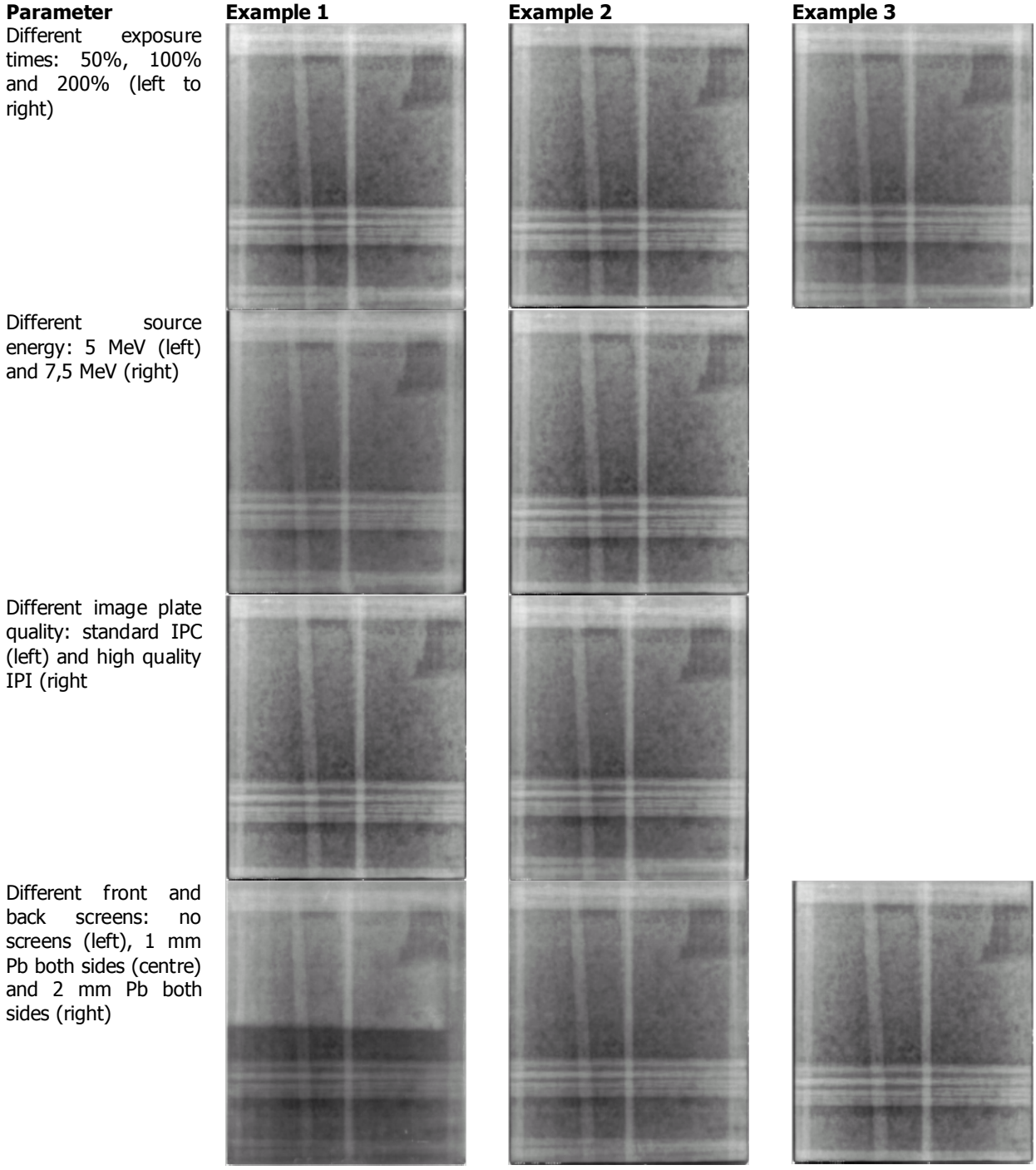

Fig. 3.5.8: Images of 600 mm concrete beam and cable duct in an attempt to get the best image quality

These investigations were all done on two 300 mm concrete blocks (total thickness of 600 mm). The block with voids was closest to the image plate.
In this example the optimum image quality in terms of void detectability, time and cost was obtained with an exposure of 244 s and energy level of 7,5 MeV on a standard (IPC) image plate with 2 mm Pb screens on both sides.

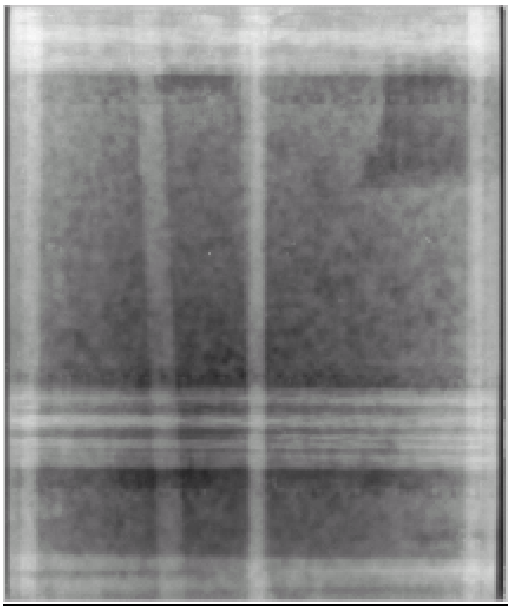

Fig. 3.5.9: Optimum image quality in terms of detectability and costs for a 600 mm concrete block. Exposure time 4 minutes at 7.5 MeV with 2mm lead screens front and back.

Optimum image quality for other concrete thicknesses can be found in a similar way.

3.5.4 Methods to improve the detectability of voids in post-tensioned cable ducts

Creating the optimum image quality for visual evaluation does not always guarantee void detectability. There are several methods that can be used to improve the detectability of voids in concrete structures. All of these are more or less based on the use of image processing and analysis.

Image processing includes:

- Contrast enhancement
- Noise reduction
- Latitude reduction

These can be regarded as basic image processing methods and are performed as a standard procedure on all images produced by any method of digital radiography.

Another standard feature is "line profile" (see Fig. 3.5.1.1) measurement to distinguish different levels of density in an image.

An example of this is shown below. In this case a bridge was inspected as it was considered that there was a risk of corrosion to the pre-stressed cables inside grouted ducts. The inspection of the bridge beams was made using computed radiography and a cobalt isotope. In order to determine whether there were voids around or inside cable ducts line profile measurements were carried out on all processed images.

Fig. 3.5.10: Skovdiget bridge in Copenhagen. This 30, year old bridge has been suffering from frost damage, asr and reinforcement corrosion. Some of the post-tensioned beams were badly cracked.

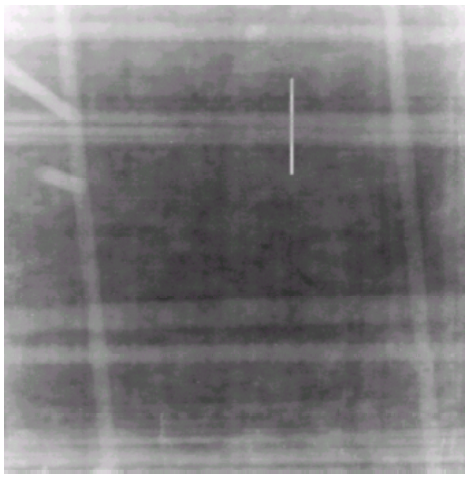

Radiographic image of beam with post-tensioned cable ducts (upper part of image). Duct diameter is 40 mm and the beam is 350 mm thick The white line indicates the density scan position.

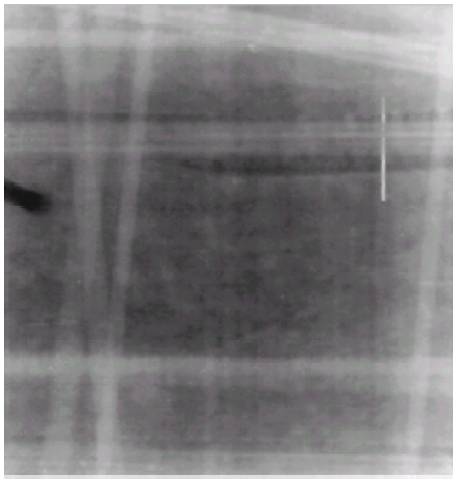

As on right but different position. The duct has voiding in the upper part above the cables. This same duct has voiding in the surrounding concrete around its underside. The white line indicates the density scan position.

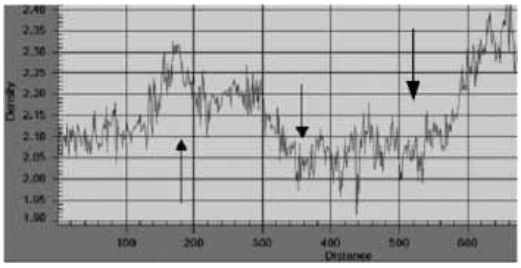

Density, scan across cable duct. The arrow to the left shows a peak in density, which is due to a narrow gap (lack of fill) at the top of the duct. The low, density area (two arrows on right) is due to the steel cables.

Fig. 3.5.11(a)

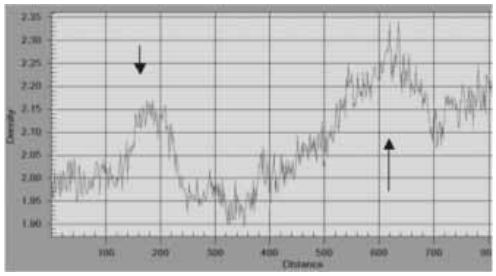

The arrow on the left indicates the high, density zone caused by the lack of fill in the upper part of the duct. The arrow on the right shows the larger voided zone, which is both outside and inside the duct.

Fig. 3.5.11(b)

In the example above there was good agreement between what is possible to see visually and what is possible to measure. This is unfortunately not always the case. Quite often the eye can be fooled into seeing apparent voids, where these do not exist. This kind of optical illusion suggesting apparent voids can occur in a confined area, which is bordered by light or low image density areas – typically light strips, as might be caused by large reinforcing bars.

Conclusion: *never trust an evaluation based* solely *on a visual evaluation, but always use a complimentary evaluation technique (line profile/ densityscan) to finally determine whether there is a void present at a certain location.*

3.5.5 Limiting conditions for void detection

Using the image processing techniques described above in combination with optimum inspection parameters does not automatically result in the kind of images required, i.e. high probability of detecting voids.

The following conditions can limit this capability:

- A *high moisture content* in the concrete increases the scatter and thereby the noise in the images. A high, moisture content also increases the exposure times by a factor of as much as three. A good example of this can be seen below from Kollekolle Bridge in Copenhagen.

- *Congested reinforcing* can make it difficult to distinguish a void in an image. This is of course due to the higher density ratio between an air-filled void and the concrete/steel combination. A void of a certain size is easier to detect in un-reinforced concrete than in heavily reinforced concrete.

- *The composition* of the concrete. It is easier to detect a void of a certain size in a homogeneous concrete with small aggregates, than in a non-homogeneous concrete with large aggregates.

- *The orientation* of the void. If the void plane lies along the path of the gamma or x-ray beam the detectability is greatest, i.e. assuming that the void size is greatest in the this plane. For a void of a given shape and size the density ratio between air and concrete will be greatest in these conditions. For example, a thin crack will be visible "in-line" but not "off-line".

- *External radiation*. If the level of external radiation on the detector side is significant compared to the level of the radiation penetrating the concrete, then the signal to noise ratio in the image produced will decrease as will the void detectability. Normally it is possible to shield the detector from this external radiation, but if the dose rate and/or the mean energy of the background radiation is too high then the probability of void detection decreases significantly.

- *Radioactive contaminated* objects. If the object being examined is, contaminated by radioactive substances then it may be impossible to produce images good enough for evaluation.

"Kollekolle" is an example of a very noisy image taken from a bridge inspection. The reasons for the image being poor and "noisy" were that the correct screens were not used, the concrete was very moist and the reinforcement was congested at the inspection point.

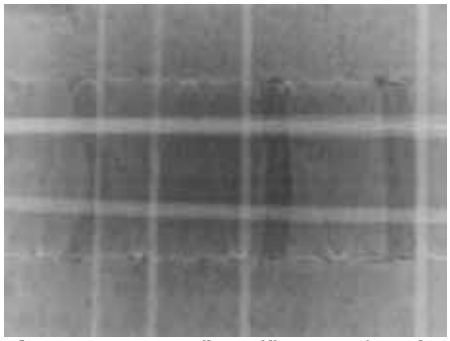

Fig. 3.5.12: A "good" example of an image produced on new and undamaged concrete with small aggregates. Thickness 300 mm.

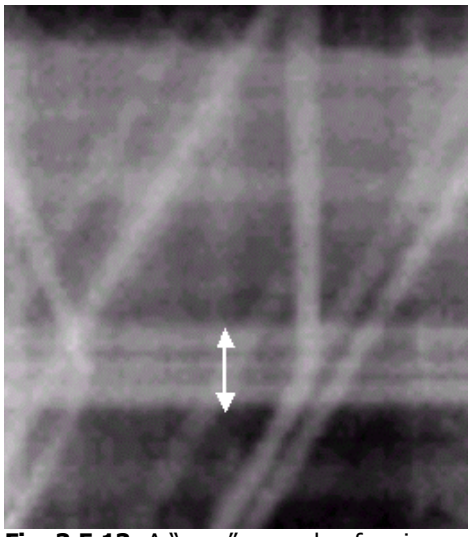

Fig. 3.5.13: A "poor" example of an image from Kolle Kolle bridge – damaged concrete with high moisture content and chlorides. The arrow indicates the cables inside the duct (arrow equivalent to 60 mm).

3.5.6 Exposure times for digital radiography of concrete structures

The exposure times for digital radiography of concrete structures depend on a number of factors:

- The type of source used for the inspection
- The thickness of the concrete structure
- The position of the detector and source
- The type of detector used for inspection
- The condition of the concrete structure
- The magnitude of the signal to noise ratio
- The object of the inspection

Depending on the thickness of the concrete being inspected then either an Ir192, Co60 or a high-energy x-ray source can be used. Ir192 can be used for thickness up to 300 mm. Co60 up to 600 mm and the high-energy x-ray can be used up to a thickness of 1500 mm. For *conventional film* radiography the maximum practical thickness will normally be lower due to the much longer exposure times.

The optimum position of the detector is usually close to the concrete structure, assuming that screens are used. The effects of scatterred radiation can otherwise reduce the image quality.

The chosen SSD is often a compromise between exposure time and field of view or, in other words, area encaptured in the image. Long exposure times can provide a big field of view, and short exposure times a shorter SSD and consequently smaller field of view.

The best detector to use on site is an image plate (storage phosphor plate) because of its robustness, flexibility and the low exposure times compared to on-line flat panel detectors. Furthermore, the image plate can be used for all the different sources commonly used for digital radiography of concrete structures.

The longer the exposure times the better the signal to noise ratio will be. For certain applications, for example inspection for corrosion of pre-stressed cables in cable ducts, a high signal to noise ratio is essential in order to achieve the necessary probability of detection.

Some typical exposure times for different sources and concrete thicknesses can be seen in the table below. All of the exposure times are based on the use of computed radiography.

Table 3.5.1

Concrete thickness (mm)	Exposure time film Agfa D8 (sec.)	Exposure times CR (sec.)	Scanning resolution (µm)
300	40	24	105
600	300	159	210
800	1017	468	210
1000	3516	1380	210
1200	14400	4500	210

Note: The equivalent "film" density for these exposures is 2.5.

Example

Mock-up, loss of reinforcement section

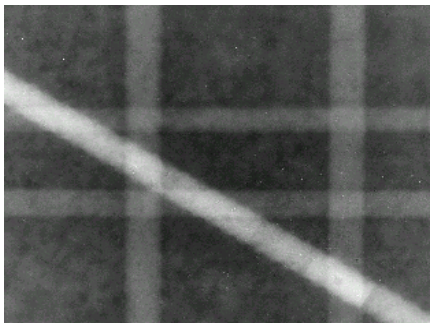

Fig. 3.5.14: Radiographic (CR) image of a reinforced concrete block. Sections of the diagonal bar have been cut out in order to calibrate the sensitivity of the technique for loss of re-bar section.

3.6: Electromagnetic techniques – "Feeling inside concrete"

The technique described here is Radar

Fig. 3.6.1: A GPR system consists of a laptop, a control unit and an antenna. Battery operation is normally used.

Fig. 3.6.2: The antenna is pulled along the surface of the concrete. The measurements are thus made continuously. No contact medium is required between the antenna and the concrete surface.

Electromagnetic methods such as the standard covermeter and radar use electrical induction and electromagnetic wave transmission respectively. The covermeter is a simple tool, which is normally only used to locate rebars close to the concrete surface. The radar equipment is based on the ground penetrating radar but for concrete it usually operates at a much higher frequency. Radar provides us with information on the wave transmission/reflection times and the amount that the wave energy is damped. The strongest asset of radar for concrete inspection is the fact that embedded metals give strong reflections. This property makes radar extremely sensitive to rebars and metallic cable ducts and of course any other metallic interface. The fact that this method can be used in a continual scan mode (antenna slides along the surface) and does not require good physical contact with the concrete surface, means that large amounts of information can be collected quickly. The extremely high sampling rate and advanced electronics provide high-resolution images, and consequently good accuracy when positioning rebars and ducts. The technique is sensitive to the conductivity of the concrete and is not suitable if the conditions are very moist, particularly if there are salts present. If the concrete is quite dry then it is possible to use radar to detect rebars and ducts 250-500 mm from the surface. Under the right conditions radar will detect large air- or water-filled voids in concrete and can also be used to measure the thickness of relatively slender reinforced concrete members.

The radar transmitter antenna produces a short pulse of high frequency (10- 2000 MHz depending on antenna) electromagnetic energy, which is transmitted into the material (concrete). The propagation of the electromagnetic wave is dependent on the high frequency electromagnetic properties of the concrete. The information received is based on the differences in the ability of the concrete (and steel) to promote or reject the transmitted electromagnetic wave. The rejected (reflected) part of the signal, the amplitude and the two way travel time, are stored digitally. By recording the reflections along a survey-line versus the travel time, a depth section along the surveyed path is mapped.

The equipment consists of one to four main parts depending on the instrument, configuration and manufacturer. These are, a control unit, transmitting and receiving antennae, and a storage / display unit. The transmitter/receiver antennae can either be separable or built together into one unit. Some modern systems have the display unit built into the control unit or the control unit built into the antenna and so forth.

The control unit receives the vital parameters (Sampling frequency, Number of samples, Number of stacks and Trace separation) from the operator. It then "tells" the antennae what to do and when to do it. The transmitter emits an electromagnetic wave into the concrete and the energy is then

partly reflected and partly refracted at interfaces that have different electromagnetic properties.

The reflected wave can be seen as a wave travelling back "through" the receiving antenna. The variations in amplitude of the wave are recorded along with the time lapse since the wave was transmitted. To be able to store this wave digitally, samples* of the wave amplitude are taken within a certain time interval (Sampling frequency). The recorded wave is called a trace.

Recorded data can be displayed instantly if preferred, but for concrete measurements it usually need post processing to be of acceptable appearance to enable interpretation. It may or may not be possible to do this in real time depending on the type of post-processing.

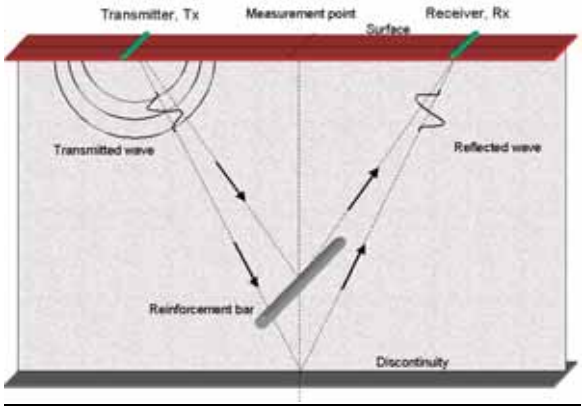

Fig. 3.6.3: The principle of Radar (GPR.) The transmitter sends a signal into the material. The signal is reflected at discontinuities and this, is recorded by a receiver. The example shown is of a reinforcing bar in concrete.

There are, many survey modes but three basic types are recognised; survey along a line, tomography, and down-hole. The most common method for concrete is to measure along a series of parallel straight lines at some fixed separation. This can then be used to produce a 3-D data cube, which is a powerfull tool for detailed studies. A trace (one single measurement) is recorded every 2-5 mm along the survey line resulting in a detailed cross section of the material.

The antenna does not need physical contact with the surface, which means that it can be pulled across the surface of the concrete while collecting data.

The number of samples collected and the sampling frequency used determine the "time window", that is, the depth of the survey if the velocity of the medium is known. Stacking (averaging of several samples at the same position) is used to attenuate incoherent noise. The wave velocities are extremely high (around 100 000 km/s for concrete), which means that the equipment has to be "fast" in order to record the trace (a wave form at one measuring point). This must be done before the operator has had time to pull the antenna to the next measuring point. The number of points (traces) used in a survey is dependent on the size of the target and the horizontal resolution required. Triggering the traces can be done manually, at time intervals, and by distance with the aid of a trigger or thread wheel.

Different antenna configurations can be used for concrete. The choice is based on the object being investigated and the amount of reinforcing in the concrete.

3.6.1 Example

Positioning reinforcement and cable ducts

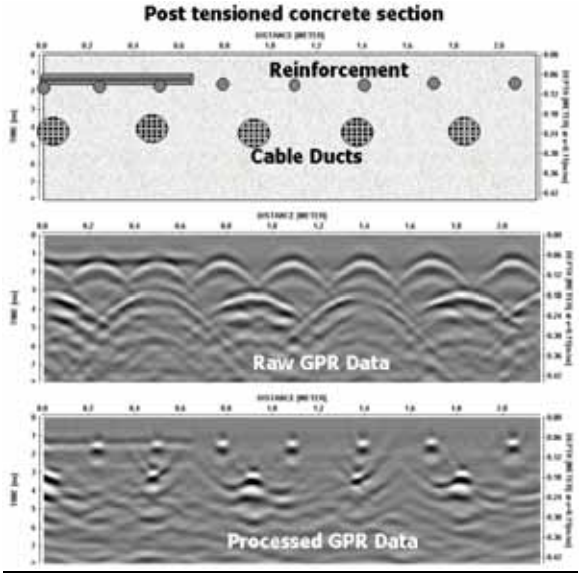

Fig. 3.6.4: Radar images of a concrete wall showing reinforcing bars and pre-stressed cable ducts. In the raw-data the reinforcing/ducts appear as hyperbolae. Raw data can be processed to provide clearer images of each individual bar and ducts which lie "behind" the near-surface reinforcing. The ducts in this case lie at about 250 mm from the surface.

* Measuring the amplitude at a particular moment in time. Many samples can recreate the waveform.

Ghost reflections from a re-bar

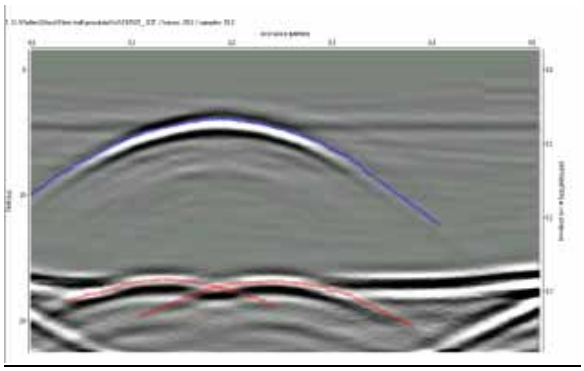

Fig. 3.6.5: A mock-up test revealing false hyperbolic reflectors, "Ghosts", below the single reinforcement bar seen as a large hyperbola in the upper part of the data.

4.0 Applying Non Destructive Evaluation, NDE

In this chapter we bring together the two previous chapters - problem cases and NDE techniques. Here some data from NDE surveys is presented and this should give an insight into the complexities of NDE applied to concrete. Some method capabilities are described for various techniques. However, it is an impossible task to try and present accurate capability data, due to the great number of influencing factors. These are usually not realized prior to the start of an NDE survey.

4.1 Introduction: Definition of the problems (objects of investigation)

A list of the types of problem considered are given below:

- Locating reinforcing bars and cable ducts
- Inspecting rebars and cable ducts*
- Locating voids in concrete and cable ducts
- Measuring concrete thickness with one and two-sided access
- Determining concrete quality
- Other problem cases - miscellaneous

* Inspection by radiography

It is rare that NDE involves only one technique. One reason for this is that there are usually several unknown factors apart from the problem in question. For example, locating voids in a cable duct (radiography) requires that we first locate the duct (for which we might use radar or U.P.E.); measuring the diameter of a reinforcing bar (radiography) requires that we know the depth to the bar (for which we might use a Covermeter or Radar); determining the quality of concrete by measuring P-wave velocity (Impact Echo) requires that we know the thickness (for which we might use SASW).

4.2 Measuring concrete thickness

This is a fundamental task for which there is a selection of suitable methods. Care should however be taken in selecting the method and interpreting the results. If we are to use a pulse-echo method then we must know the wave velocity to calculate the thickness. We can determine the wave velocity by measurement between fixed points on the surface or by measuring through a section of known thickness. However, the wave velocity at the surface can vary considerably from the velocity at depth and can thus lead to considerable errors in estimating the total thickness. Neither is it always possible to check the wave velocity by calibration against a known thickness, as this is not always known or can be determined.

4.2.1: Thickness measurement using ultrasonic pulse echo

U.P.E. is based on the propagation and reflection of mechanical waves, known as shear waves (as opposed to compression waves). The waves are generated at the concrete surface by an array of transducers that resonate parallel to the surface. The waves produced have frequencies in the range 33 to 250 kHz. The measurement of thickness involves converting the wave travel time through the concrete to a distance. This is done either by *knowing* the shear wave velocity or by *measuring* it. The shear wave velocity can be determined by measurement between two transducer arrays along a line on the concrete surface or by measurement through concrete of known thickness (see Fig. 4.2.8) or by conversion of a known compression or Rayleigh wave velocity.

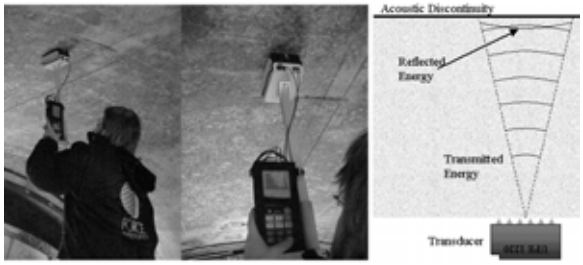

Fig. 4.2.1: The picture on the left shows thickness measurement in the field using the U.P.E. technique. The diagram to the right shows the principle of technique– a relatively narrow beam of high frequency waves are transmitted through the concrete and back to the receiving part of the transducer array.

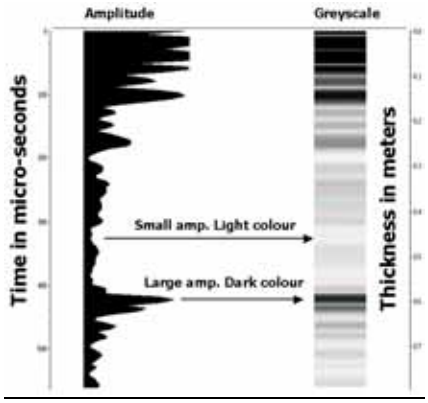

Fig. 4.2.2: The received signal (right) is converted to a grey-scale plot using a colour table.

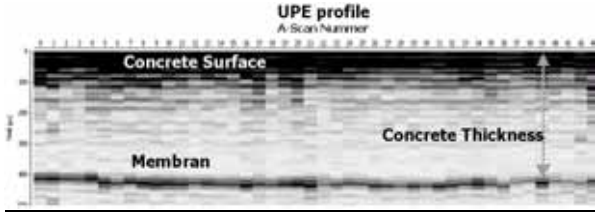

Fig. 4.2.3: A result from a U.P.E. profile along a concrete lining in a tunnel. The diagram shows the result of a series of measurements made along a line (in this case with separation 400 mm). The thickness of the concrete is about 650 mm. The thin dark line represents the echoes from the backside of the concrete lining.

The result shown in Fig. 4.2.3 is a good example of thickness measurement using the U.P.E. technique. The concrete in this case is of good quality and not reinforced. In addition, the maximum aggregate size is 25 mm, which is beneficial for good ultrasonic "sound" transmission. (Compare the clear bottom echo signal from 650 mm thick concrete with that shown in the example below in which the thickness is only 300 mm.)

In less favourable conditions, e.g. in poorer quality concrete or if the aggregates are larger, then we cannot expect such good results. The reason for this is that the wave energy is dissipated by irregularities and scattering from larger aggregates. In Fig. 4.2.4, we can see the result of U.P.E.-measurements on a 300 mm slab with some cracking and delamination.

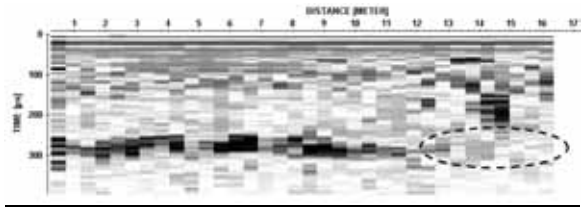

Fig. 4.2.4: U.P.E.-scans of poorer quality concrete. In the diagram, the bottom echo can be seen quite well along most of the scan length. However, there is a poor zone in the right hand region, which interrupts the signal. This could be caused by discontinuities quite near the surface. (This might be checked by choosing a higher frequency and wider time window to provide more detail around the suspected anomoly)

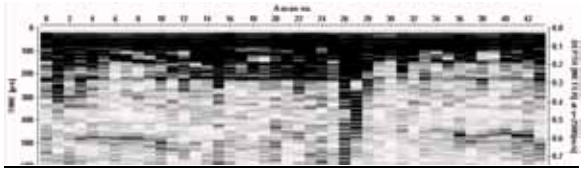

Fig. 4.2.5: In this diagram, the reflections in the near surface region are strong along the entire length of the scan. This is seen as a dark region near the surface (dark corresponding to many strong reflections). Most of the wave energy is thus dissipated before it can reach the bottom of the concrete slab. Only faint bottom echoes can be seen to the left and right ends of the scan.

The U.P.E. technique described here uses dry contact transducers and thus does not require a contact medium like ultrasonic gel or paste to provide acoustic coupling with the concrete surface. Since the transducer tips are needle shaped and spring-loaded, the antenna can operate on quite rough surfaces. This means that each measurement requires only a few seconds. The wave spread from the transducer array is narrow and this means that we have little interference from interfaces (to the side of the survey line, e.g. such as the edges of a block).

In concrete of reasonable quality and thickness (around 600 mm or less), this is the favoured technique for thickness measurement. If aggregates are around 16 mm or less then it is possible to use this method for thicknesses up to 1000-1200 mm. (Ref. Fig. 4.2.9)

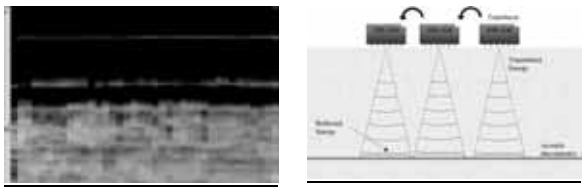

Fig. 4.2.6: U.P.E.-scan with c/c 50 mm (single transducer array). The bottom echo is not clearly visible. The dark region in the top indicates that there are many reflections in the near-surface region.

Concrete wall. Thickness 800-850 mm. Concrete compressive strength 50-70 M Pa. Maximum aggregate size 32 mm (crushed granite). Age at test approximately 30 years. Some near-surface irregularities. Pre-stressed in horizontal and vertical directions.

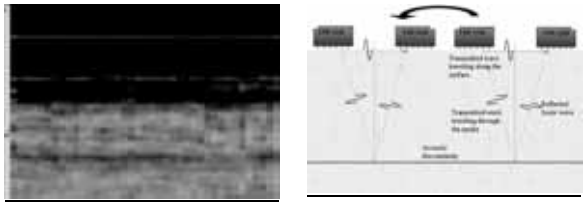

Fig. 4.2.7: Same wall as shown in previous Fig. 4.2.6. U.P.E.-scan with double transducer array, increasing the strength of the signal. The bottom echo can now be seen although faintly. The frequency used in both cases was 33 k Hz.

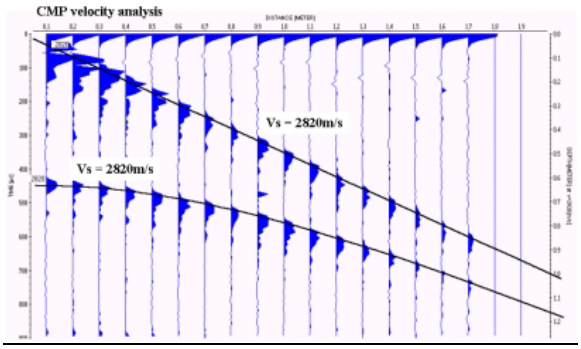

Fig. 4.2.8: Measurement using two transducer arrays (one as sender and one as receiver) on a 600 mm thick concrete slab showing the surface and average (through-slab) shear wave velocities (upper and lower sloping lines respectively). In this manner it is possible to compare the near-surface velocity with the average value through the full thickness. In this case they are the same.

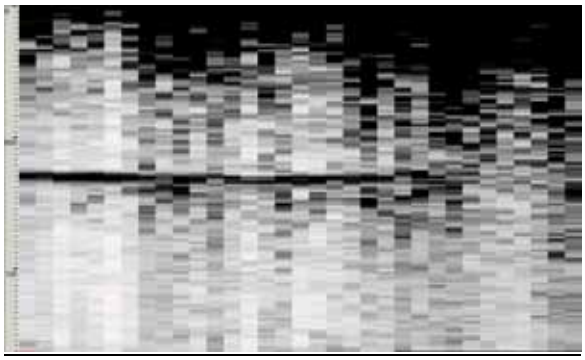

Fig. 4.2.9: This profile was made along a 750 mm thick wall at c/c 50 mm. The bottom echo signal can be seen clearly over most of the section, which is due to the fact that the maximum aggregate size is 16 mm. The transition to concrete with larger (32 mm) aggregates can be seen (right hand side), as the bottom echo is no longer visible. A single transducer array was used for this test. The back wall echo is from a concrete: steel-interface. The scan length is 4000 mm.

Fig. 4.2.10: Newly constructed bridge in Norway. The bridge slab is 850 mm thick and tapered at the edges. Some drying-shrinkage cracks appeared in the top surface. The w/c-ratio of the concrete is 0.4 and the maximum aggregates are 25 mm. The visibility of the back wall (underside of the bridge slab) tells us that the surface-opening cracks are probably shallow and that the concrete is otherwise free from internal damage. See Fig. 4.2.11.

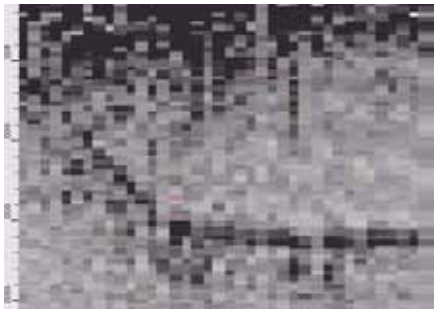

Fig. 4.2.11: U.P.E.-scan at c/c 50 mm from the edge of the bridge towards the centre. The underside of the bridge slab gives quite a clear reflection and we can see the bridge profile quite well. The reflections from the sloping edges are not as strong, as expected since the wave energy is partly deflected. No significant defects are suspected in the concrete apart from the surface cracking.

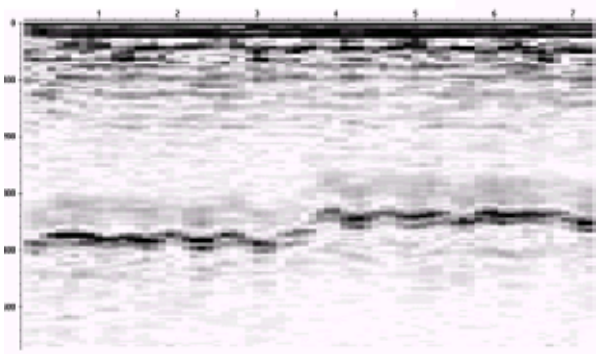

Fig. 4.2.12: U.P.E. thickness measurement on 650 mm thick concrete lining. The tests were made with c/c separation 200 mm. The bottom echo can be clearly seen and a detailed image appears of small variations in the thickness due to ripples in the far surface due to the flexibility of the formwork sheets used. The length of the scan shown is about 7 m.

4.2.2 Thickness measurement using Impact Echo

By striking the concrete surface with a hammer or similar, we generate compression waves, which propagate into the concrete and are reflected from the backside and return to the surface of impact. The reflections back and forth between the surfaces will continue in the form of a standing wave with a frequency, **f** dependant on the velocity of the compression wave, $\mathbf{v_c}$ and the thickness of the section, d:

$$f = \left(v_c \cdot \frac{1}{2d} \right)$$

The reflected waves are transformed into frequency content using Fourier analysis with the result that we obtain a frequency peak corresponding to the depth to the reflecting interface. For a simple, homogenous slab of infinite size in the x- and y-directions, the only reflecting surface will be the backside and we will obtain a single dominant frequency in the frequency spectrum, see Fig. 4.2.2.3. The waves are generated by a single impact, e.g. using a hammer. A large hammer has a larger impulse time and creates low frequency and high-energy waves. A small hammer or ball bearing has a short impulse time and produces high frequency, low energy waves. The choice between the two depends mainly on the depth and size of the concrete or defect being examined. In order to obtain sufficient sensitivity to detect a small shallow crack then a light hammer or ball bearing would be used.

The method is excellent for structures with simple geometries, such as slabs and walls. The fact that the input energy is relatively high and the frequencies low, means that we can obtain results for relatively thick structures with varying quality and coarse aggregates. Impact echo is generally not sensitive to aggregate size. The wave energy is spread on a broad front and it is not possible to detect relatively small or narrow regions in which the thickness varies (the ability to detect such variations depends on their size relative to the thickness). A fundamental rule of impact echo (observed by Sansalone and others) is that, the lateral dimensions should be more than about 5 times the thickness to avoid edge effects. Bounded structures respond in an entirely different manner from plates.

Care should be taken when testing thick structures if there is a likelihood of surface damage or variations in concrete properties with depth. A thick concrete wall in a relatively dry indoor environment may have considerable variations in both moisture content and mechanical properties with depth (due to long-term drying and/or strength gain). The value of P-wave velocity used to calculate thickness of a member should obviously be accurate for the full thickness and not just the surface layer.

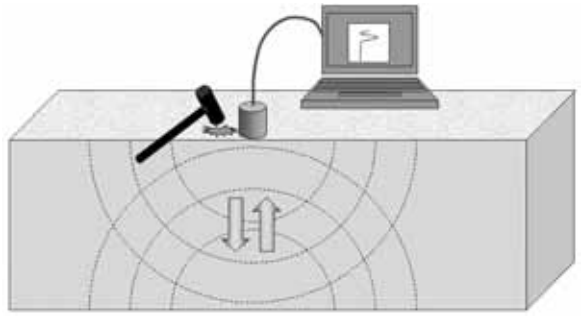

Fig. 4.2.2.1: Impact Echo - The concrete is struck with an impactor creating mechanical waves that propagate back and forth between the surfaces. The frequency of this resonance is used to determine thickness, depth to interfaces and P-wave velocity.

Impact echo testing requires good contact between the transducer and the concrete surface, which can involve some preparation time. Some types of equipment are quite rapid however and do not require surface preparation. Impact Echo is otherwise a robust method and flexible in the sense that it is possible to vary the input energy (and frequencies) according to the concrete thickness and quality, as well as the size of the object/defect to be detected. It is normally possible to obtain a clear and distinct bottom echo when measuring thickness. It is best suited to simple geometries such as slabs since geometries that are more complicated cause reflections from other boundaries/interfaces. Care has to be taken not to misinterpret other wave-modes, for example, flexural modes caused by flexural vibration of the concrete element or layer, as well as other wave types. The flexural response of thin layers of concrete is a feature that allows Impact Echo to detect delaminations, for example those caused by rebar corrosion.

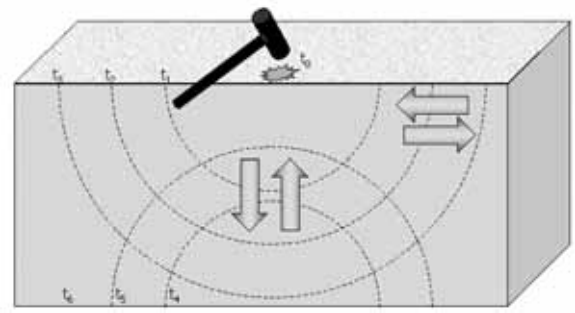

Fig. 4.2.2.2: Even a simple structure will produce echoes from many boundaries. Several wave types exist and this can cause interpretation errors particularly if the geometry is complicated. (Dashed lines visualize the mechanical energy fronts at different times after the impact of the hammer)

Calculating thickness

Here V_C and C_P are the same, i.e. compression wave velocity.

Compression wave velocity of concrete, C_P = 4000 m/s

Frequency of reflected wave, F = 4 k Hz

$\Rightarrow$ Thickness, D = C_P /(2F) = 500 mm.

Thus, if we know the compression wave velocity then we can calculate the thickness of the concrete.

This is the simplest situation and is demonstrated by the example from a mock-up measurement below (Fig. 4.2.2.3). The same principle is used to measure the depth to voids, cracks, pipes and other interfaces.

The above relationship between frequency, depth (thickness) and compression wave velocity, C_P apply for an infinate medium. For plates the IE-compression wave velocity is taken to be 96% of the value for an infinate medium.

For other structures like rectangular and circular columns the fundamental frequency (first modal frequency) is F_1 where:

$F_1 = \beta . C_P/(2F)$

The value of β is 0.92 for circular columns and 0.87 for square columns/beams. The value for rectangular columns/beams depends on their aspect ratio, i.e. ratio of depth to breadth.

Mock-up example

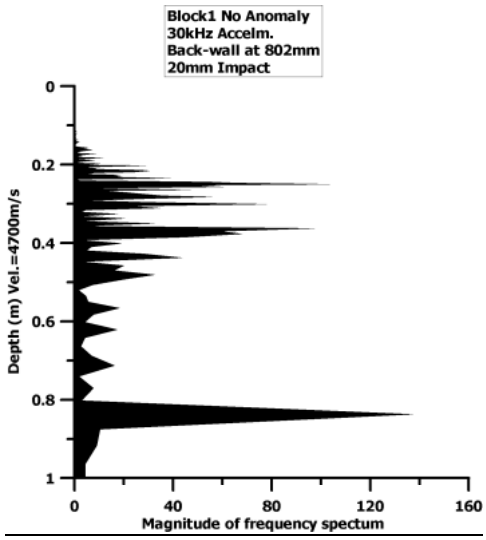

Fig. 4.2.2.3: Impact Echo result from a concrete slab 803 mm thick. The dominant echo is from the underside of the slab, while several weaker reflections from internal discontinuities can be seen. The frequencies have been converted to thickness by using the compression wave velocity of 4700 m/s. The impact was made with a ϕ 20 mm steel ball. The dominant echo is the large peak or "spike" visible at the bottom of the y-axis. The value of C_P in this case is that of an infinate medium.

4.2.3 Thickness measurement using SASW

SASW can be a useful tool for thickness measurement. It can provide us with the thickness of concrete directly, i.e. without knowledge of wave velocities. This however requires the right conditions. Examples from site tests are shown in Fig. 4.2.3.2 and 4.2.3.3. The technique is well suited for simple geometries in situations where other techniques cannot be used or calibrated.
The accuracy has been found to be about 3-8% for thickness measurement depending on the survey conditions. SASW is often used to determine wave velocities, which can then be used to calibrate other techniques (UPE or IE) for thickness measurement.

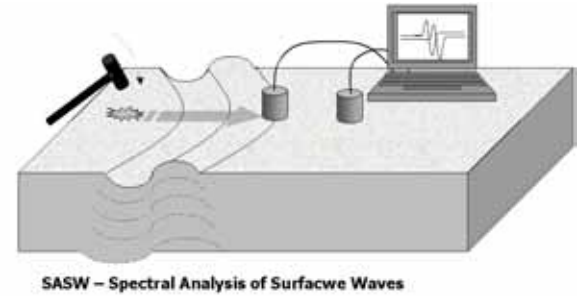

Fig. 4.2.3.1: An impact creates waves that travel along the surface of the concrete – concrete with a free surface. These surface (Rayleigh) waves are influenced by the sub-surface conditions – high frequency waves by near surface and low frequency waves by near and far surface. The wave passage is recorded by two accelerometers placed at suitable distances from the impact point.

The deviation in the dispersion curve that can be seen in Fig. 4.2.3.3 below indicates quite accurately the thickness of the concrete. It is thought that this deviation is an effect of the standing (P-wave), which reflects from the interface (back side). It will also coincide with a large drop in data coherence at a corresponding frequency. It is thought that the accuracy of this method in measuring thickness can be better than ± 5%. See also Appendix 5, Fig. A.5.3.

Grouted concrete lining

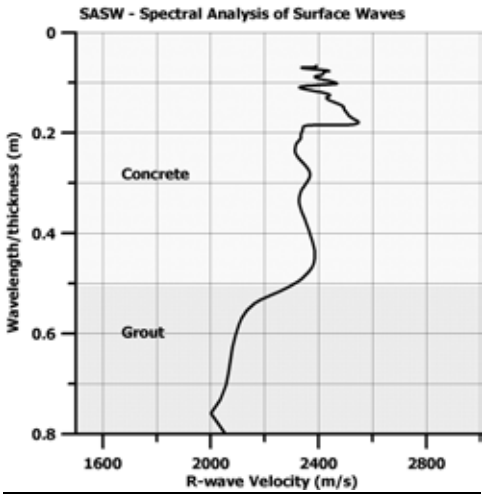

Fig. 4.2.3.2: The result from a SASW measurement on a concrete wall with grout fill behind (lower strength and G-modulus). The graph shows the velocity variation with wavelength. The wavelength can be converted to depth. The graph thus shows the velocity variation with depth. This information can be used to determine the thickness of layers with different stiffness properties, e.g. a strong concrete layer above a weak grout as shown above.

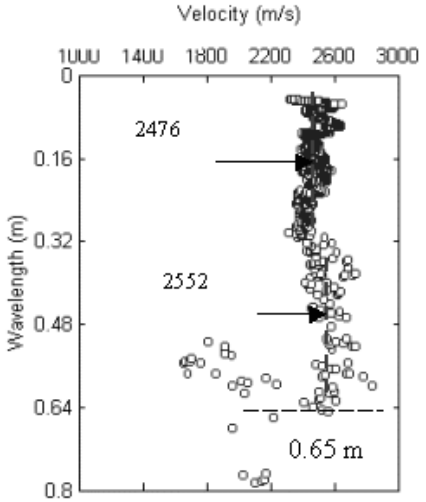

Fig. 4.2.3.3: Result from a SASW measurement on a tunnel lining. The dispersion curve deviates in typical fashion at a wavelength corresponding to the thickness of the concrete. The Rayleigh wave velocities are indicated.

4.2.4 Thickness measurement using radiography

In some situations, it is not possible to measure wall thickness (easily) even if there is access to both sides. A large cylindrical structure, for example, may not be accessible in a way that will enable wall thickness to be measured directly. Since there can also be some difficulty in accurately determining the acoustic wave velocities needed to measure thickness, it may be necessary to use a technique like radiography.

If the structure is quite thick (> 400 mm) then HECR can be used. The procedure is quite simple as shown below in Fig. 4.2.4.1.

1. The SOD has to be measured
2. A detector (image plate) must be placed in contact with the concrete and centred on the beam of radiation
3. A form of reference object (tungsten or lead marker) must be placed on the source side of the concrete structure in the centre of the beam of radiation. The size of the reference object (SCO) has to be measured. The reference is usually two markers at a fixed separation.
4. The enlargement of the reference on the projected image is measured (MOC)

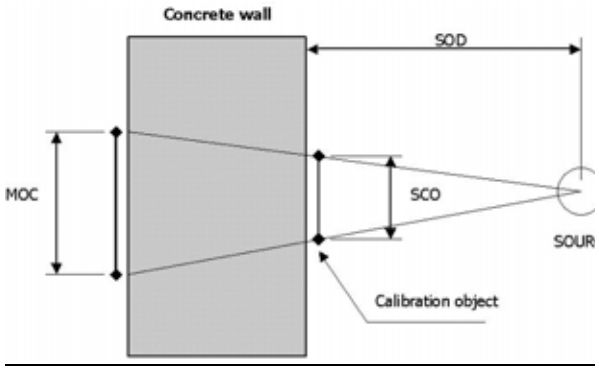

Fig. 4.2.4.1: Principle of thickness measurement using radiography.

Two markers consisting of lead or tungsten (Wolfram) are placed equidistant from the centre of the radiation beam on the source side of the wall. Their image will be projected on to the image plate. Another marker is placed at the centre of the film on the other side of the wall. By simple triangulation, we can calculate the wall thickness:

$$CT = \left(\frac{MOC}{SCO} \right) \cdot SOD - SOD$$

The typical accuracy that can be expected for this kind of measurement is approximately +/- 5% of the actual thickness.

To check that the alignment is correct, the film-side marker should be midway between the images of the source-side markers.

4.2.5 Thickness measurement using radar

In favourable conditions, then Radar can be used to measure concrete thickness. For this to be viable however, the concrete should be relatively slender and not heavily reinforced. If Radar is able to transmit a signal through the concrete, the travel time can be determined and thus a relative measure of the thickness can be obtained. To convert the travel time of the Radar wave to actual thickness the velocity of this electromagnetic signal must be determined. This is possible by calibration or by determining the appropriate physical parameter.

The technique is well suited to measuring *relative* thickness variations of thin structures. It is a usefull alternative to acoustic methods if, for example, the concrete surface is covered in a soft material or thick layer of paint.

Concrete beam

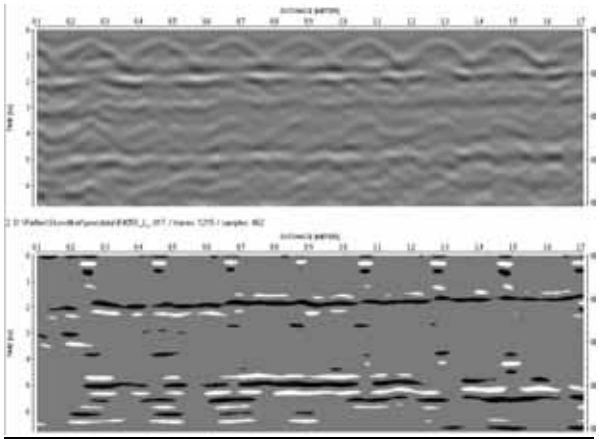

Fig. 4.2.5.1: A GPR profile that shows reinforcement (hyperbolae), a surface-parallel cable duct (upper horizontal reflector) and the back wall reflection. The lower picture shows the processed data.

Thickness against a steel liner

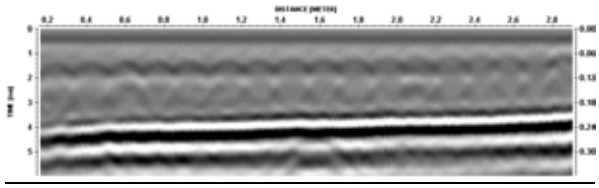

Fig. 4.2.5.2: The back wall reflection has in this case, been enhanced by the fact that it is lined with a steel plate. This plate reflects 100% of the incident energy, which can be compared with about 50% for a concrete – air interface.

The advantages of using radar (if conditions allow) are mainly speed and the fact that no surface couplant is required. It can be compared to other uses of radar, e.g. those mounted on vehicles to enable rapid scans of road surfacing.

4.2.6 Thickness measurement – summary of techniques and recommendations

The best technique should be used for the job in question. If possible, try two or more techniques on site. Choose the best technique and use a second or even third technique to confirm the results. Beware of the effects of low velocity layers and be aware of the risk of gradual velocity variations globally and with depth. Depending on the technique used, e.g. IE, make the necessary corrections for geometrical effects.

U.P.E.

Concrete quality	Max. Aggregates	Thickness (mm, max)
High	< 16 mm	1000-1100
High	< 25 mm	800-1000
High	25-32 mm	600-800
Low-Medium	25-32 mm	300-600

If the concrete is of good quality then the conditions are probably right for using the U.P.E.-method. This is the favoured method for reasons of speed, accuracy, ease of use and resolution in thickness and variations in thickness in the horizontal direction. The maximum thickness of concrete that can be tested depends very much on the size of the aggregates. Measurement (data collection) is considered to be easier and quicker with this method than others.

IE

Concrete quality	Max. Aggregates	Thickness (mm, max)
High	32 mm	>1500
Low-Medium	32 mm	>1500

If the concrete is more than 800-1000mm thick and the maximum size of the aggregates is, 32mm or more then IE is the favoured technique. Also, if the concrete is of low-medium quality, then IE would be chosen. The resolution in depth measurement and detection of spatial variations in thickness is not as good as U.P.E. IE is not affected by aggregate size to the same extent as U.P.E.

SASW

Concrete quality	Max. Aggregates	Thickness (mm, max)
High	Not applicable	1000 -1500 (our experience)*
Low-Medium	Not applicable	As above
Different layers	Not applicable	As above

*In principle no max thickness applies

SASW can give quite accurate depth measurement and has the advantage that it is not always dependant on the operator knowing the wave velocity of the concrete. This is a good way of checking other methods. The thickness of different layers of material, e.g. weak concrete on hard concrete can be calculated based on the form of SASW-dispersion curves. The maximum depths referred to above are only those measured in this work. In principle there is no "maximum" depth. In civil engineering this will be determined by the accessible surface on which the tests are made. The method is quite slow and would normally be used only for spot checks and calibration of other methods.

HECR

Concrete quality	Max. Aggregates	Thickness (mm, max)
Not applicable	Not applicable	<1500

HECR can be a suitable method if access to both sides is possible and other methods are difficult to calibrate. The maximum practical thickness that can be measured with the 7.5 MeV Betatron is 1500 mm. Accuracy is determined by how accurately the equipment and markers can be placed on respective sides and their alignment with the source of radiation.

Radar

Concrete quality	Max. Agg	Thickness/resolution in x and z
High	NA	0.3 m/ 10%
Low	NA	0.2 m/ 10%
Dry/in-door	NA	0.5 m/ 10%

In special cases such as relatively thin and unreinforced concrete, then radar can provide a rapid alternative to acoustic techniques.

4.3 Detection of voids in concrete

The capabilities of NDE methods are often described in terms of their ability to detect and characterize voids of a certain size in concrete. It is very rare however for voids of well-defined shape and size to be found in concrete. Instead, voids usually take the form of volumes of diffuse shape and size, with or without aggregates or binder, for example aggregates and sand from which the cement has been washed away. The sensitivity of the techniques in locating voids must however first be established on mock-ups in which we are familiar with the smallest detail, bearing in mind that performance can often be expected to be poorer in the real world.

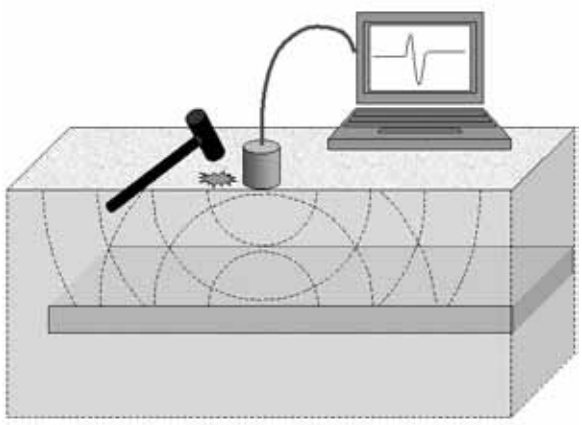

Fig. 4.3.1: Ideal case with echoes from a well-defined void with reflecting surface perpendicular to the direction of wave propagation

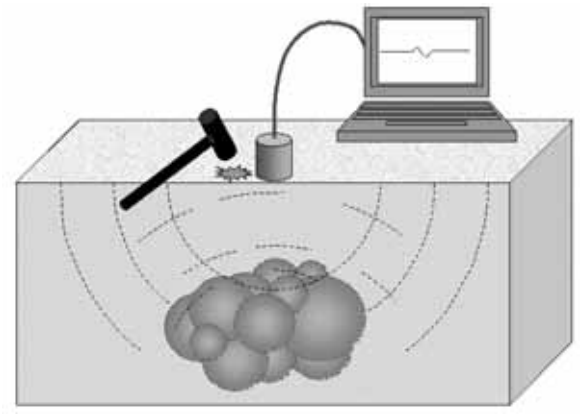

Fig. 4.3.2: Realistic case, for example due to honeycombing in concrete. Here the reflections are weaker and less easily detected

The detectability of voids depends on their size, shape and depth, as well as the aggregate size and quality of the concrete. The methods that we consider here are (in order of sensitivity):

Technique	Confirmed sensitivity – examples
Radiography	Detect 20 mm void in 1200 mm thick concrete
U.P.E. *	Detect 200 mm void at 500 mm depth
I.E. *	Detect 200 mm void at 220 mm depth
S.A.S.W. *	Detect 200 mm void at 220 mm depth
Radar *	Detect 200 mm void at 220 mm depth
* Single-sided access	

Table 4.3.1: Confirmed, "void sensitivity" for selected NDE techniques.

Radiography is by far the most sensitive (and reliable) technique for detecting voids in concrete, as well as for measuring their shape and size. It does however require 2-sided access. The other techniques can detect voids but normally cannot distinguish these from other types of discontinuity, e.g. from a surface-parallel crack. In this work, we have found U.P.E. to be extremely good at rapidly detecting and to a certain degree sizing voids. The U.P.E. technique considered is revolutionary and cannot be equalled by any other U.P.E. instrument that we know of. It of course requires only single-sided access.

Most of the work reported here refers to the radiographic and U.P.E. techniques. Many tests have been made with both I.E. and S.A.S.W on the mock-up (Block 1 – see below and Appendix 4), but it has been found that only a few of the larger voids can be reliably detected with these techniques. All techniques are however dealt with to some extent.

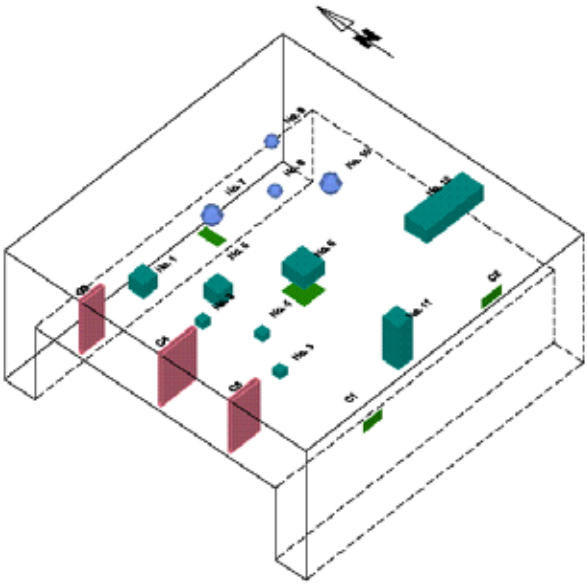

Fig. 4.3.3: View of Block 1 including the defects in the form of voids and thin plates to represent cracks.

A detailed description and enlarged image including photographs of the mock-up is given in Appendix 4.

4.3.1 Detection of voids using the U.P.E. technique

The structure considered is, Block 1 as shown in Fig. 4.3.3 and Appendix 4. The tests have been carried-out in two ways:

1. Tests in a grid over the surface without consideration of void position

2. Detailed tests over the known positions of the voids

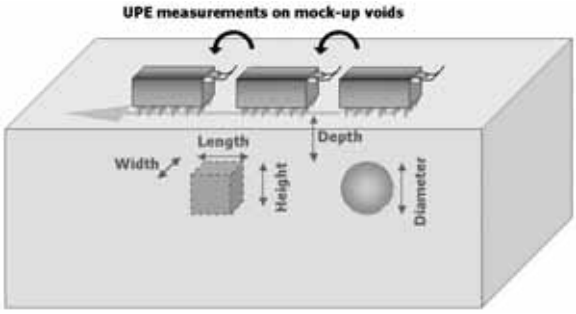

Fig. 4.3.2.1: Grid scanning over upper surface. The surface area is divided into a grid (fixed x and Y-spacings) and a survey made without prior knowledge of the void positions.

A series of tests was made over the upper surface of the block in a systematic manner at x- and y-separations of 200 mm. The objective was to check if the voids could be detected without prior knowledge of their position, i.e. if scanning in this manner was sufficient to detect the voids and if so which voids.

The UPE-technique was quite outstanding in this test, as all voids with the exception of two small voids close to the surface have been clearly detected. There were also indications of these two small voids. There is also very little tendency for false indication (non-relevant indications) in these results. See Fig. 4.3.2.2.

A similar series of tests was made over this block using direct echo (from the voids) and back-wall echo as criteria. The results are shown in Appendix 4. The grid size in this test was different to that shown here.

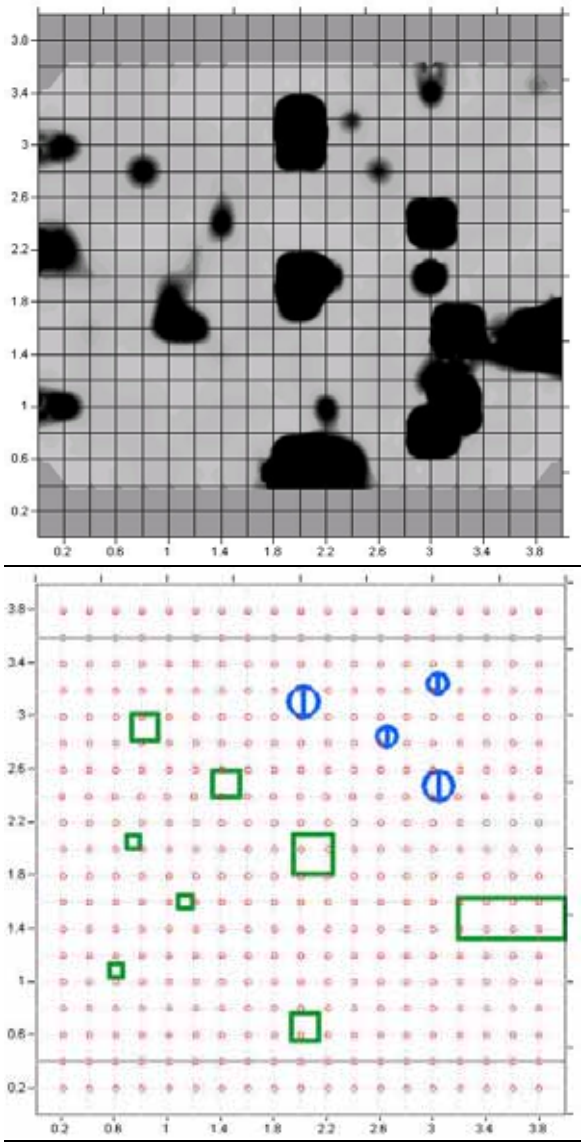

Fig. 4.3.2.2: Grid-scan of block no. 1 using U.P.E. The upper diagram shows the result of time-delay calculation for the wave back-wall reflection, with dark areas representing suspect positions. The lower diagram shows the actual position of the voids (this diagram does not include the three voids on the left edge of the block or the large steel plate with attached air voids in the lower right region (detected by upe)). See Appendix 4 for more details of all the defects in this Block.

The results show that the transducer array produces a relative narrow wave front. This is of course good in most situations since it focuses the limited energy to a certain area. However, small voids close to the surface will not be detected unless the test point is very close to the void.

U.P.E Survey strategy for voids

A preliminary coarse survey is made to rapidly scan a larger surface and if a suspect area is found then a detailed survey at this point follows. The coarse survey will tend to reveal a "gap" in the bottom echo from the slab underside at 800 mm if there is some internal void or similar. The more detailed survey can then be made, for example, using higher frequencies, a closer time window and closer spacing between measurements.

In this example shown in Fig. 4.3.2.3 we see Void no.5 (200 mm cube at 490 mm). There is a clear "gap" in the bottom echo profile, i.e. no reflection from the underside of the slab, at the position above the void. The void interferes with the waves and disturbs the bottom echo even when the transducer array is 100 mm from its edge. The first survey has been made at c/c 100 mm and frequency 33 k Hz. The second survey (inset) was made with c/c 10 mm and a frequency of 70 k Hz. In this case, it is possible to see the individual reinforcing bars and the void at 490 mm in greater detail.

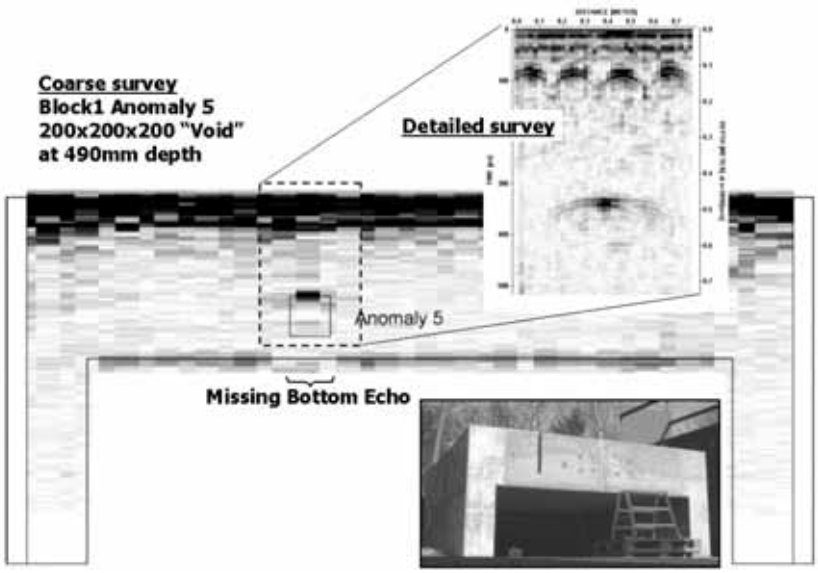

Fig. 4.3.2.3: A typical survey would be made in two steps. The initial coarse grid survey that would indicate suspect areas. These areas would then be surveyed in a denser and more detailed grid.

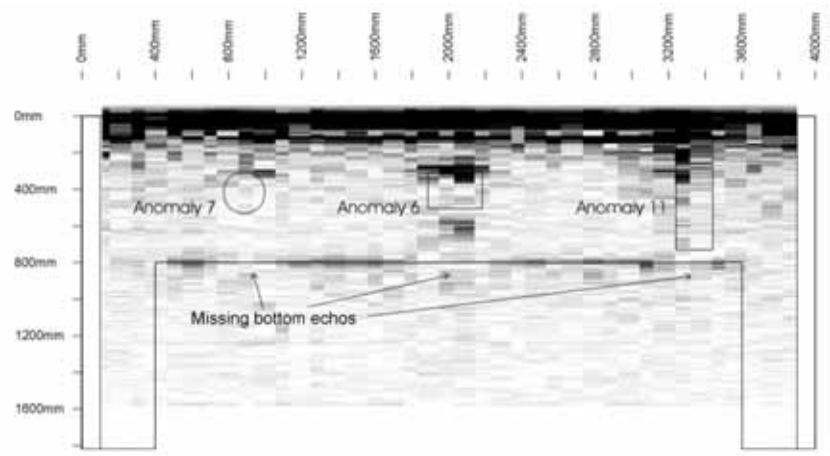

Fig. 4.3.2.4: U.P.E.-survey at c/c 100 mm across Block 1 revealing three voids (no.'s 6, 7 and 11) by direct reflection and interrupted bottom echo.

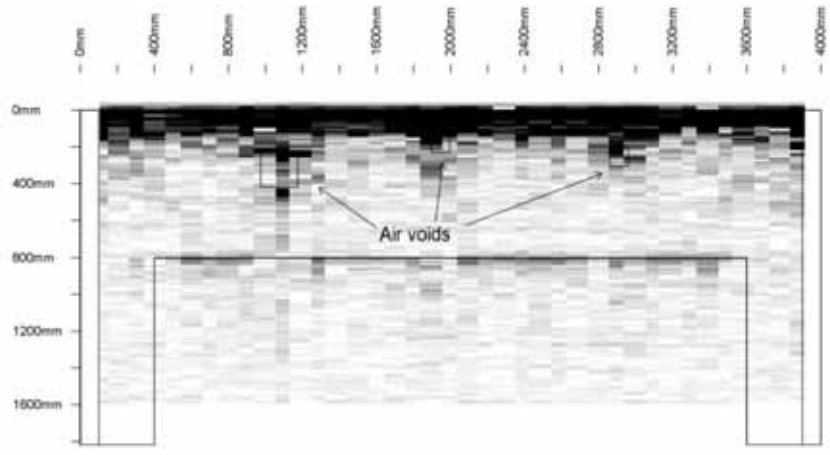

Fig. 4.3.2.5: U.P.E.-survey at c/c 100 mm across Block 1 revealing voids no.s 1, 2 and 3

Detailed investigation of voids using U.P.E – Reflections

The UPE tests over the voids are evaluated below on the basis of direct reflections from the voids. The tests were made in the form of B-scans at 10 mm A-scan intervals.

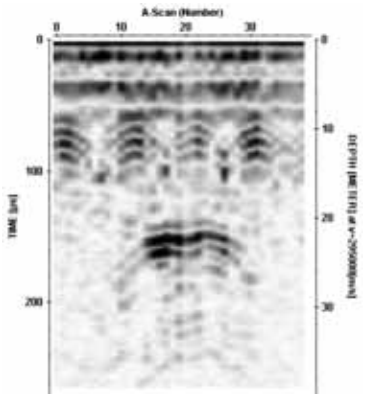

"Void" No. 1 (200x200x200 at 220 mm). Very clear. See also Appendix 4.

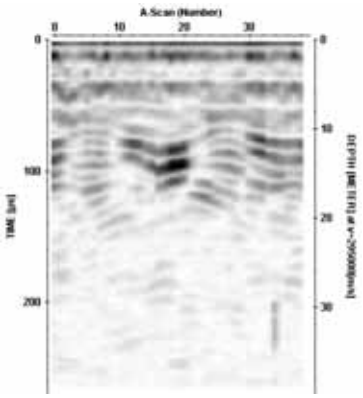

"Void" No. 2 (100x100x100 at 130 mm). Not very clear as void is directly under reinforcing.

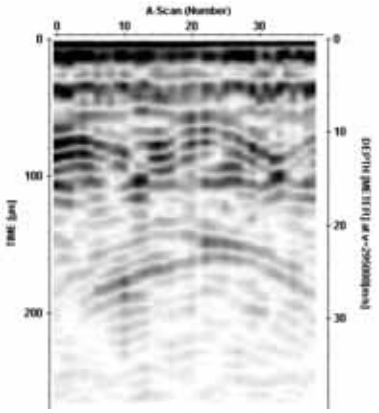

"Void" No. 3 (100x100x100 at 205 mm). Void quite clear.

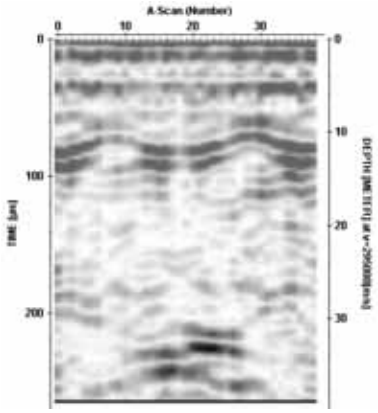

"Void" No. 4 (100x100x100 at 305 mm). Void quite clear but not definate.

Fig. 4.3.2.6: B-scans over known voids in Block 1

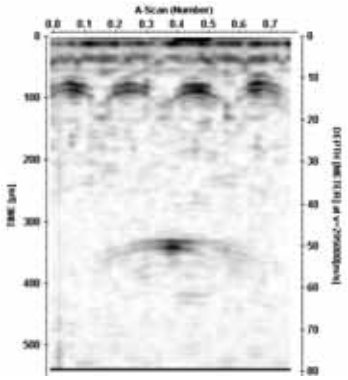

"Void" No. 5 (200x200x200 at 490 mm). Very clear.

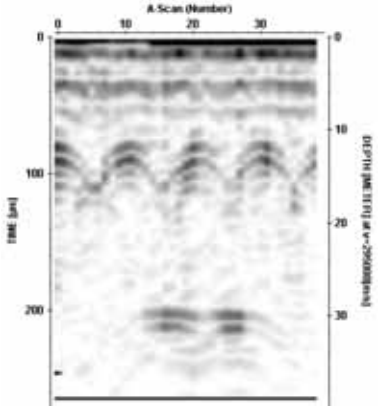

"Void" No. 6 (300x300x200 at 305 mm). Very clear.

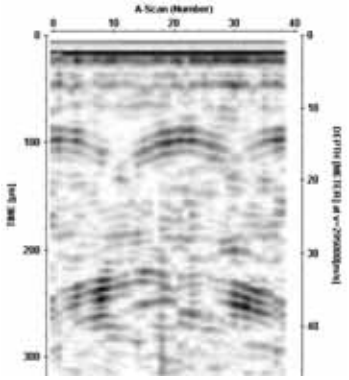

"Void" No. 7 (ϕ 225 mm at 305 mm). Clear with strongest reflections with antenna offset from centre.

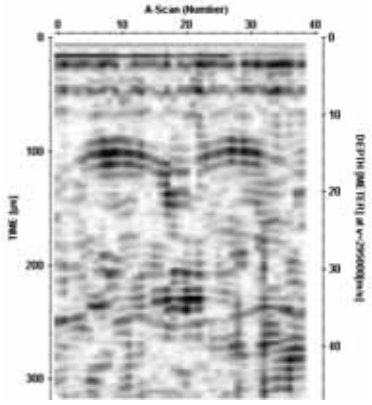

"Void" No. 8 (ϕ 150 mm at 305 mm). Quite clear.

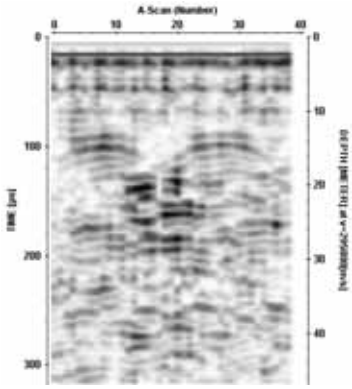

"Void" No. 9 (ϕ 150 mm at 175 mm). Quite clear.

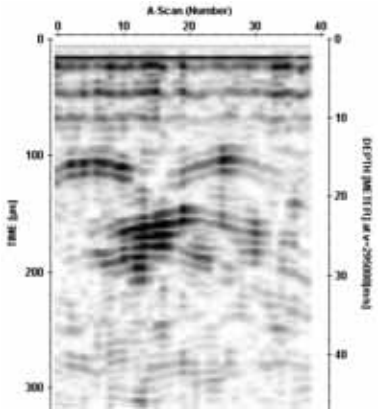

"Void" No. 10 (ϕ 225 mm at 190 mm). Clear.

U.P.E. Void detection Block 1 – Summary of results

Void no.	Echo from void	Bottom echo block	Grading	Estimate size of void
1	Yes	Yes	1	Yes
2	Yes	Yes	3	No
3	Yes	Yes	3	No
4	Yes	Yes	2	Possible
5	Yes	Yes	1	Yes
6	Yes	Yes	1	Yes
7	Yes	Yes	2	Possible
8	Yes	Yes	2	No
9	Yes	Yes	2	No
10	Yes	Yes	2	Possible

Table 4.3.2.1: U.P.E. Void detection Block 1 – Summary of results

Grading criteria

1. Very clear echo from void. Bottom echo blocked. Effect at side.
2. Very clear echo from void. Bottom echo blocked. No effect at side.
3. Fairly clear echo from void. Bottom echo blocked.
4. No reliable indication.

In 8 of 10 cases the voids can be clearly "seen" by both reflected waves from the void and a gap in the back-wall echo. The results are not so clear for the 100 mm cubic voids at 130 and 205 mm from the surface. In the case of the void at 130 mm, the reflected waves are probably disturbed by reflections from the two layers of reinforcing immediately above. The 100 mm void at 205 mm is visible in this case but it is unlikely that it would be detected in a poorer concrete. In all cases the voids interrupt the back-wall echo.

It is interesting to note that the strongest reflections from a spherical void often occur when the antenna is off-centre by about half the diameter of the sphere. Almost no reflection can be seen when the antenna is directly above the centre of the sphere. See Fig. 4.3.2.7.

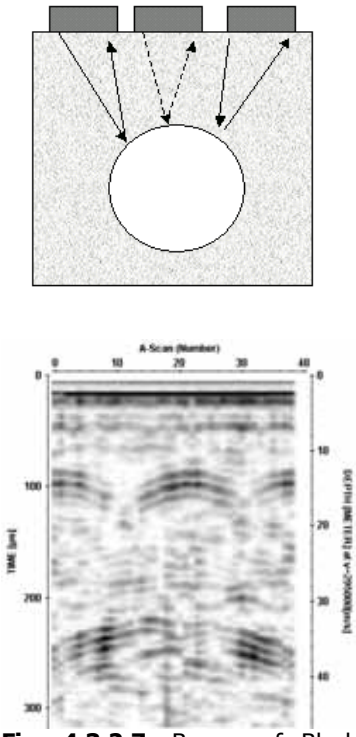

Fig. 4.3.2.7: B-scan of Block 1"void" No. 7 (ϕ 225 mm at 305 mm).

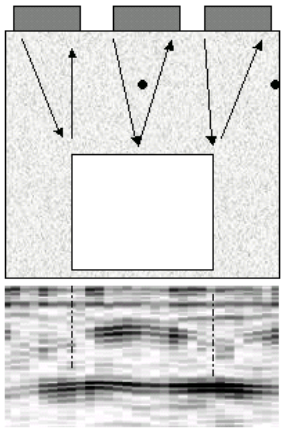

Fig. 4.3.2.8: B-scan of Block 1 "void" no.1 (200 mm cube at 220 mm). The strong reflection is uniform (depth) over a B-scan length of 190 mm. The void first becomes visible with an antenna offset of about 60 mm in this case.

The rebar weakens the signal a little around the centre.

4.3.2 Investigation of voids using I.E.

We have found that IE is suitable for detecting relatively large voids in structures with simple geometries. As demonstrated in the results from Block 1 below we found that the capability of IE in detecting "smaller" voids is less compared with UPE.

A "Yes" or "No" in the figures below indicates whether the void is visible.
This is based on direct echoes from the voids and the back wall echoe.

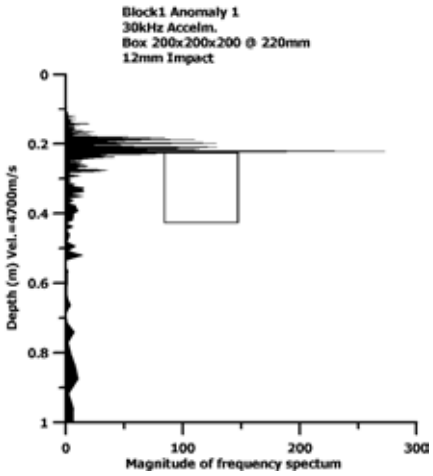

(200x200x200 at 220 mm) **YES**

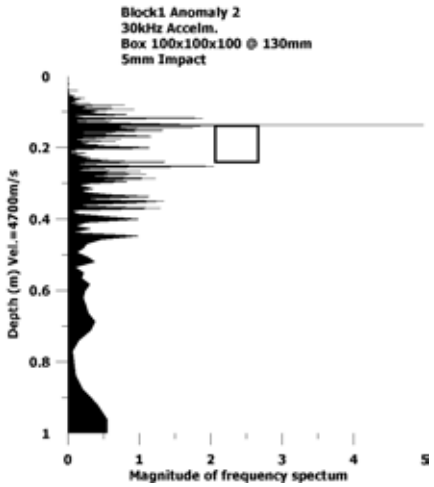

(100x100x100 at 130 mm) **YES**

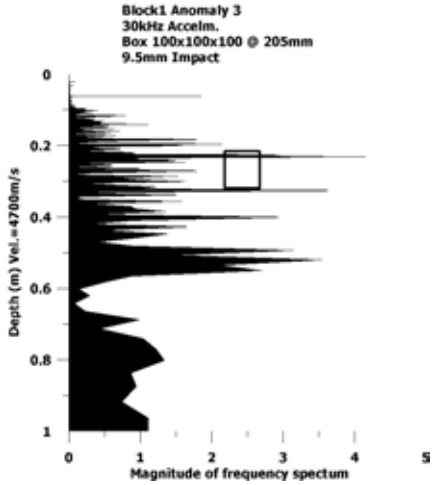

(100x100x100 at 205 mm) **NO**

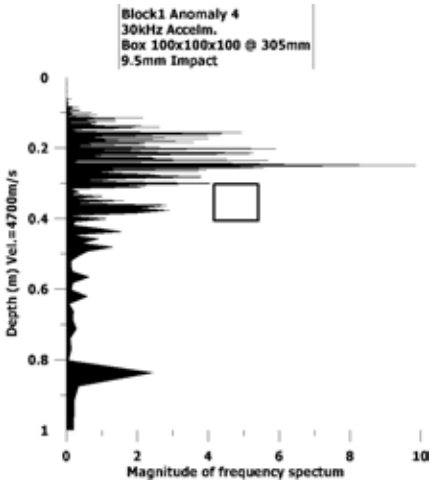

(100x100x100 at 305 mm) **NO**

Fig. 4.3.5.1: Impact echo frequency spectrum for tests above voids in Block 1

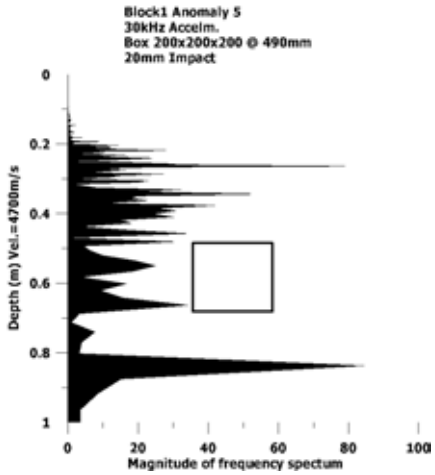

(200x200x200 at 490 mm) **NO**

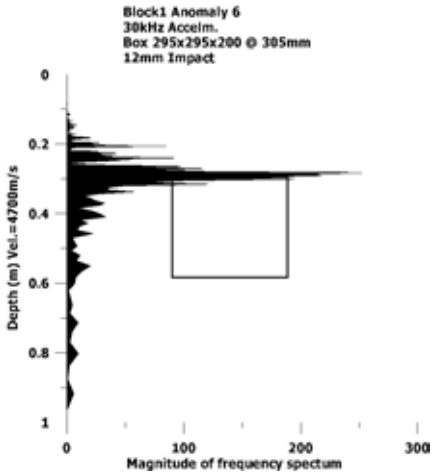

(300x300x200 at 305 mm) **YES**

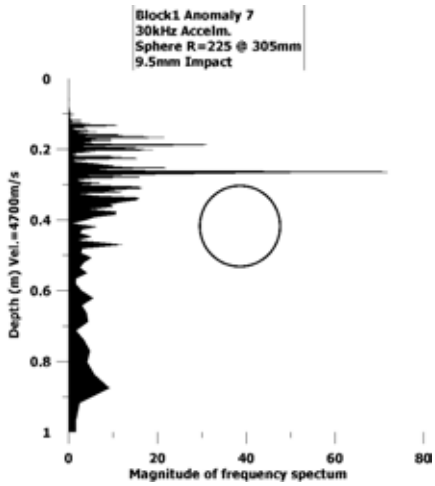

(ϕ 225 mm at 305 mm) **NO**

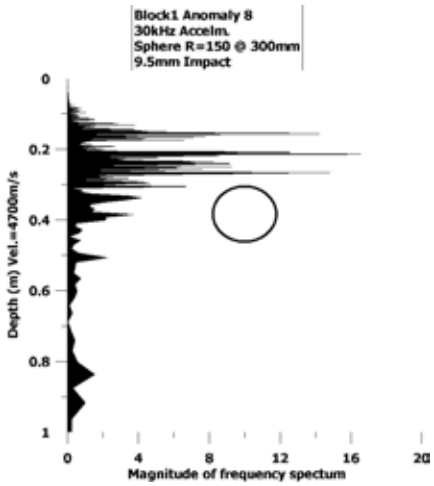

(ϕ 150 mm at 305 mm) **NO**

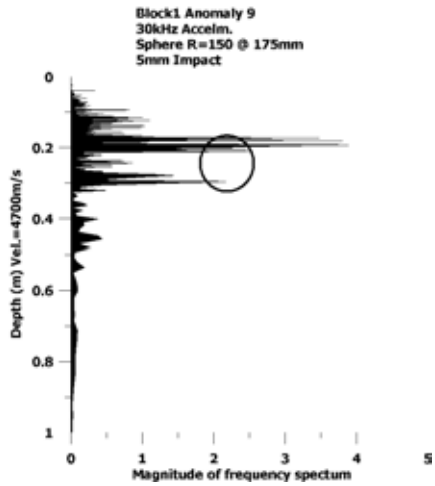

(ϕ 150 mm at 175 mm) **YES**

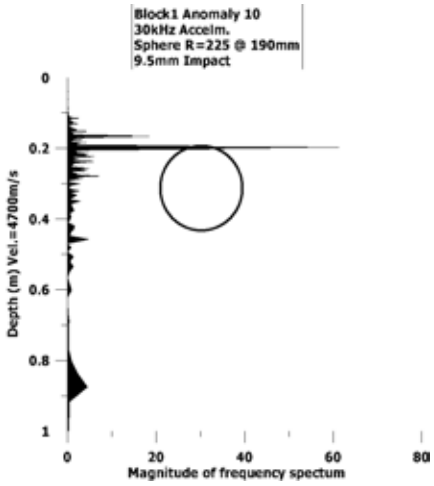

(ϕ 225 mm at 190 mm) **YES**

IE Tests made in May 2000 on Block 1.

The following tests were made with Impact Echo on Block 1, a couple of months after the Block was cast. The tests were made in a grid over the surface with separation 300 mm. The grid was adjusted to coincide with the nearest void where this applied.

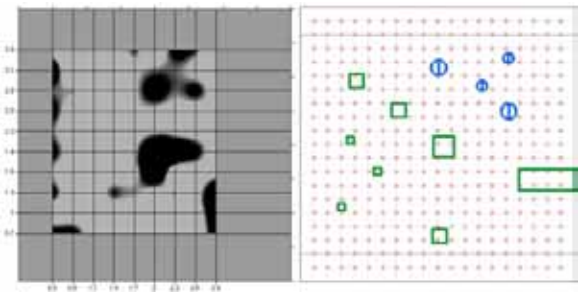

Fig. 4.3.5.2: Coarse IE survey on Block 1. Notice that only part of the block has been surveyed.vThree small sperical voids (top right) are not included.

The coarse survey over the block gave indications of the larger of the voids.

Further tests were made with 7, 11, 20 and 24 mm spherical impactors as well as a small hook and light hammer above the voids. In the case of Void no.5 (200 mm cubic void at 490 mm) at total of 30 different tests were made with different impactors and positions above the void. It produced no distinguishable echoes, however, and no effect was seen on the bottom echo.

Void number	Echo from void	Be-delay	Grading
1	Yes	Possible	2
2	Yes	No	3
3	Yes (weak)	No	4
4	No	No	5
5	No	No	5
6	Yes	Yes	1
7	Yes (weak)	No	3
8	Yes (weak)	Possible	3
9	Yes	No	4
10	Yes	No	3

Table 4.3.5.1: Impact echo - void detection, Block 1

Grading criteria

1. Very clear. Dominant echo from void with all impactors and delayed bottom echo.
2. Clear. Clear echo from void with all impactors. No bottom-echo delay.
3. Fair. Echo from void with correct choice of impactor. No bottom echo delay.
4. Uncertain. Not dominate echo from void. No bottom echo delay.
5. No indication.

The 200 mm void at 220 mm and the 300 mm void at 300 mm were clearly visible. Note however that these could be missed by the incorrect choice of impactor. It must be said that the remaining voids were either fairly visible or not visible at all.

4.3.3 Investigation of voids using S.A.S.W.

The results shown here are from Block 1, as is the case with U.P.E. and IE-tests. These results are examples of the *best* data obtained after considerable effort. It should be remembered that the variation in velocities with wavelength in apparently sound concrete could be considerable, particularly in a congested structure like this. In other words, the Block may not be suitable for void detection using SASW. On the other hand, SASW may require special conditions for succesfull void detection, which cannot always be expected in the field.

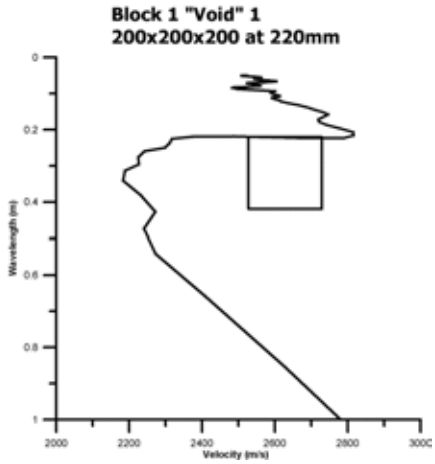

200 mm transducer separation. In this case we can see the void. See also Fig. 4.3.6.2.

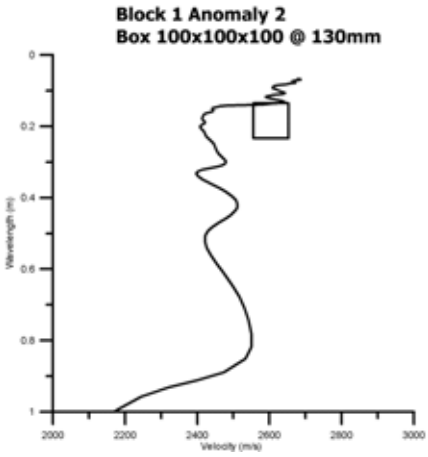

200 mm transducer separation. There is some indication although the effect is probably insufficient to make a reliable judgement. See also Fig. 4.3.6.3.

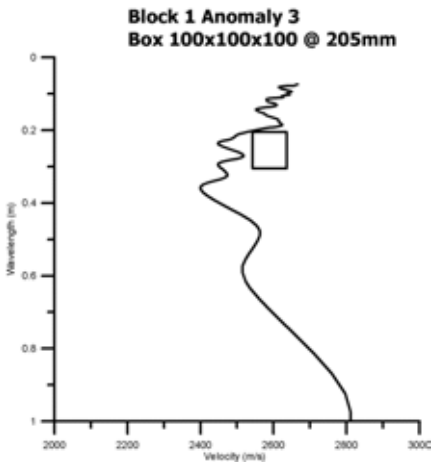

200 mm transducer separation. Possible weak indication.

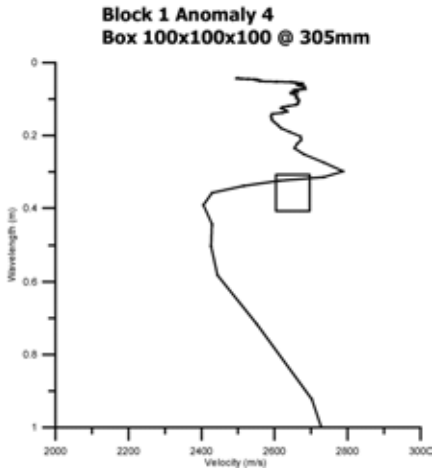

200 mm transducer separation. Apparent indication.

Fig. 4.3.6.1: SASW dispersion curves for tests made above voids in Block 1

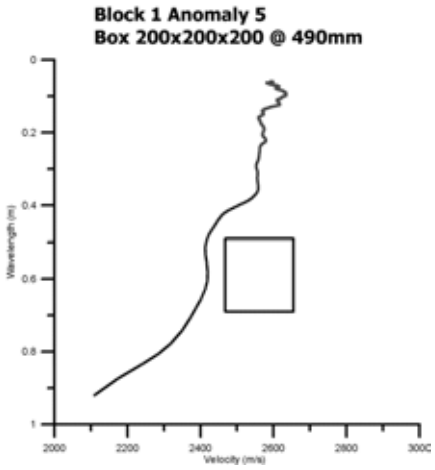

300 mm transducer separation. Possible weak indication, but compare with solid concrete.

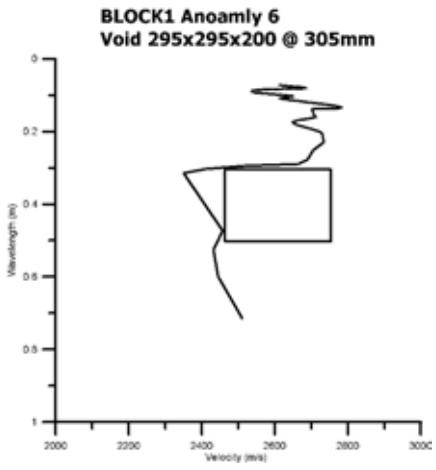

400 mm transducer separation. Clear indication.

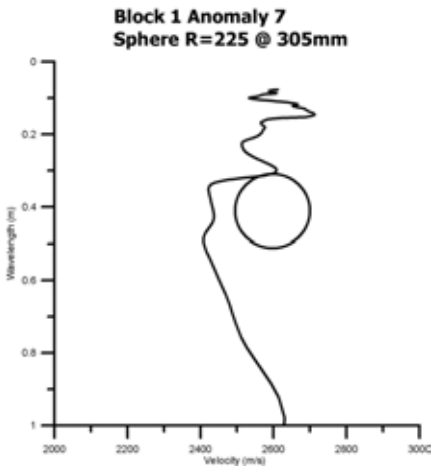

200 mm transducer separation. Possible weak indication.

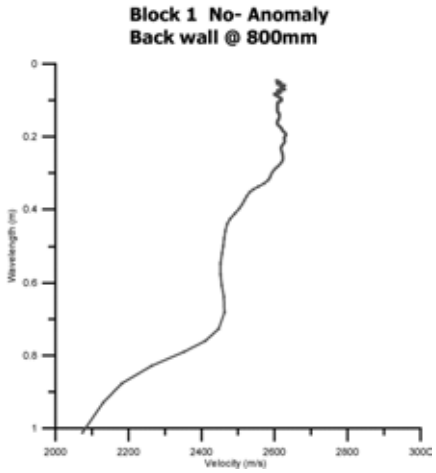

400 mm transducer separation. Solid concrete. Note that the dispersion curve drops away at a wavelength about half the block thickness. This is to be expected. The curve drops further at wavelengths equivalent to the full thickness.

Summary of results – Void detection with SASW

It should be stressed that Block 1 may not be the ideal structure to test with this method, due to the fairly congested internal geometry (voids, cracks, reinforcing etc).

As can be seen in the following two diagrams, the response from a void can have many signatures depending on the measurement configuration. It is possible to entirely miss large defects if the wrong configuration is used and thus the technique requires experience and is not regarded as the most suitable technique for this purpose. It can have applications in special circumstances.

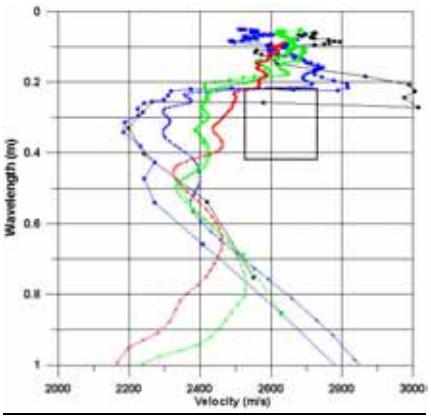

Fig. 4.3.6.2: Results using different accelerometer separations to investigate void 1 (200 mm cube at 220 mm)

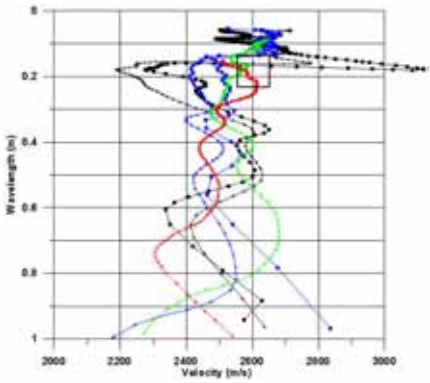

Fig. 4.3.6.3: Results using different accelerometer separations to investigate void 2 (100 mm cube at 130 mm)

Due to the multitude of responses seen in the data from the SASW measurements it is difficult to categorize these and come up with a general summary about performance for void detection. It remains one of those techniques for which it is difficult to predict response. However, it should be tried from case to case as it does give some information about the depth of voids, and may be useful in distinguishing voids from cracks that are parallel with the surface. In other words the technique can give an indication of the size of the void (in the vertical direction). It is quite a time consuming process however to produce dispersion curves, as shown here.

4.3.4 Investigation of voids using Radiography

If the voids of interest are too small to be detected by other methods, for example if they are less than 100 mm in size, then we must resort to radiography. Also, if the voids are in awkward geometries or near joints, for example above a pipe entry in a wall then radiography is required. It is in our opinion the only reliable method of detecting voids inside cable ducts cast in concrete.

Void detectability as a function of concrete thickness and void size

The size of a void is almost always of interest regardless of whether it is located inside a cable duct or the concrete. Most of this work was however done with cable ducts in mind. There are (radiographic) methods that can be used to determine the size of a void in all three directions. Whether the voids are inside or outside the cable ducts has no bearing on these methods.

Tests were made on mock-ups with various void sizes inside an embedded cable duct and concrete. The thickness of the concrete was varied from 300 mm to 1200 mm using a number of other blocks. The fact that the blocks are assembled to make up the required thickness has no bearing on the technique. The smallest (air-filled) void we have investigated is 15 mm square. This was visible in our 1000 mm thick mock-up. Very small voids and even air pores a few mm in size can be clearly seen in some of the images.

Fig. 4.3.7.1: The Betatron accelerator in the laboratory while making tests on 1500 mm thick concrete. A 8 mm thick steel plate has been sandwiched between 1200 mm and 300 mm concrete. Holes in this steel plate can be seen in the radiographic images. See also Appendix 4, Fig. A 4.18.

Note: The radiographic images presented in the form of "pictures" in this report will not be of the same quality as is experienced when analysing results on a proper workstation. The quality will also be better in the electronic version compared with a printed version.

Various types of voids have been investigated in the field and in mock-ups.

Field

Void type	Duct diam. (mm)	Concrete thickness (mm)	Voids detected
Voids in post-tensioned cable ducts	30/35 mm (corrugated ducts with 12 x ϕ 6 mm strands)	330 mm	Yes
Voids in post-tensioned cable ducts	60 mm	1000 mm	No

Table 4.3.7.1: HECR results from field investigations

Mock-up

Void type	Void size (mm)	Concrete thickness (mm)	Voids detected
Voids in concrete	15-70	300-1200	Yes all
Voids in ducts encast in concrete (air-filled voids)	15-70	300-1200	Yes all
Hole in 8 mm steel plate encast in concrete	ϕ 10, 20 and 50 (x 8mm thickness)	1000-1500	Yes
Voids in ducts encast in concrete (water-filled)	Approx 15mm thick x 30, 50 and 70mm	300-800	Some

Table 4.3.7.2: HECR results from mock-up trials

Results, of tests on mock-ups.

Tests were made on mock-ups with various void sizes. These voids were either inside an embedded cable duct or in the concrete. Whether the void is inside the cable duct or not has no bearing on the performance of this technique. At the same time it can be difficult to tell if a void is inside or outside the duct.

The thickness of the concrete was varied from 300 mm to 1200 mm using a number of modular blocks. The fact that the blocks are assembled has no bearing on the results. Thus Radiography is one of the few techniques that can be used in the laboratory with good resemblance to actual site performance. It is not affected by boundary conditions or the fact that there are many open joints between blocks that make up a larger block.

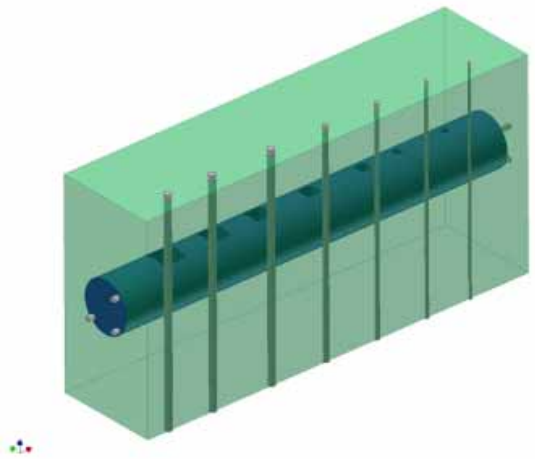

Fig. 4.3.7.3: Mock-up with cast in cable duct that has a number of voids inside.

Description of the mock-up with cast in cable duct

The mock-up beam is 300 mm thick and the cable duct is 150 mm in diameter. The duct contains 3 VSL* cables and has been filled with cement grout. Voids have been made in the grout as shown. The voids are 15, 20, 30, 40, 50, 60 and 70 mm rectangles. The beam is also reinforced as shown with ϕ 8, 10, 12, 16 and 20 mm bars.

Fig. 4.3.7.4: Sketch of the block with encast cable duct and voids (seen from above). The voids are placed centrally in the injection grout and are therefore not in contact with the thin walls of the duct.

Images of the block were produced with a 7.5 MeV Betatron. See Fig. 4.3.7.5 (300 mm) and 4.3.7.6 (600 mm) below. The total thickness was increased in stages up to 1200 mm using extra blocks 100 mm and 300 mm thick. Results are presented in the two following figures.

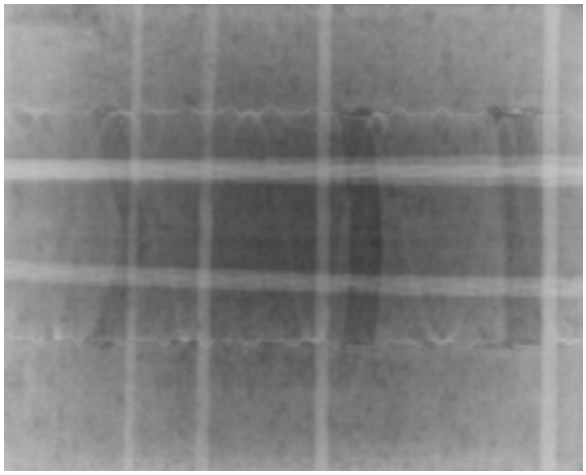

Fig. 4.3.7.5: Image of 300 mm thick concrete. The 15, 20 and 30 mm voids (from left to right) can be seen as dark vertical lines inside the cable duct. Small voids (pores) can also be seen above and below the outside of and adjacent to the duct. The light vertical lines are re-bars and the horizontal light lines are cables inside the duct. The thin wall of the duct can also be seen. The mottled texture of the concrete is normal.

*

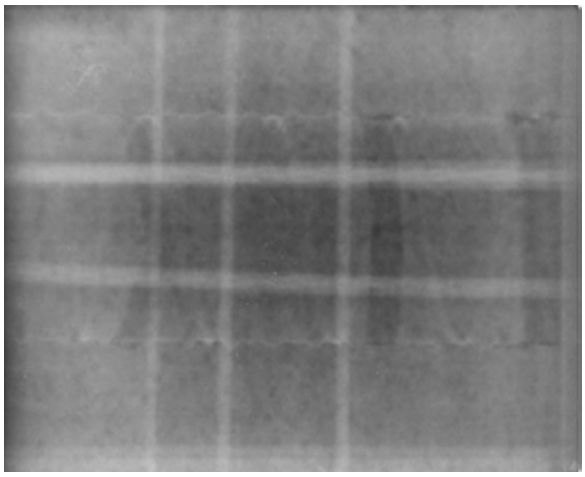

Fig. 4.3.7.6: The same image as above but this time through 600 mm thick concrete. The voids are still clear but the quality of the image is less compared with 300 mm thick concrete. Note that the contrast in image density between voids and solid concrete is less compared with 300 mm thickness.

The size of the voids relative to the thickness has been investigated.

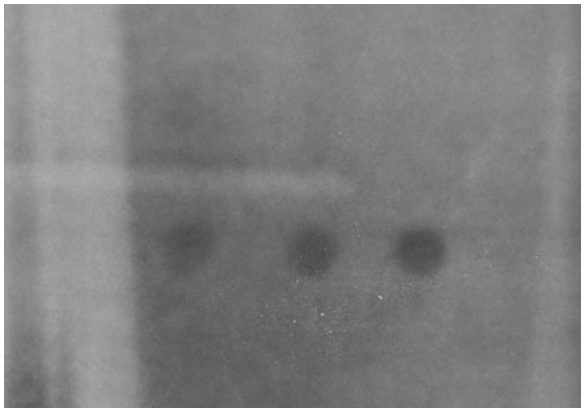

Fig. 4.3.7.7: This image is from 1200 mm thick concrete with 3 voids each ϕ 20 mm and depth (in the direction of radiation) 15, 20 and 40 mm (left to right). The voids are on the image plate side of the block.

The detectability of a void in a concrete construction varies of course depending on some of the limiting conditions mentioned above. However, under ideal conditions it is possible to detect:

- a void size in a plane perpendicular to the beam of radiation down to minimum of 1 to 1.5 % of the total penetrated concrete thickness (in other words the minimum width of the void)
- a void size in the direction (parallel to) the beam of radiation down to 1.5 to 2 % of the total penetrated concrete thickness (in other words the minimum depth or thickness of the void)

To determine the size of a void in the plane perpendicular to the direction of the radiation (x and y axes) requires that the depth of the void (from the surface) is known. This depth can be determined by taking two exposures of the void with two known angles of incidence. This is a well-known technique and is called stereographic exposure. When the depth of the void is known then the magnification of the void can be calculated and, of course, its size.

To determine the size of a void in the direction of the beam of radiation (z axis) is a little more complex. This can be done by measuring image density, and by calculating a void density factor (vdf). In the example below this has been done for 4 different thicknesses of concrete.

Determination of the size of a cavity

In order to establish if there is a relationship between the thickness of the concrete and the size (depth or thickness of the void) of the void, a void density factor was calculated for all the void sizes and for 4 different thicknesses of concrete. The size, or more correctly the depth, of the void is calculated in the direction of the beam (z-axis). This factor is defined as:

$$vdf = \frac{D_V - D_C}{D_C} \cdot 1000$$

Where D_V is the grey level value of the image corresponding to the middle of the void and D_C is the corresponding grey level value adjacent to the void. The latter, i.e. 'void adjacent density' is based on the average of the grey level values measured on each side of the void at the same horizontal position.
This void density factor plotted as a function of the size of the void for 4 different thicknesses of concrete can be seen below, Fig. 4.3.7.8.
A clear correlation between the depth of a void and the thickness of the surrounding concrete can

be seen even although it decreases with increasing concrete thickness.

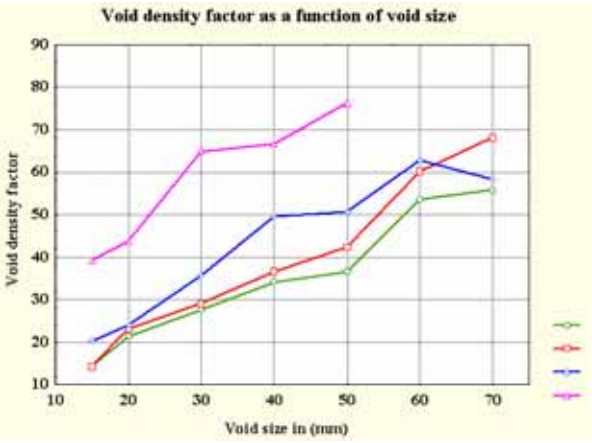

Fig. 4.3.7.8: Void density factor plotted as a function of the size of the void for 4 different thicknesses of concrete.

This equation is of course only valid for a certain source and set-up parameters and should only be used by experienced inspectors with care.

Voids in cable ducts – another example

The example shown above is perhaps less realistic, as cable ducts are usually quite congested with cables or strands. In the example below an attempt has been made to imitate a congested cable duct.

Fig. 4.3.7.9: Cable duct being prepared with air- and water-filled voids. The cable duct has a diameter of 70mm and contains 12 x 12.5 mm vsl cables, i.e. a heavily reinforced and congested cable duct. The "voids" are placed around and outside the cables. The duct was then cast in a 300 mm thick concrete beam

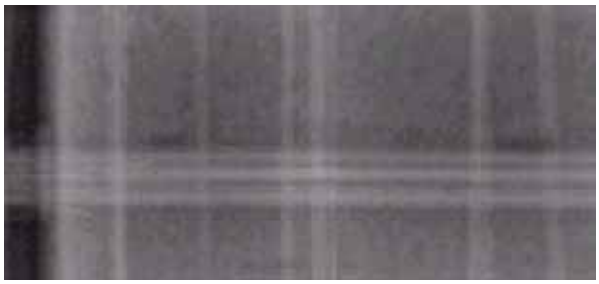

Fig. 4.3.7.10: Two radiographic images from the cable duct with water filled voids. These cannot be seen with the eye behind the cable strands. In this case they can be seen quite well above the cables.

The duct contains quite a massive amount of steel with little empty space available. The voids in this experiment have a thickness of only 12 mm. The voids can be seen with the eye above and below the cables, but not behind the cables. The air-filled voids are easier to see than the water-filled voids. A line profile will indicate the voids behind the cables but this is at the limit of what can be detected.

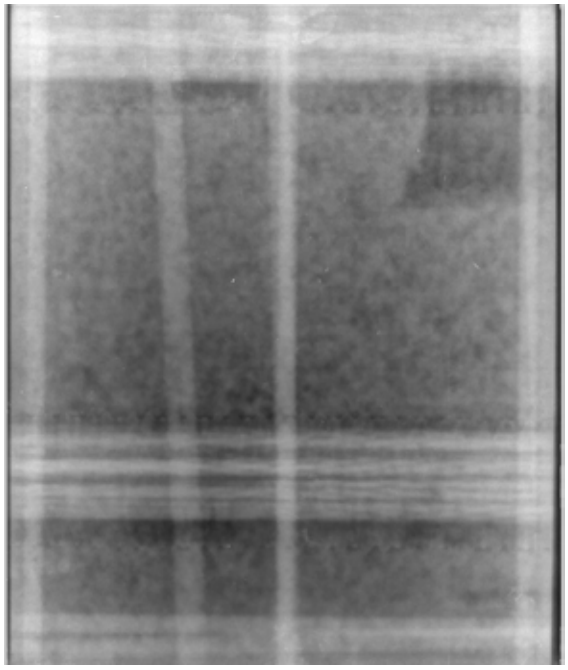

Fig. 4.3.7.11: Cable duct with two voids, which can be seen above and below the cables. Note that there appears to be 4 cable strands inside the duct whereas there are in fact 12.

Example from site - KolleKolle Bridge

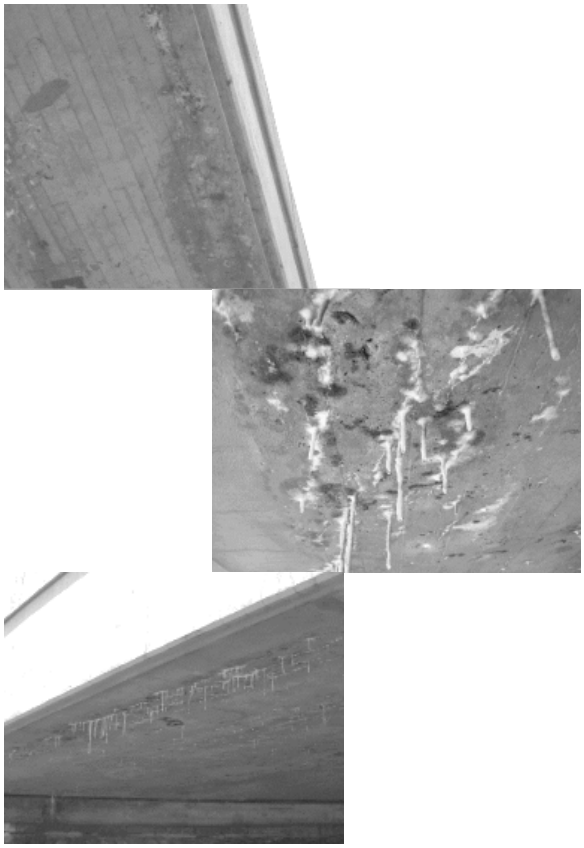

Fig. 4.3.7.12: KolleKolle bridge in Copenhagen. There was extensive cracking and leakage of chloride-contaminated water through the post-tensioned slab. The concrete in the upper side of the slab had some severe freezing damage and reinforcement corrosion.

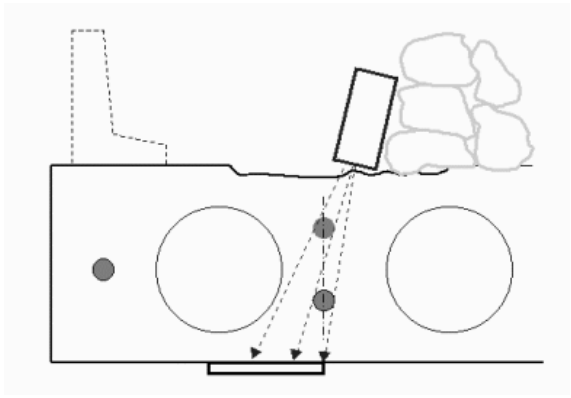

Fig. 4.3.7.13: Set-up for radiography. The Betatron was positioned on top on the bridge while the image plate was attached underneath.

The 1000 mm thick slab has post-tensioned cables as shown as well as large air-filled tubes. The slab was checked using the Betatron and the computed radiography system. The Betatron was positioned as shown in Fig- 4.3.7.13 on top of the slab and an image of both cables projected on to the image plate, care being taken so that they did not superimpose. The bridge was under heavy traffic yet it was possible to shield the Betatron using sand bags so that traffic was not interrupted. The radiographic image below in Fig. 4.3.7.14 shows a cable duct and reinforcing. The upper cable duct has also been projected on to the image and is significantly enlarged. No voids were suspected in the cable duct fill.

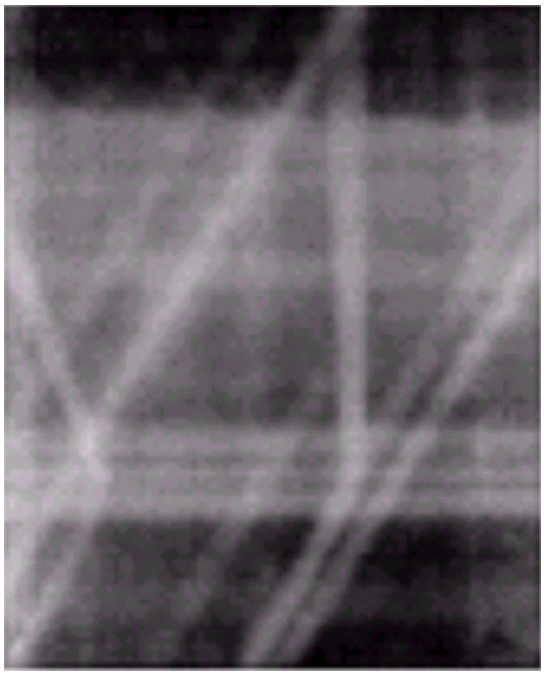

Fig. 4.3.7.14: Results from radiographic investigation at Kollekolle bridge. The film side (lower) duct is seen in the lower part of the image. The Upper duct is spread out over a large portion of the upper part of the picture.

The exposure time used for this 1000 mm slab was 40 minutes, which is twice that needed for the laboratory mock-ups. The reason (or part reason) could be that the concrete was very moist.

The Radiographic technique requires that care is taken to account for geometric effects like displacement and enlargement of projected images.

4.3.5 Investigation of voids using Radar

Very limited experience has been acquired from this type of investigation and we are thus not able to provide any detailed information.

A few months after "Block 1" had been cast one GPR profile was made across it. The "only" information that could be extracted from the profile was the location of the two layers of reinforcing. Two years later a couple of profiles were made across some of the voids in this block. This survey was more successful and the voids can in fact be seen. The improvement in data quality that enabled this was probably due to two things. Firstly, the concrete after two years was less electrically conductive and this allowed information from greater depth to be collected. Secondly, the Radar equipment had been improved.

Air void in mock-up

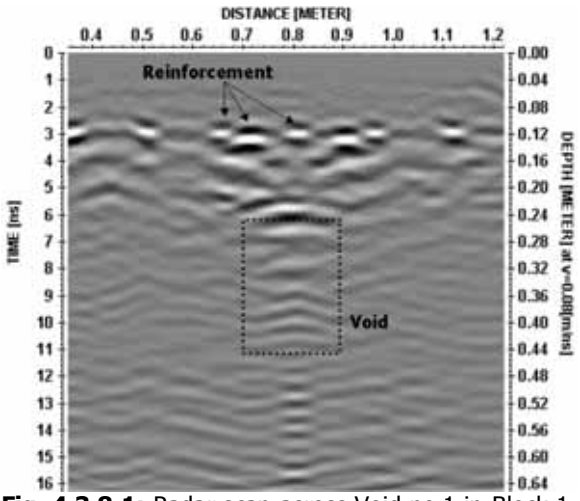

Fig. 4.3.8.1: Radar scan across Void no.1 in Block 1. The void can be seen. The antenna orientation is "Broadside", which is a mode sensitive to objects perpendicular to the profile (in this case the reinforcement).

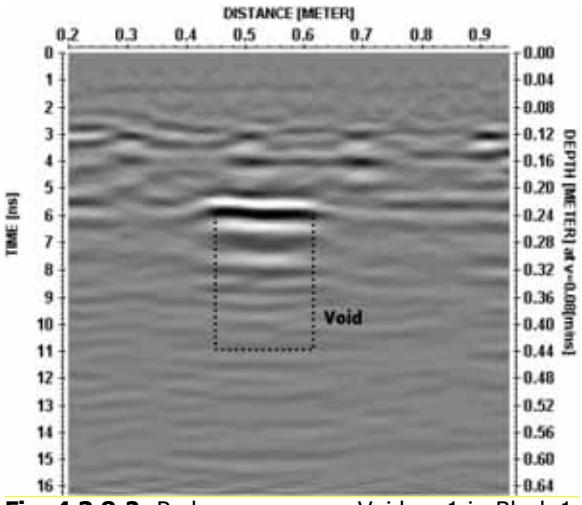

Fig. 4.3.8.2: Radar scan across Void no.1 in Block 1. The void is very clear. The antenna orientation this time is "Inline", which is a mode that is sensitive to objects with orientation along the profile. Compare with Fig. 4.3.8.1 above.

As seen in the figures above the Radar technique can detect voids in concrete and even give very clear indications of the voids. The antenna orientation chosen is very important. The huge difference in results between these two profiles is simply due to the orientation of the radar antenna relative to the survey direction.

The main disadvantage of using radar to locate voids is that the structure or part of it under investigation is usually quite complicated. There can be many layers of congested reinforcing, which will tend to act as a shield.
The advantages of speed, non-contact and continual scanning and high resolution, as well as one-sided testing, could under the right conditions make radar a favourable technique for void detection.

4.4 Detection of re-bar and cable duct position

There are many situations in which it is necessary to locate re-bars and ducts. Here are some examples of typical situations:

- Compliance checks – to see if the details are as design, for example, as a post construction check
- When drilling and cutting concrete so as not to cause serious damage to re-bars
- When examining the condition of a structure then the cover thickness to re-bars is a vital parameter.
- When there is reason to suspect voids in cable ducts or damaged cables then it is first necessary to locate their position accurately.

The techniques that can be used for this purpose are many, although the amount of information they provide varies. The techniques are listed in the table below:

Technique	Position /depth	Size	Condition
Covermeter	Yes/ Yes	No	No
Radar	Yes/~Yes	No	No
U.P.E.	Yes/~Yes	No	No
Radiography	Yes/ No*	Yes	Yes

Table 4.4.1: NDE, techniques for locating reinforcing bars in concrete.

* The depth can be calculated with radiography if two images are taken (stereographic imaging).

4.4.1 Re-bar and cable duct position using UPE

In some situations, UPE can be the preferred technique for locating cable ducts, despite the fact that it is relatively slow and clumsy compared to radar. If the concrete is electrically conductive or contains steel fibre reinforcing then UPE could be the only way. In the right conditions then UPE can locate ducts quite accurately. Also, if the duct is non-metallic then UPE could be the best method.

Locating rebars with UPE.

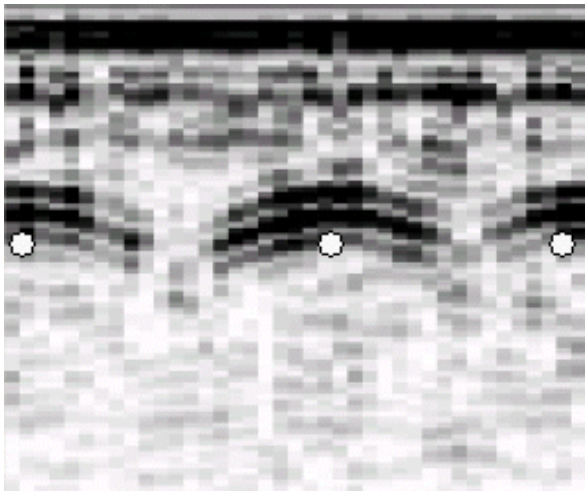

Fig 4.4.1.1: UPE data that shows how well reinforcing bars can be located. The bar positions are at the centre of the hyperbolae created in the scan made perpendicular to their axes (re-bars shown here as grey dots superimposed on the upe image (B-scan)). Each re-bar produces three reflections, which is an effect of the time-delay between the three sets of transducers in the array (transducers separated by 20 mm). This effect is accentuated by the shallow measuring depth.

4.4.2 Re-bar and cable duct position using IE

The technique is not suitable for locating pre-stressed/post-tensioned cable ducts, according to the experience gained in this project. It has however been found to be useful in locating large ducts and pipes cast into bridge decks, in situations where other techniques were not suitable. There are reports that suggests that IE is a good technique for positioning cable ducts. This is however not our opinion and we can cite other methods in almost any situation that are more informative and reliable.

4.4.3 Re-bar and cable duct position using SASW

SASW is not a suitable method for locating cable ducts. The presence of cable ducts will however affect the Rayleigh wave velocities, which will be visible in dispersion curves. This is not sufficient to constitute "detection " or visualisation of cable ducts such as can be achieved with radar, upe or x-ray.

4.4.4 Re-bar and cable duct position using radiography

This is probably one of the most common uses of radiography in civil engineering.

A radiographic image of reinforcing can be very detailed, enabling reinforcing bar size, depth, spacing and configuation to be established. The projected image of reinforcing must be correctly interpreted, as rebars will usually be enlarged, projected out off position and distorted. This can usually be overcome with the help of more than one image and complimentary techniques like radar and covermeter.

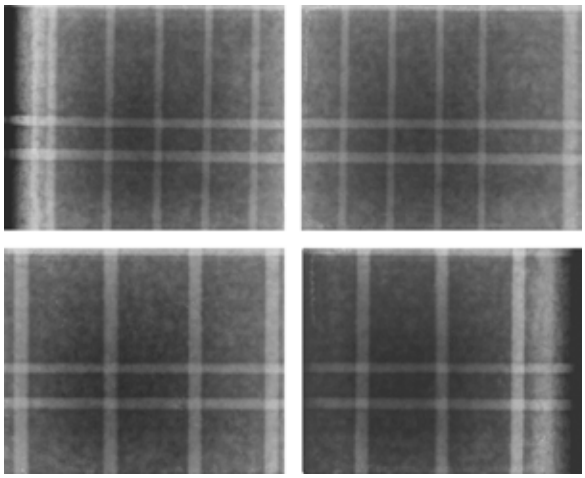

Fig. 4.4.4.1: *Above left*: ø12 mm reinforcing bars at depths ranging from 40 mm to 160 mm. *Above right*: ø12 mm reinforcing bars at depths ranging from 130 mm to 260 mm. *Below left*: ø20 mm reinforcing bars at depths ranging from 35 mm to 175 mm. *Below right*: ø20 mm reinforcing bars at depths ranging from 175 mm to 265 mm. This set up was used to test the accuracy of the technique in determining bar diameter and depth.

It is not possible to determine the depth of a reinforcing bar of unknown diameter by using a single radiographic exposure. If however, the diameter is known, then the depth can be calculated by measuring the size of its projected image. The accuracy of this method has been investigated.

The SDD (Source to Detector Distance) used for all exposures in this investigation was 1400 mm. The results are shown in Table 4.4.4.1.

Nominal diameter (mm)	Measured diameter (mm)	Nominal depth (mm)	Calculated depth (mm)	Deviation in %
11.7	14.10	262	238	-9.16
11.7	13.68	229	203	-11,35
11.7	13.47	200	184	-8.00
11.7	13.26	169	165	-2.37
11.7	13.05	138	145	5.07
11.7	12.53	105	93	-11.43
11.7	12.31	77	69	-10.39
11.7	12.07	40	43	7.50
19.8	24.76	269	280	4.09
19.8	23.71	220	231	5.00
19.8	22.43	172	164	-4.65
19.8	21.70	125	123	-1.60
19.8	21.00	82	80	-2.46
19.8	20.30	36	34	-5.56

Table 4.4.4.1: Measured and calculated, depth of reinforcing bars in block 8.

The poorer accuracy obtained in the case of the smaller diameter bar is due to the fact that the measurement accuracy is the same with the same magnification in the image processing software. This measurement accuracy is approximately +/- 0.05 mm. It is very important that the accuracy is of this magnitude in order to be able to determine the depth of the reinforcing bars with a deviation as small as 10%.

When the diameter is known, it is also possible to determine if there are one or more reinforcing bars superimposed on each other on basis of the grey level value in the image. It is not possible however to determine which bar is nearest and which is farthest away (unless their diameter is known).

Example from site – Positioning cable ducts in a bridge box-beam

A large post-tensioned bridge was to be modified and this included drilling a large number of holes for anchours in the side of the box-beam. In order to avoid cutting or damaging the pre-stressed cables, their position was fixed using radiography. Both cobalt and iridium isotopes were used for the main investigation. The CR-imaging system was used.

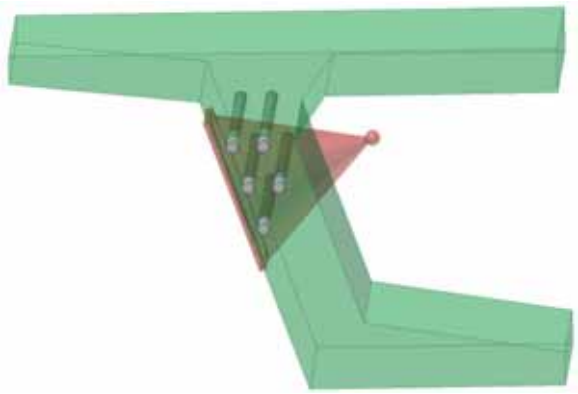

Fig 4.4.4.2: Positioning cable ducts in bridge beam. The isotope was placed on the inside of the structure and the image plate fixed to the outside.

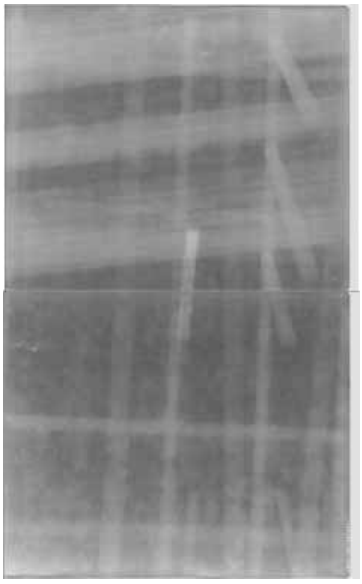

Fig 4.4.4.3: Two images plates have been joined in one exposure. The sloping cable ducts can be seen in the upper image. Vertical and horizontal reinforcing can also be seen.

4.4.5 Re-bar and cable duct position using radar and covermeter

Covermeter

The simplest and most common instrument for mapping reinforcement is the covermeter. This can rapidly show the position of most of the rebars near the surface, i.e. normally within 60 mm. In our experience it is very difficult to confidently locate rebars that lie deeper than 100 mm using this technique, unless they are large (>20 mmϕ) and well spaced. The covermeter will not identify single bars if these are closely spaced (for example c/c < 50 mm) and closely spaced rebars can lead to faulty depth measurement. For example, two bars adjacent to each other will result in apparently smaller cover thickness if the instrument is calibrated for a single bar of known diameter. The covermeter is not affected by the moisture content or quality of the concrete being tested. This is probably the most used NDE technique on site and does not require a great deal of experience or skill. It is an essential part of any site investigation, like a hammer and a good eye.

Radar

Radar is quite a common technique for mapping reinforcing. It is also rapid and can locate bars up to 500 mm from the surface, although normally this is restricted to 200-300 mm. Radar has very high resolution and will identify bars that are closely spaced, for example it will distinguish two bars with a separation of 30 mm at a depth of 100 mm. One advantage of this method is that it can identify several layers of reinforcing. It will also detect cable ducts that lie deeper (behind) the surface rebars.

This is quite a sophisticated technique and data processing enables 3-D images to be created of the reinforcing arrangement. Unlike the covermeter, radar is sensitive to variations in moisture content and the electric conductivity of concrete. This means that the maximum measuring depth is affected. The best results are obtained in "dry" concrete. The velocity of the radar wave (electromagnetic wave) has to be calibrated against a known depth since variations in velocity are to be expected. Radar is not affected by the magnitude of the embedded steel, so that cover thickness to bars can be determined accurately regardless of the bar size or whether the bars are spliced etc.

Covermeter and radar can be used together to solve the shortcomings of the individual techniques.

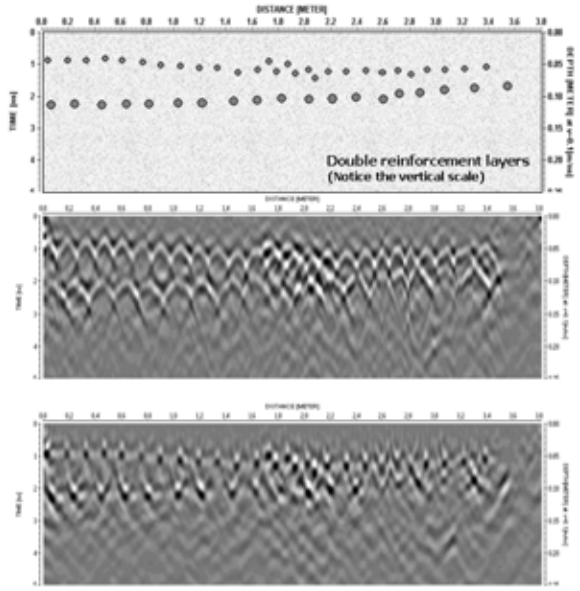

Fig. 4.4.5.1: Re-bar mapping with radar. The upper diagram shows the reinforcing in the upper side of test block no.1, with a layer of mesh (ϕ 6 mm with c/c 150 mm) topmost and the main reinforcing (ϕ 16 mm with c/c 200 mm) below. The "raw" radar data is shown in the centre diagram, with each bar producing a hyperbola. The lower diagram shows the same data but processed. Here each bar is clearly indicated by a small dot. Note that in the centre portion the mesh has been overlapped by about 200 mm. Despite the congestion the individual bars can be seen, as can the three layers.

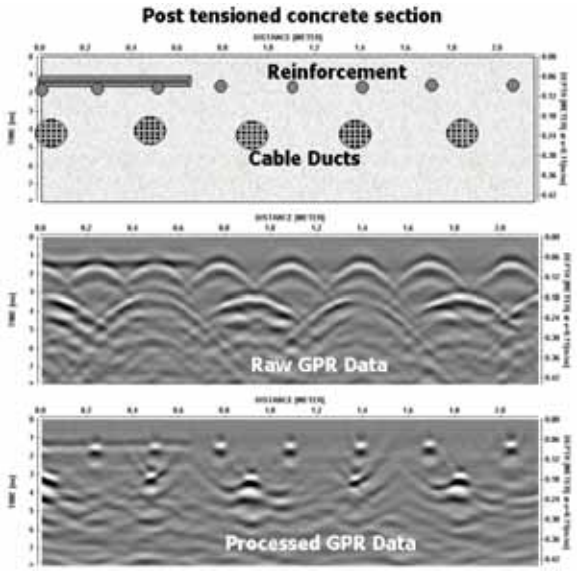

Fig 4.4.5.2: Radar scan of a pre-stressed wall. The rebar and cable duct layout is shown in the upper diagram. The raw data is shown in the centre diagram and processed data in the lower. Here we can see evenly spaced rebars at a depth of about 40 mm. In addition, there is a short length of rebar, which lies parallel to the antenna scan.

In the centre diagram, both the uppermost parallel and underlying (perpendicular) bars can be seen, together with large hyperbolae from the deeper lying cable ducts (depth around 200 mm).

The processed data shown in the lower diagram enables each bar and duct to be clearly distinguished – each appearing as a dot.

The subject of detecting and inspecting cable ducts and reinforcing bars with radar and UPE is dealt with in more detail in Appendix 4. This also deals with other mock-ups and the detailed work carried-out with these two techniques, as well as the improvements made to radar antenna.

4.5 Inspecting reinforcement and cable ducts/cables

Locating and mapping reinforcing and cable ducts can be a comparatively easy (and cheap) task compared with examining their condition. A direct (instantaneous) inspection of the condition can only be made using radiography.

Technique	Position /depth	Size	Condition
Covermeter	Yes/ Yes	Yes*	No
Radar	Yes/ Yes	No	No
U.P.E.	Yes/ Yes	No	No
Radiography	Yes/ No**	Yes	Yes

Table 4.5.1: General capabilities for NDE techniques regarding reinforcement

* Estimate of bar size can in certain circumstances be made using some types of covermeter

** If more than one radioraph is made of the same rebar then the size can be calculated

There are three problems of interest to consider here:

1) Condition of reinforcing

2) Condition of cable duct and fill inside cable duct

3) Condition of pre/post-tensioned cables inside cable duct

We refer to the physical condition, for example loss of rebar section, break in pre-stressed cable and void inside cable duct (injected). The condition with respect to corrosion activity of reinforcing or steel plate directly cast in concrete can be established using electro-chemical methods, such as half-cell potential and corrosion rate using the Galvanostatic Pulse method. These methods refer to the instantaneous risk and rate of corrosion and not to the physical state, e.g. loss of section.

In this work it has not been possible to replicate conditions of reinforcing corrosion or corrosion to pre-stressed cables. Neither are good examples from site investigations available that will allow a proper evaluation of capabilities. Our experience has shown that in order for rebar corrosion to be detected using radiography, then the bar section should be locally reduced by at least 20% of the original diameter. The condition (corrosion risk) of cable duct injection has been quite closely examined (see Section 4.3.7).

4.5.1 Inspecting reinforcing and cable ducts using UPE

UPE will not provide information about the physial state of reinforcing according to our experience. It can provide some indirect information that will help in establishing if corrosion has occurred or if there is a risk of it occurring. For example, it is sensitive to concrete damage such as delamination, as might be caused by corrosion or local deterioration in concrete that will increase the risk of corrosion.

Some effort has been put into the problem of trying to locate voids in cable ducts with various methods including Impact Echo and U.P.E. There are obvious advantages in being able to do this, as it would mean that a survey could be made relatively quickly from one side of a structure.

More details on this subject are presented in Appendix 4.

Our preference is very much for radiography however.

4.5.2 Inspecting reinforcement and cable ducts using IE

According to our experience IE is not a good tool, either for inspecting the reinforcement or cable ducts. There are some examples in various publications suggesting that it is possible. This is however beyond our experience.
The comments made above about indirect information, which may give a clue as to the corrosion conditions apply also to this method to some extent.

4.5.3 Inspecting reinforcement and cable ducts using SASW

Not suitable.

4.5.4 Inspecting reinforcement and cable ducts using radiography

Detection of corrosion in reinforcement and pre-stressed cables in reinforced concrete

The sensitivity of radiography in establishing rebar section loss was investigated. For this purpose, a ø20 mm reinforcing bar was milled in sections of length 40 mm, each corresponding to 5%, 10%, 20%, 30%, 40% and 50% reduction of the nominal thickness. This bar was added to a 300 mm thick mock-up. In addition several 100 mm blocks were available to increase the thickness of the concrete examined.

It should be noted that the mock-up is "idealised" in the sense that the rebar section reductions are perfectly formed and there is neither, concrete damage around the bar or corrosion products, both of which are factors which would be expected to affect results in a real situation.

Description of test

Two exposures were made - one with the reduced thickness in the direction of the beam and one perpendicular to the direction of the beam, see Fig. 4.5.4.1 and 4.5.4.2.

Exposure parameters: 7.5 MeV, 150 sec. and SDD = 1400 mm

Scanning parameters: scanning resolution 210 µm, scanning sensitivity 8.

The low scanning sensitivity and the fact that the concrete was still 'green' caused a significant increase in exposure time compared to the Block 1(A) and 2(A).

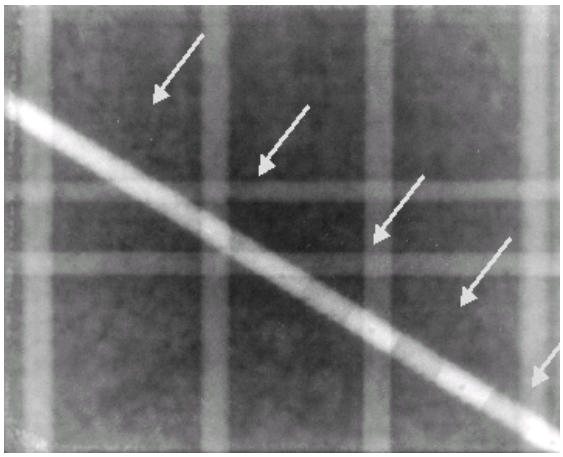

Fig 4.5.4.1: Radiographic image that shows the ø 20 mm reinforcing bar (diagonal) with small milled sections in the direction of the beam. The milled sections can be seen as darker areas along the bar (indicated with arrows).

In the second set-up, Fig. 4.5.4.1 the milled sections have been turned 90° to the direction of radiation.

By using grey level value profile lines along and perpendicular to the reinforcing bar it is possible to detect 10% - 20% loss of section in the direction parallel with the radiation and down to 5% in the direction perpendicular to the radiation.

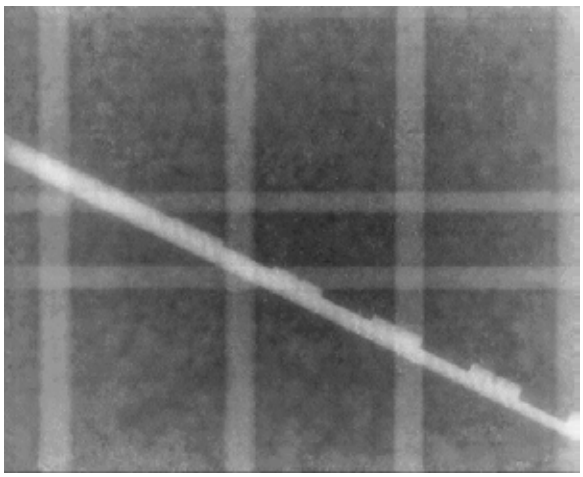

Fig 4.5.4.2: Radiographic image that shows how the technique can show loss of re-bar section. The milled sections in this example are turned 90° to the direction of radiation.

4.6 Concrete quality and condition

The quality of concrete in structures has often been described "non-destructively" using measured wave velocities and some statistics showing their variation. This is often where the gap widens between the inspecting engineer and those who hope to use the results. An abstract definition of quality like this does not tell us how the structure will perform the functions it is intended for and what changes can be expected in the future. A more usefull non-destructive description is needed. Modern NDE can provide a much more detailed picture of quality and condition, that makes it possible to describe how various functions might be affected. The best and most reliable recipe is still to combine NDE with intrusive testing and other traditional inspection methods, as the conditions are often too complex to describe concrete quality using NDE alone.

Quality: the state of the structure after construction, the standard of the materials used and of the workmanship

Condition: the state of the structure at a given time, which will be decided by the quality and loading it has been exposed to

In the table below, some NDE methods are listed together with a description of the information they can provide concerning quality and condition. The problem of voids of finite size has been dealt with earlier in this report.

NDE method	Parameter measured	Information obtained
Radar	Velocity, attenuation, penetration	Moisture level (relative), conductivity (salts)
Radar	Reflections, damping	Cracks (wet or moist) Voids
HECR	Density	Voids, porosity, cracks (beam parallel)
U.P.E.	Shear wave velocity	Shear modulus Approximate strength and mechanical properties
U.P.E.	Reflections	Cracks, voids, honey-combs, joint and bond strength (relative)
SASW	Rayleigh wave velocity and dispersion	Variations in mechanical properties with depth, damaged and deteriorated concrete and presence of layers Shear modulus
IE	P-wave velocity	Elastic modulus Approximate strength and mechanical properties
IE	Reflections	Cracks, voids, honey-combs, joint and bond strength
IE	Flexural response	Delamination
U.P.E., SASW and IE	Shear, Rayleigh and P-wave velocities	Poisson's ratio (dynamic), Elastic modulus (dynamic), Isotropy

Table 4.6.1

Quality *can* be broadly described by the wave velocities measured in a structure and parts of it and the degree to which the velocities vary. This applies mainly to mechanical waves although some information (not related to strength) can also be obtained by radar waves and x-ray. The velocity of mechanical waves is directly related to strength, and the variation of velocities can give quite a good picture of the uniformity and homogeneity of the concrete.

The velocity of mechanical waves travelling through concrete is determined by the elastic properties of the concrete (strength) and the homogeneity. We must be able to distinguish these effects. In other words, we have to know if the velocity of a wave travelling through the concrete is reliably measured as the *true* value, or if it has been affected by some internal defect or by the geometry of the structure (apparent velocity). (It could be argued that the measured *apparent* wave velocity reflects the quality even without distinguishing the effects of mechanical properties and homogeneity.)

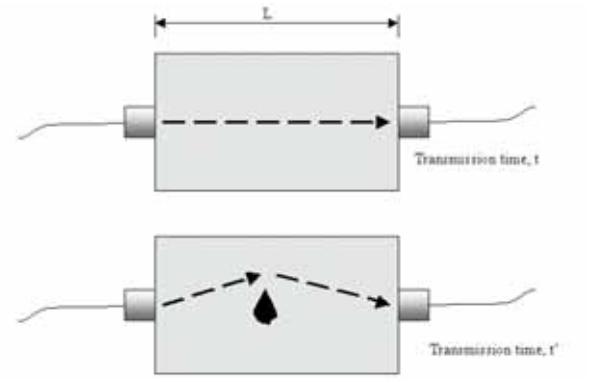

Fig.4.6.1: Simple through transmission of ultrasonic waves in a concrete block. In the upper case, the concrete is homogeneous and the sound waves take the shortest path between the sending and receiving transducers. Knowing the size (L) of the concrete and the travel time, t, we can easily calculate the true wave velocity. In the lower case, there is a defect inside the concrete of unknown size and position. The transmission time, t' is thus affected by the defect and we obtain a velocity that is "apparent". This velocity will be lower than the true velocity as the wave path is longer.

Quality and strength

The quality of concrete has been described by the coefficient of variation of wave velocities, typically in the case of simple P-wave through transmission measurements. This is a reasonable way of describing "older" structures, for which it might be expected that the consistency of concrete quality delivered and placed can vary. The coefficient of variation of wave velocities in a modern structure should be very low (less than 1), yet even if this is so the structure may be in a dangerously poor condition from the time of casting. For example, the integrity of a cooling water channel might be seriously affected due to porous casting joints and subsequent rebar corrosion. Likewise a bridge may have potentially serious weaknesses due to lack of compaction around pre-stressed cable anchors. A general survey of wave velocity variation on these structures may not reveal this type of problem. On the other hand, a low coefficient of variation will tend to reflect that the structure has been made with care and this is in itself an indication that the likelihood of hidden defects is small.

We cannot describe the condition of concrete in a quantitative manner if the "defects" are diffusely and randomly spaced and varied in nature. The capabilities of NDE are in proportion to the quality of the concrete and the ability to describe a discrete defect is reduced if the surroundings (concrete) are in a poor condition. Generally speaking, if the NDE methods work well then we know that the concrete is most likely of good quality and vice-versa. If the concrete is of poor quality generally then we must rely more on traditional inspection methods and combine NDE with coring.

4.6.1 Quality based on apparent wave velocities

When investigating a structure, particularly an old structure, of which little or nothing is known, then we should be extremely careful in drawing conclusions about the quality of the concrete on the basis of apparent wave velocities alone. This is particulary true if the concrete is only accessible from one side, if it is thick and if the surface has been concealed by paint or similar. The difficulties in interpreting data can arise if the many factors that affect the wave velocities are not known – these could be (combinations of):

- Material strength variation
- Construction defects
- Deterioration or damage
- Internal geometry
- Global geometry
- Variations in moisture content

The number of variables and potentially important conditions demonstrates the need to have access to several NDE techniques, an understanding of the structure in question and preferably also intrusive test data.

4.6.2 Strength based on wave velocities

There is rarely need to use wave velocity to estimate the strength of concrete, particularly in newly produced and modern concretes for which the strength development can be quite accurately predicted. There are other means of more accurately measuring strength. In the case of older structures, it is usually quite simple to remove cores or make other intrusive tests of compressive strength. However, in some situations, it can be

invaluable to have the means of measuring wave velocities, either for speed, size of sample or safety reasons:

1. Old structures with many elements, e.g. columns, for which the variation in strength properties should be established (strongly varying concrete quality)

2. Structures that have a safety function, and for which practical considerations make it difficult to take cores

In the first case the quality of concrete, i.e. mainly w/c-ratio, may vary considerably throughout the members if these have been constructed over a long period and with insufficient checks during construction. Exposure conditions and changes in work teams and foremen can cause variations in both quality and strength. It may be important to identify weak zones or elements, particularly (as we have seen) if the concrete strength in supporting structures can be 10 M Pa or lower.

In the second case, the problem is quite specific. A relatively thick wall section exposed to one-sided drying over a long time will likely have very different strength properties across its section due to drying rate and long-term strength gain. This will be reflected by variations in wave velocities with depth – normally and logically increasing with depth. The long-term ageing of the concrete can be monitored non-destructively by measuring seismic wave velocities.

4.6.3 Concrete strength based on true wave velocities

There is no unique relationship between wave velocity and strength of concrete but the two are directly related. The amount and size of the coarse aggregates has a significant effect on wave velocities. The result is that different wave velocity: strength relationships are obtained for different mix proportions.

It is not possible to accurately estimate concrete strength based on measured wave velocities alone. It is possible to estimate if the concrete is of low strength, medium or high strength. It is also possible to delineate areas of weaker concrete and to see trends that might indicate changes that the concrete has undergone with time or if the concrete in part of a structure deviates from the normal in some other way, e.g. the mix proportions.

The results, from site investigations, that are shown in Fig. XX represent structures from all over Europe, varying in age from 2 to 60 years. The variation in concrete quality is considerable, most notably the type, size and quality of the aggregates, but also the compactness of the concrete. In the lower end of the scale we have a low strength concrete (11-20 MPa compressive strength) containing calcareous aggregates; in the medium range (20 to 40 MPa) the samples are mainly from older structures (30 to 60 years) with in some cases poor aggregate grading; in the higher range (40 to 70 MPa) more modern concretes (2 to 30 years) with good quality aggregates (mainly granite) and good aggregate grading.

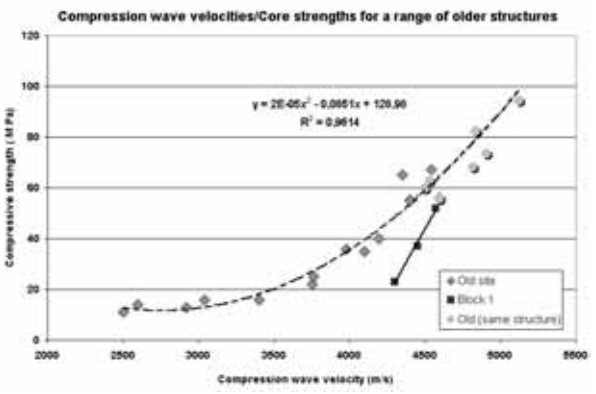

Fig. 4.6.3.1: Measured compressive strength on site and corresponding P-wave velocities. These results are taken from a range of structures from Scandinavia to southern Europe with ages from 2 to 60 years. Also shown are 3 results from Block 1 (Note that the results from Block 1 were obtained from cubes during the first 28 days of hardening and not from mature concrete). Some of the results shown are based on Rayleigh wave velocities, which have been converted to compression wave velocities according to the relationships shown below. The data has been chosen from various projects conducted over a ten-year period. (Diagram enlarged in Appendix 6)

Despite the widely varying concrete types, reinforcement configurations, environment conditions and ages represented by Fig. 4.6.3.1 there is a clear trend – a reasonable estimate of strength could be made. The following categories might be chosen based on compression wave velocity:

Low strength	Low-medium strength	Medium strength	Medium-High strength	High – Exceptional
2500-3000	3000-3700	3700-4200	4200-4700	4700-5000

We do not use the terms "poor" or "good" to describe the concrete, as most of the structures considered are un-damaged, and fulfill the requirements asked of them. The classification of should be made with reference to how it performs its function.

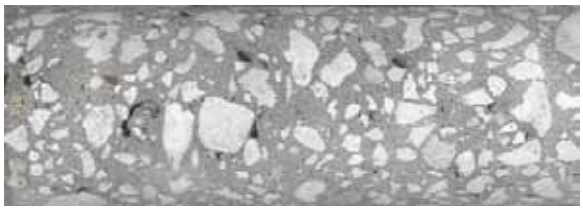

Fig. 4.6.3.2: Example of low strength concrete. Age at test 30 years. Compressive strength/wave velocity found to be 14 MPa/ 2600 m/s. Calcareous aggregates mostly <15 mm. Concrete from a column, southern Europe. Exposed concrete surface and sheltered outdoor environment – carbonation depth 55 mm. Possibility of long-term strength gain is small due to dry environment (thin members and dry, hot climate).

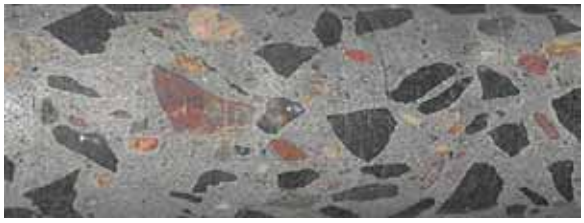

Fig. 4.6.3.3: High strength concrete. Age at test 30 years. Compressive strength/wave velocity found to be 94 MPa / 5100 m/s. Mostly crushed granite aggregates with maximum size 32 mm. Slow rate of hydration cement (Limhamn, Sweden). Concrete from a nuclear containment building, Scandinavia. Painted surface with normal indoor environment – carbonation depth 1mm. Long-term strength gain due to slow drying (> 90% relative humidity after 30 years).

4.6.4 Wave velocities and elastic modulus of concrete

The velocity of sound waves through concrete can be used to determine the dynamic modulus of elasticity. It has been suggested that the relationship between the static and dynamic moduli is a function of the density of the concrete, as is the case between the static moduli and strength and the relationship between wave velocity and strength. The relation between wave velocity and dynamic modulus of elasticity can be written:

$$E_{dyn} = \alpha \gamma v^2$$

Where
$\mathbf{E_{dyn}}$ is the dynamic E-modulus, "α" a factor depending on Poisson's ratio, "γ" the density of the concrete, and **v** the compression wave velocity.

The factor α is calculated from the Poisson's ratio:

$$\alpha = \left(1+\sigma\right)\cdot\left(1-2\sigma\right) \Big/ \left(1-\sigma\right)$$

A commonly used value of σ is 0.2, although in reality this can vary between 0.15 and 0.25 for higher and lower strength concrete respectively.

Examples Block 1

Compression wave velocity is 4700 m/s and density 2400 kg/m^3. If we assume the value of Poisson's ratio to be 0.15 or 0.2 then we obtain a value of E_{dyn} of 50.3 and 47.7 GPa respectively. The difference is small but we may want to know the value of Poisson's ratio accurately.

How is the Poisson's ratio determined?

The elastic constants are interrelated. If the moduli are determined, the Poisson's ratio can be calculated. Poisson's ratio is also a function of the ratio of the compression and shear wave velocities.

$$E_{dyn} = \alpha \gamma \upsilon^2$$

$$G = \rho \cdot \left(\upsilon_s\right)^2$$

$$\sigma = \left[1 - 2\left(\upsilon_s / \upsilon_L\right)^2\right] / \left[2 - 2\left(\upsilon_s / \upsilon_L\right)^2\right]$$

We know that the compression wave velocity, v_L and shear wave velocity, v_s are 4700 m/s and 2950 m/s by measurement. We still do not know the exact value of density in the block but can quite safely assume it to be 2380 kg/m^3. The calculated value of Poisson's ratio is thus 0.175, and the corresponding value of dynamic elastic modulus is 48.6 GPa. The ratio of shear to compression wave velocities (v_s/v_L)= 0.6 to 0.62 for normal concrete. In the case of Block 1, this is 0.627.

We can also determine the compression wave velocity from the measured Rayleigh wave velocity.

An approximate value for Rayleigh wave velocity is:

$$\upsilon_r = \left[\frac{0.87+1.12\sigma}{1+\sigma}\right]\cdot\upsilon_s$$

For Block 1 this would give us a value of Rayleigh wave velocity of 2676 m/s, which is very close to the measured value (2600-2650 m/s in summer 2003).

We have found in our work that the ratio of Rayleigh to compression wave velocities is nearly always 0.56 for undamaged concrete. In the case of Block 1, we obtain a ratio of 0.55-0.56. The value of Poisson's ratio determined by wave velocity measurements is higher than that which would be obtained by strain measurements.

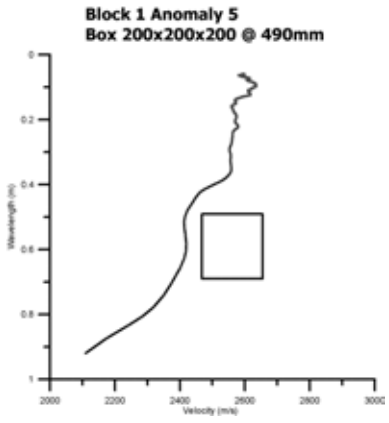

Fig. 4.6.4.1: SASW dispersion curve for Block 1 above a void at 500mm. The un-disturbed Rayleigh wave velocity is 2600 m/s.

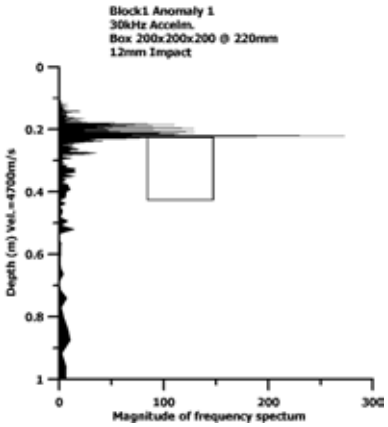

Fig. 4.6.4.2: Impact Echo response for Block 1 and void at 220 mm depth. The frequency of the echo from the void is 10.7 k Hz, which means our compression wave velocity is 4700 m/s.

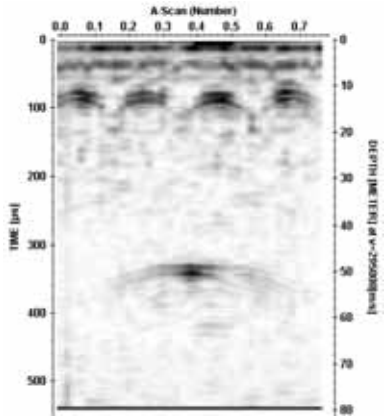

Fig. 4.6.4.3: U.P.E. response from void at 500 mm in Block 1 (as SASW on left). The shear wave velocity is 2950 m/s.

There are obvious advantages in having access to two or more methods that can be used to determine the velocities of the various wave types. This can be used to calibrate some techniques, e.g. compression and shear wave velocities based on a Rayleigh dispersion curves.
A un-balance between velocity, ratios would tend to suggest that the concrete has been damaged in some way, for example micro-cracking causing anisotropy in the outer layers of a structure exposed to freezing and subject to ASR.

4.6.4.1: Wave velocities measured in Block 1 during the hardening phase

These are presented briefly to give an impression of how strength and wave velocities can be related.

This block was cast in February 2000. The temperature of the concrete during setting and hardening was checked using cast-in thermo sensors to ensure that measures could be taken to avoid extreme temperature differences that might cause cracking. No cracks have been observed on the surface or detected by NDE. The whole casting process was recorded every minute and there is no reason to suspect any kind of defect, for example, cracks, honeycombing or cold-joints. The various wave velocities described below for Block 1 are thus considered to be true values with the possible exception of some Rayleigh wave values.

Cubes were cast simultaneously together with extra reference blocks in order to monitor maturity and compressive strength as well as compression wave velocity. These samples were stored in the open air beside Block 1.

Block 1 was fitted with temperature sensors, maturity gauges and LOK-test inserts to enable some in-situ compressive strength measurements.

It can be seen that the wave velocity: strength relationship is not linear. A strength gain from 35 to 53 MPa results in a P-wave velocity increase of only 4% as seen in Fig. 4.6.4.4. (The strength of the concrete was measured on the cubes, as were compression wave velocities. The compression wave velocities were also measured at four positions each over a span of 1000 mm on two sides of the block.)

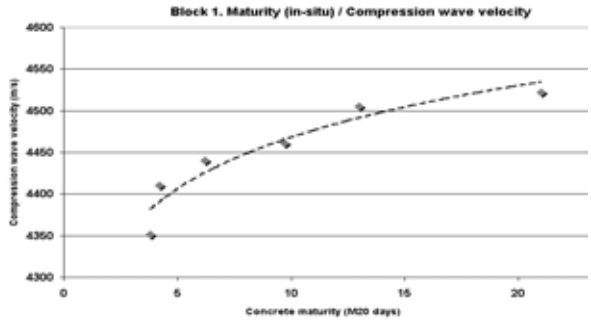

Fig. 4.6.4.4: These measurements were made on Block 1 itself. After 4 M20 days, the compression wave velocity is already 96% of the value at 28 days.

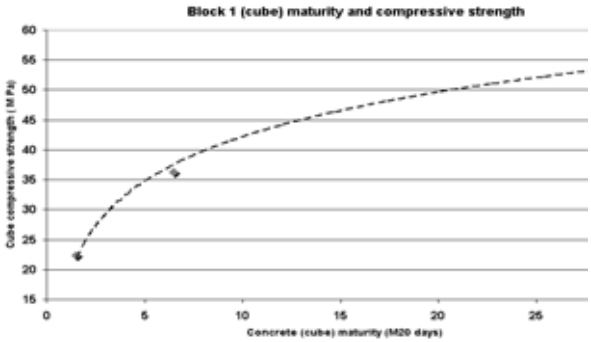

Fig. 4.6.4.5: These cubes were stored beside Block 1 during hardening. The strength gain is rapid and it can be seen that already after 1.5 M20 days the compressive strength is between 20.2 and 25.4 M Pa., i.e. almost half of the 28-day strength.

Further test results from Block 1 during hardening are to be found in Appendix 1.

4.6.5 Deterioration of concrete

Example 1 – Dam with frost damage and ASR

Several examples of typical responses from deteriorated concrete are given below. Note that it can be extremely difficult to distinguish deteriorated concrete from the effects of construction defects if NDE alone is used. In principle, a crack caused by deterioration such as ASR will have the same effect on wave propagation as a crack produced by shrinkage. NDE alone can therefore not describe the mechanism that causes deviating wave velocities. The advantage of NDE is that it will reveal patterns that suggest deviations, which indicate that something is wrong, and this can be used to plan how samples should be taken and analysed.

Freezing and thawing is a deterioration process, which affects the cement paste and is progressive from the surface of the concrete.

ASR is a process that results from cracking of aggregates and swelling in the cement paste. The damage is normally greatest at the free surfaces and takes the form of large expansion cracks perpendicular to the surface. The concrete will also crack at depth although the process of expansion is constrained internally.

Since both of these processes lead to cracking and porosity of the concrete, and both rely on moisture ingress, then in many situations the two can combine to form a particularly aggressive form of deterioration.

Fig. 4.6.5.1: Dam structure northern Sweden. Concrete cracking caused by ASR. The surface cracks are significant – running perpendicular to the concrete surface. The outer 100 mm has separated on drilling out. Internal cracks and porosity can be seen by the dark, moist pattern

Fig. 4.6.5.2: Crack pattern as seen on the concrete surface. The picture covers an area of about 400 mm x 400 mm and was taken near the most severely damaged concrete close to water level.

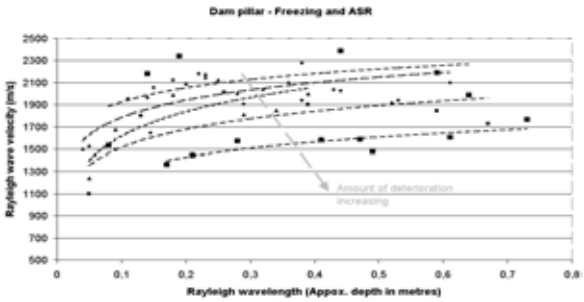

Fig. 4.6.5.3: Dam pillar subject to freezing and ASR. These are results from SASW measurements showing Rayleigh wave velocities versus wavelength (depth from surface). The various plots are results from different levels on the dam pillars and show how the extent of damage increases in the parts most exposed to water. Based on measurements on un-damaged concrete in the same structure the Rayleigh wave velocity should be around 2500 m/s. The lowest Rayleigh wave velocity measured and what seems to be a lower boundary is 1100 m/s, which reflects a physical sate of the concrete similar to building blocks of stone with loose binding, but not rubbly or soft. The lowest velocities are near the surface and this corresponds to the degree of cracking, which is greatest near the surface.

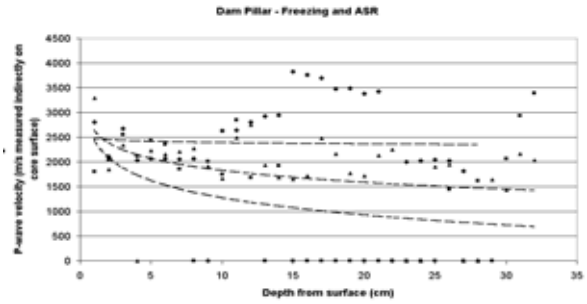

Fig. 4.6.5.4: Dam pillar as above. P-wave velocities measured indirectly along the surface of a core using the UK 1440 instrument. The values are low and there is no increase in velocity with depth from the surface generally. This would suggest that there is cracking throughout the concrete and not just near the surface. The measured wave velocities are thought to be in three categories reflecting the mode of measurement and the sensitivity of the instrument – near normal P-wave, shear wave and at the lowest end of the scale no measurable transmission. The latter reflects the severity of some of the cracks, which were not visible to the naked eye.

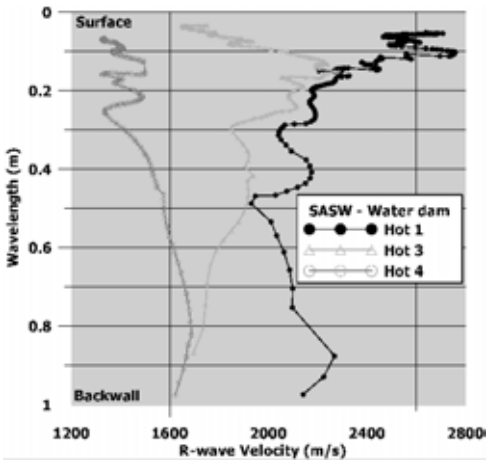

Fig. 4.6.5.5: Dispersion curves for the dam pillar. In the case of "Hot 1" the measured Rayleigh wave velocities are highest reflecting the fact that damage in the dryer parts of the structure is least. Note that at short wavelengths the velocity is near the expected value for undamaged concrete. This is probably because the data is obtained with transducer separations that are smaller than the spacing of the macro-cracks at the surface. We thus obtain velocity values which are unaffected by the macrocracking. As we see, the apparent velocity decreases with increasing wavelength, which is probably due to a combination of internal cracking and geometrical effects, but also due to the fact that the lower frequency (longer wavelength) data was obtained with larger transducer spacing (the curves are "merged" data, i.e. several sets of data with gradually increasing transducer separation). The results Hot 2 and Hot 3 reflect the increasing degree of damage nearer the water level, i.e. increasing moisture levels and thus more severe asr and frost damage.

Example 2 – Bridge column with ASR

Fig. 4.6.5.6: Bridge column with map cracking (shady and moist-like edges suggestive of ASR.) Larger vertical surface open cracks appear at regular intervals around the column, as well as map cracking.

Fig. 4.6.5.7: View of the column. The cracking is obvious along the whole length of the column, but most clearly on the side, which is exposed to the prevailing weather (higher moisture levels).

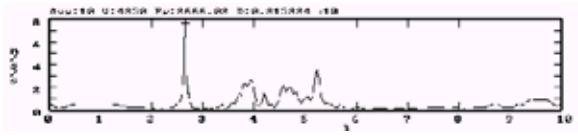

Fig. 4.6.5.8: Impact Echo from bottom of C1. The lowest dominant peak is 2.66 k Hz and there are a number of higher frequency peaks (higher modes) although these are not distinct. The dominant peak is the fundamental frequency. Based on a P-wave velocity of 4920 m/s the fundamental frequency of this column (diameter 726 mm) in an un-damaged state would be 3.1 kHz. The fact that the measured fundamental frequency is lower suggests that the column is damaged.

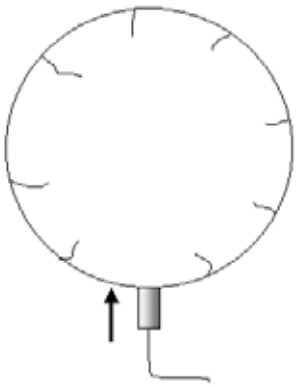

Fig. 4.6.5.9: Impact Echo measurements on the column. The fundamental and higher frequency modes are obtained.

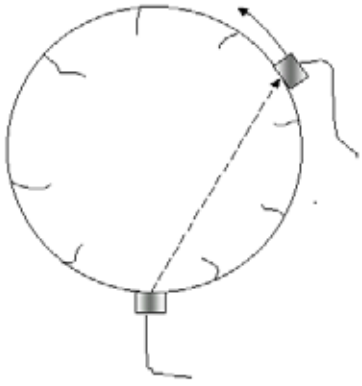

Fig. 4.6.5.10: UPV-measurements around the circumference of the column.

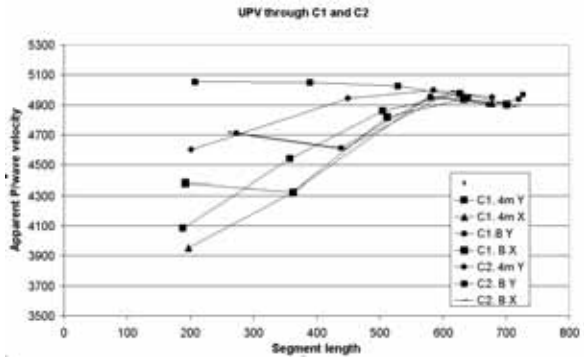

Fig. 4.6.5.11: UPV around columns. Plot of apparent P-wave velocities for various segment lengths. The annotation C1 and C2 refers to the column number. The figures "4 m" refers to the height above ground level and "B" means bottom of column at which the tests were made. The slope of the curves reflects the depth of the surface open cracks between the transducers.

According to this, the P-wave velocity seems to be striving towards an upper limit of between 4900 m/s and 5050 m/s.

The average separation between vertical cracks (visible) around the mid-section of C1 and C2 is 204 mm and 223 mm respectively. The crack widths for C1 were estimated to be between 0.1 and 1mm for C1 and on average 0.1- 0.2 mm for C2.

Based on the curves and assuming that the wave is affected by a single surface-opening crack half way between the transducers then the approximate depth of the crack in the worst case is estimated to be 100 mm. Since the cracks are more frequent then we assume that the first crack is 100 mm from the transmitting transducer. Then the depth of the crack would be approximately 40 mm (presumably open crack depth). We assume that the latter case is true, as the frequency of cracks around the column has been measured. This is based on the worst case, i.e. C1.

Both impact echo and wave velocity tests suggest that the two columns are damaged at all investigated sections. The damage extent and pattern seems to be uniform – the difference in measure values of fundamental frequency (F_1 equal to about 2.6 k Hz) measured at all points is less than 0.12 kHz, which is quite low (4% of the theoretical value).

The wave velocity tests suggest that the open crack depth is approximately 40mm, if we assume that the damage consists only of this type of damage and that no internal cracking exists. The wave velocities measured between opposite faces of the columns give P-wave values of 4900 m/s, which we assume to be normal for undamaged concrete. The impact echo results suggest that there are no significant internal cracks reinforcing this supposition.

Impact echo gives fundamental frequencies for the columns, which are lower than expected based on an assumed P-wave velocity of 4900-5000 m/s. If we assume that the surface damage results in an effective reduction in diameter by 80 mm (40 mm deep surface opening cracks around the column) then the resulting fundamental frequency calculated (assuming a column diameter of 726-80 mm) is 2.7 kHz, i.e. approximately that measured.

We suggest therefore that the surface cracks have an effective depth of about 40 mm and that this has resulted in an effective "reduction" in column diameter by 80 mm.

Since the crack depth is the same as the design cover thickness to the reinforcing then this could lead to corrosion and will almost certainly reduce the durability of the columns. Corrosion measurements along the column suggest some degree of active corrosion, although confined to "patches". The cover to the stirrups on opposite faces of two columns was on average 54/39 mm and 48/40 mm (reinforcing cages a little "off centre" in both cases). The high strength and resistivity of the concrete has most likely prevented any extensive reinforcement corrosion. There was no outward sign of corrosion. The bridge was 40 years old when inspected.

Rayleigh wave velocities near the surface of the column were around 1200 m/s. This would suggest that the damaged layer of concrete has a dynamic elastic modulus of around 15% of the undamaged concrete. A P-wave velocity of 4900 m/s would suggest that E_{dyn} is about 53 GPa. Based on our curve in Fig then the compressive strength of the uncracked concrete should be about 80 MPa or more.

Example 3 – Dam with frost damage

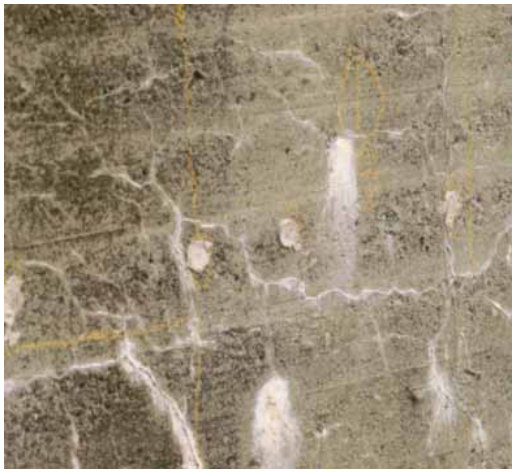

Fig. 4.6.5.12: Dam wall with signs of cracking and leaching.

Fig. 4.6.5.13: There were obvious signs of frost scaling also.

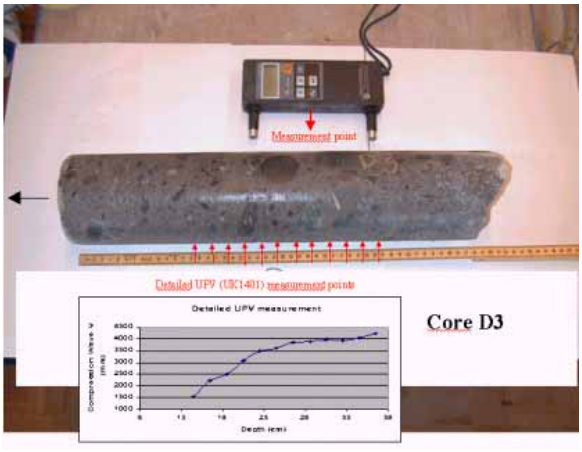

Fig. 4.6.5.14: A typical core from the dam wall. Concrete 60 years old. The core has broken at around 400 mm from the surface along a crack plane. This crack is thought to be a temperature-shrinkage crack from the time of casting. To the eye there is no obvious damage in the outer (near-surface) concrete, but as can be seen from the velocity curve values as low as V_P=1500 m/s have been measured. The instrument used for velocity measurements is the UK 1440 and is seen in the picture.

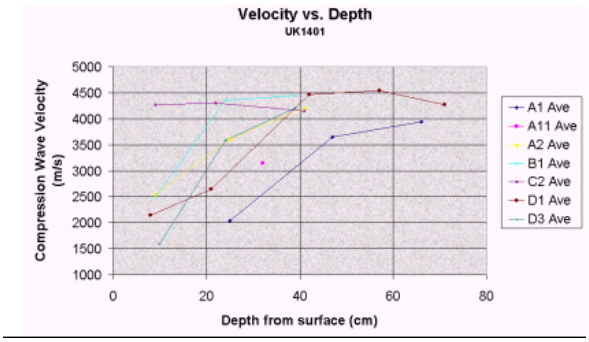

Fig. 4.6.5.15: The P-wave velocities have been measured indirectly on the surface of a core using the UK 1440 instrument. The un-damaged P-wave velocity appears to be 4500 m/s. Most of the damage to the concrete appears to be 200-300 mm from the surface. The curves tend to suggest a lower bound of compression wave velocity of around 1200 m/s.

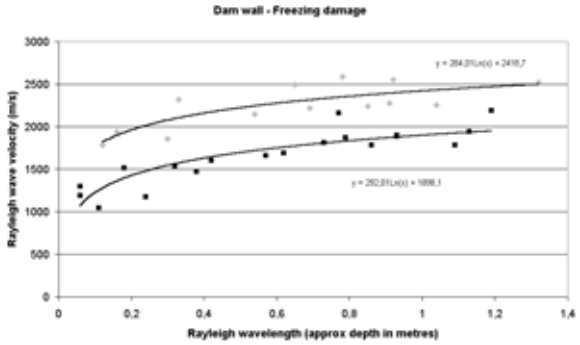

Fig. 4.6.5.16: Dam wall with freezing damage as above. The values shown are Rayleigh wave velocities measured with SASW on site. The upper line is the average of two sets of data from relatively "good" concrete. The lower line is the trend for the 3 "poor" concrete areas. (This is based on the outward appearance of the concrete surface and amount of visible damage). The data at wavelengths less than about 100 mm is very poor, which reflects the amount of damage in this region. In the upper case the Rayleigh wave values approach what is expected for un-damaged concrete, i.e. around 2500 m/s. The sets of curves are similar if offset by about 500 m/s which is thought to be due to the degree of near-surface damage. There is nothing to suggest damage to the concrete at depth.

Example 4 – Bridge beam with frost damage and ASR

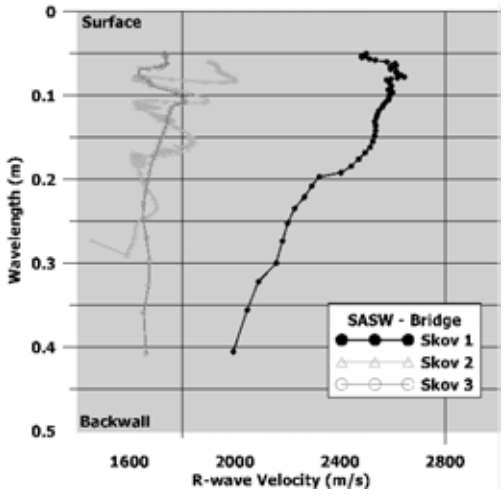

Fig. 4.6.5.17: SASW dispersion curves for two 320 mm thick post-tensioned concrete bridge beams.

The dark curve (Skov 1) is from an apparently un-damaged beam. Max R-wave velocity 2600m/s. the Rayleigh wave velocity begins to drop at wavelengths around half the beam thickness, which is expected and is probably an effect of the finite size of the beam.

The other results, Skov 2 and 3 are from a beam with visible surface cracking. The curves (velocities around 1700 m/s) suggest that the cracking extends all through the beam.

Example 5 – Bridge slab repair (SASW)

A special technique was used to repair voids in the underside of a bridge slab. A shutter was first fixed under the slab and void after which aggregates were inserted from underneath. A cement grout was then injected to mix with the aggregates in the void.

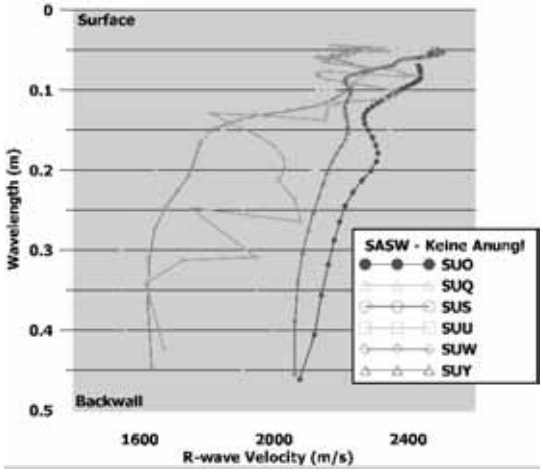

Fig. 4.6.5.18: Rayleigh wave dispersion curves obtained at various positions across the repair area. The depth into the concrete is shown on the vertical axis and the Rayleigh wave velocity on the horizontal axis. The "normal" dispersion curves show velocities around 2400-2100 m/s. Some of the curves deviate significantly at around 150 mm and drop to 1500 m/s. This sugests there is weaker material below about 150 mm into the repair.

Fig. 4.6.5.19: The mock-up used for the repair trial has been cut in sections revealing the condition of the repair along the section tested. It can be seen that the first 150 mm is reasonably well formed with both aggregates and binder. There is however a layer of grout without aggregates, which corresponds with the "weak" layer suggested by SASW.

APPENDIX 1- Description of Block 1

Block 1 is the largest mock-up constructed in this project. The slab of Block 1 has an area of 16 m^2 and thickness 800 mm. The slab was cast with two supporting walls/legs with thickness 400 mm. The Block is monolithic. The main purpose of the block is to test the capability of various NDT methods in detecting voids of various sizes and depths from the surface. The block is shown below.

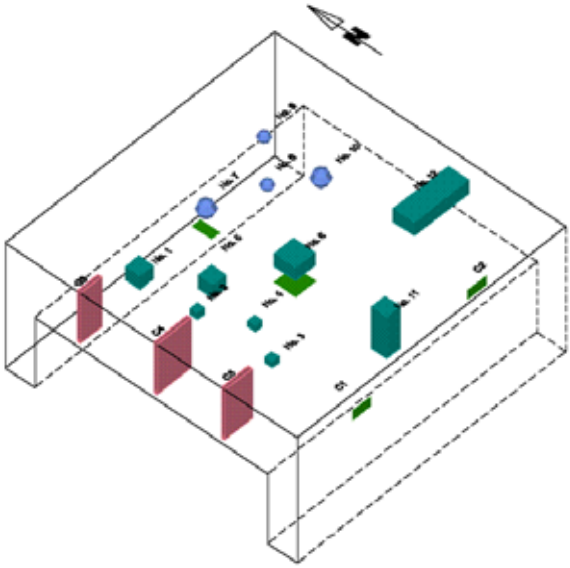

Fig. A.1.1: View of Block 1 including the defects in the form of voids and thin plates to represent cracks.

Brief description of the concrete and reinforcing

Great care was taken to produce a concrete block of good quality and homogeneity. Only the artificial defects were desired, while any accidental cracks or honeycombing would have been unacceptable. Subsequent NDT has not revealed any defects other than those designed.

The 28-day strength of the concrete was found to be on average 53 MPa. The design static E-modulus is 35 GPa and density 2350 kg/m3. The concrete was cast with a low w/c-ratio (0.37) and some plasticiser additives were used. A crushed, granite (Dalby) from the south of Sweden was chosen, with maximum size 25 mm. Low-alkali cement was chosen.
The Block was cast in February 2000, care being taken to avoid temperature cracks. Sensors were installed in three positions to check the heat of hydration and differences thereof so that the risk of temperature cracking could be minimised.

The slab is reinforced on top and bottom surfaces with a mesh of ϕ 16 bars at c/c 200 mm. The cover thickness on the upper surface is on average 90 mm. In addition a mesh of ϕ 6 mm, c/c 150 mm was placed above the main reinforcing on the upper surface.

Several methods were used to check the strength development in the initial stages after casting. These included:

- Compressive tests on 150 mm cubes cast on site and matured under controlled conditions
- LOK-test (Pullout test) on two faces of the slab
- Maturity monitoring in situ
- Measurement of compression (P) and Rayleigh (R) wave velocity

As an example, the Rayleigh wave velocity at 28 days was found to be on average 2250 m/s, with a corresponding compressive strength of 53 MPa. After 30 months the Rayleigh wave velocity has been found to be 2500-2600 m/s. On the basis of the measured wave velocities the 28-day dynamic E-modulus would have been around 35 GPa, while at 30 months this has increased by 12% to 45 GPa.

The slab was cast more or less continuously, with only short time intervals between concrete loads. Casting was made using a pump. The concrete was poured without any tendency to become plastic or any danger that the concrete could not be vibrated into a uniform and homogeneous mass. Polished plywood formwork was used on the sides and undersides, resulting in a very smooth surface texture. No special surface treatment was made on the upper surface.

No cracks or micro-cracks have been or are visible on any surface of the block. Neither is there any indication of honeycombing, entrapped air bubbles or bleeding.

Fig. A.1.2: View of Block 1 from NW. In the photo one of the three large "cracks" is seen as well as several LOK (pullout) test scars.

Fig. A.1.4: South face of Block 1 with thin plastic sheet securely fixed to the reinforcing. Notice that a thin bar has been fixed behind the sheet to prevent movement or bending.

The defects cast into Block 1

Cubic and spherical voids of various sizes were imitated using polystyrene blocks and hollow plastic spheres. These were fixed securely in the formwork using welded bars and stirrups, to guarantee that they did not move during casting.

Fig. A.1.3: Block 1 during casting with square voids fixed in place. In the upper part of the picture we see two 200 mm cubes at 220 mm and 490 mm depth respectively.

In addition to the voids, some thin plastic sheets were installed as shown in Photo 3. These were used so that the response could be compared with 3-dimensional voids.

Details, of the defects in Block 1.

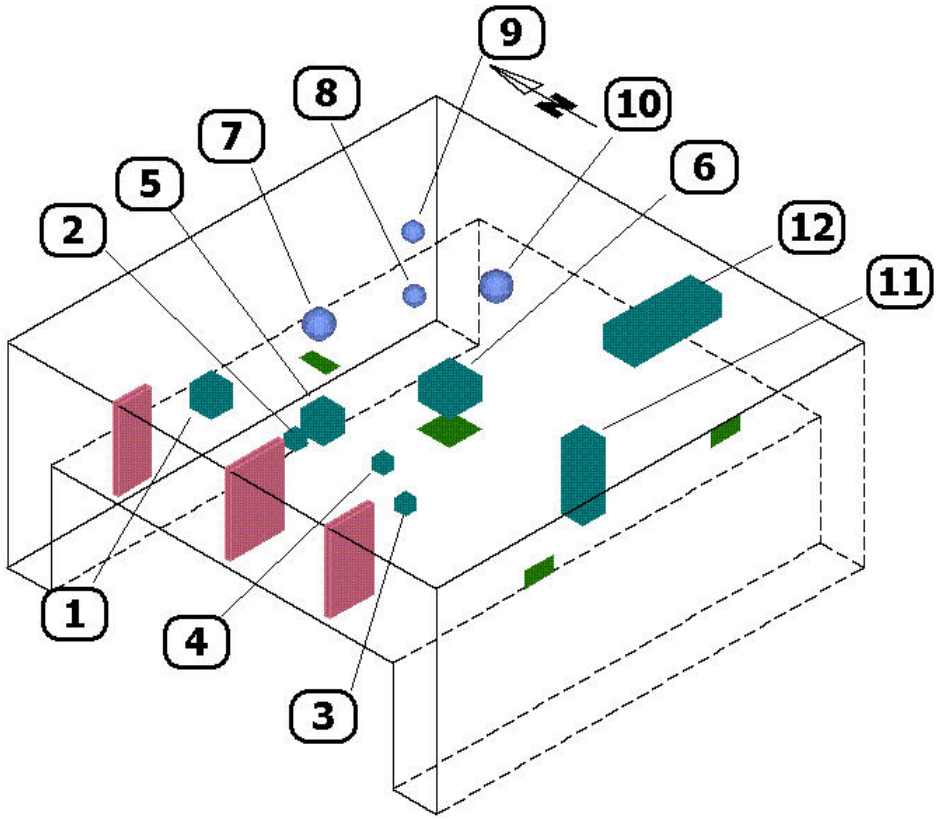

Fig. A.1.5: Drawing of "Block 1" mock-up. (4 x 4 x 0.8 m plus "supports")

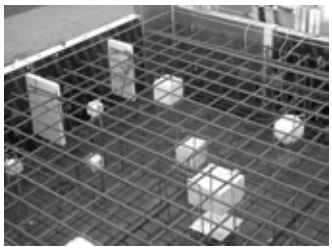

Block 1 "voids" 1 to 7.

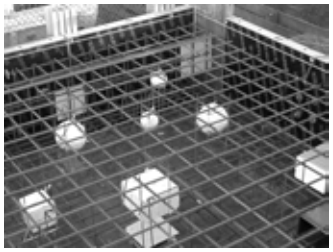

Block 1 "voids" 5 to 11.

Block 1 "voids" 6, 11, 12 and steel plate cast in with semi-spherical "voids" on upper side.

The mock-up consists of a monolithic 4 m x 4 m x 0.8 m thick slab with supporting "legs". The slab is reinforced on top and bottom sides with ϕ 16 mm rebars and is cast with a concrete of average 28-day compressive strength 53 MPa. The aggregates are crushed Dalby granite with maximum size 25 mm.
The voids vary in size from 100 to 300 mm, and they are both square and spherical, placed at various depths from the top surface.

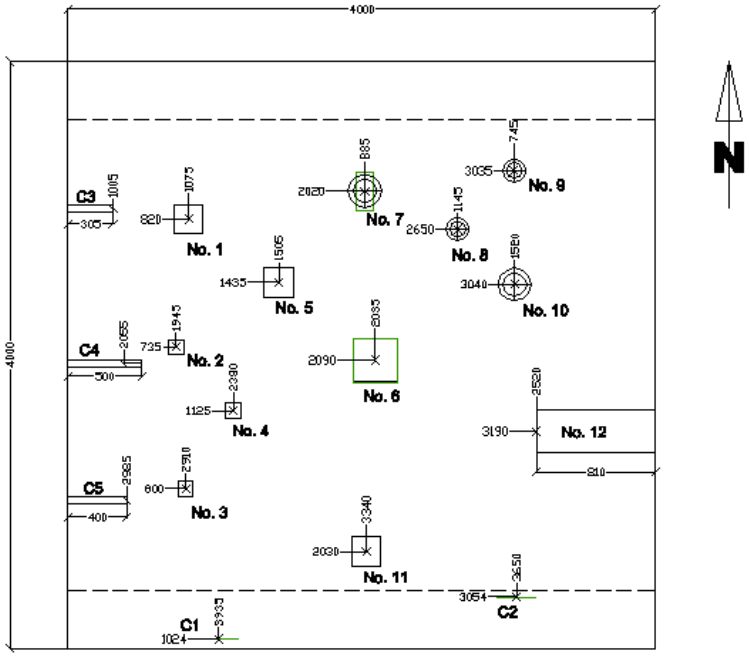

Fig. A.1.6: Plan view of Block 1 with voids and cracks numbered and their positions indicated. Not shown in the figure is a cast-in steel plate with semi-spherical voids attached to the top surface. This plate is located adjacent to the south leg between void no.11 and 12. Voids numbers 11 and 12 are designed so that access is possible in order to change the depth of voids and filler material.

Table A.1.1: Description of voids in Block 1.

Void no.	Size	Depth from top	Depth from bottom
No.1	200x200x200	220 mm below	380 mm above
No.2	100x100x100	130 mm below	570 mm above
No.3	100x100x100	205 mm below	495 mm above
No.4	100x100x100	305 mm below	395 mm above
No.5	200x200x200	490 mm below	100 mm above
No.6	295x295x200	305 mm below	295 mm above
No.7	225 mm diameter	305 mm below	270 mm above
No.8	150 mm diameter	300 mm below	350 mm above
No.9	150 mm diameter	175 mm below	475 mm above
No.10	225 mm diameter	190 mm below	385 mm above
No.11	200x200x600	100 mm below	100 mm above
No.12	810x300x200	200 mm below	400 mm above

Description of the concrete

Mix proportions			
Material	ID	Content (kg)	Density (kg/m^3)
Cement	PC(A/HS/EA/G)	295	3220
Min. additive	Danasko B1	68	2300
Min. additive	Microsilica (AVO)	19	2250
Chem. admix	Conplast 316AEA	0.7	1003
Chem. admix	Conplast 212	2.3	1170
Chem. admix	Peramin F	2.3	1210
Water		136	1000
Aggregate	RN-Avedore0-4/A	697	2630
Aggregate	Dalby 4-16	690	2750
Aggregate	Dalby 16-25	460	2750

Table A.1.2

Concrete properties	
Slump	80 mm
W/C ratio	0.37
Air content	4.6%
Density	2367 kg/m^3
28 day cube compressive strength (measured) 53 MPa	

Table A.1.3

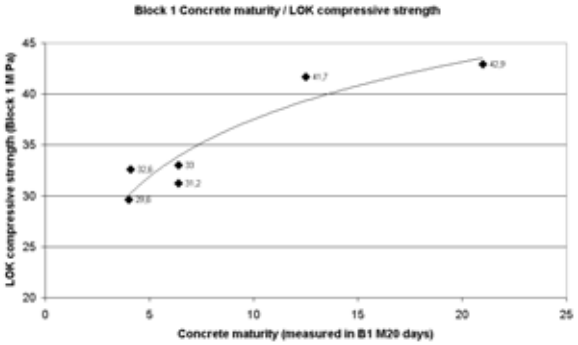

Fig. A.1.7: These measurements were made on Block 1 using cast-in maturity probes and LOK-test inserts. The spread in the LOK-test results is more than desired and they show generally lower values than the cube compressive strengths. The inserts were placed along the side of the Block.

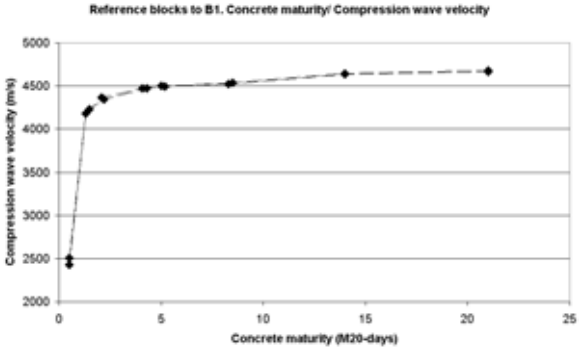

Fig. A.1.8: These results are from two reference blocks, which were cast and stored with Block 1. The P-wave velocity after only 0.5 M20-days is 2500 m/s. The increase in velocity after 1 M20-day is relatively small. There is almost no measurable difference between 14 and 21 M20-days.

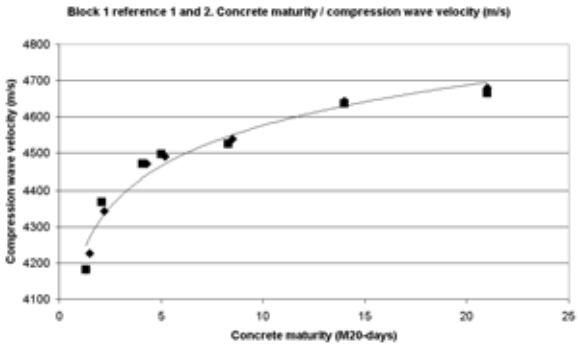

Fig. A.1.9: Concrete maturity and compression wave velocity development from 1.3 to 21 M 20-days. These figures are from the extra reference blocks.

APPENDIX 2 – examples of NDE on site

In the following tables examples are given of work carried-out over a 12, year period in which NDE has played a central role.

Table A.2.1

Structure	Objective	Motivation	Result	Method
Bridge slab (Depth < 150 mm)	Locate depth of ducts	Hole punctured in slab during re-surfacing	Depth to ducts varied (too close to surface)	I.E.
Nuclear containment (1000 mm)	Check for voids at pipe entries	Leakage through wall	Voids located	H.E.C.R.
Parking deck corbel (300 mm)	Position of reinforcement and detail	Collapse of corbel and wall section	Defect corbels located – wrong reinf. Detail	Ir-radiography
Bridge column (<1500 mm)	Locate internal rubble pockets	Cracks visible	Loose areas located	S.A.S.W
Nuclear containment (600-1200 mm)	Map reinforcement compliance	Safety assessment	Changes from available drawings	H.E.C.R. and radar
Floor slab (Depth <150 mm)	Position of reinforcement	Prior to coring to avoid damage	Mapped and found irregular reinf. spacing	Radar
Nuclear structure (1200 mm)	Position of reinforcement	Prior to coring to avoid damage	Mapped and found not compliance position	H.E.C.R.
Fuel tank (350 mm)	Delamination due to corrosion to be mapped	Visible damage	Mapped with accuracy	U.P.E.
Iron ore storage silos (300 mm)	Wall thickness	Visible abrasion on inside	Mapped with accuracy	U.P.E.
Airport roof (150 mm)	Thickness and reinforcement details	Historical value. To be transported to other site	Mapped and found to comply	I.E. and radar
School building	Extent of fire-damage	Fire	Mapped (estimated)	U.P.V.
Column plinths (400 mm)	Extent of cracks	Visible cracks	Cracks shallow	U.P.V. and I.E.

Examples of older structures, for which N.D.E. has been specifically, required, usually as a result of some accident, incident or planned change to the structure. The figures given in brackets in the left-hand column refer to the thickness of concrete through which the tests were made.

Table A.2.2

Structure	Objective	Motivation	Result	Method
Bridge slab (900 mm)	Check for internal voids and cold-joints	Visible damage at surface	Global mapping of condition	U.P.V. and S.A.S.W.
Bridge slab (depth <300 mm)	Check repair quality	Quality check	Weak layer (lack of binder) located	S.A.S.W. and I.E.
Bridge slab (1000 mm)	Check for internal damage (cracks)	Visible settlement during casting	Qualitative assessment	S.A.S.W. and I.E.
Bridge abutment (850 mm)	Check for internal voids	Visible damage at surface	No voids detected	U.P.E.
Tunnel lining (600 mm)	Check thickness and for internal voids	Leakage risk	Accurate mapping of thickness and homogeneity	U.P.E.
Building support columns (900 mm)	Check depth of cracks	Visible damage	Accurate mapping of delamination and reinforcement position	U.P.E. and U.P.V.
Office building support columns (600 mm)	Reinforcement detail and fill of ducts in pre-fabricated columns	Extensive cracking	Reinforcement accurately mapped and voids located in ducts	H.E.C.R.
Swimming pool (450 mm)	Bond between tiles and concrete base slab	Cracking in tiles	Full area mapped and bond quality established	U.P.E.
Concrete tank (600 mm)	Concrete homogeneity (voids and honey-combing)	Visible damage at surface	Some void areas located	I.E., U.P.V. and S.A.S.W.
Bridge column (depth < 150 mm)	Post-construction check of cover thickness to reinf.	Quality check	Good.	Radar and covermeter.
Suspended floor slab (250mm)	Check bond of extra 100mm concrete layer	Quality check	No defects found (lack of bond)	U.P.E.

Examples of new structures, for which N.D.E. has been specifically required, as a form of post construction check. The figures given in brackets in the left-hand column refer to the thickness of concrete through which the tests were made.

Table A.2.3

Structure	Objective	Motivation	Specific tests	Method
Football Stadium (50 years old)	Condition assessment / lifetime	Decision regarding modernisation	Concrete quality and bond of shotcrete. Reinforcement compliance.	U.P.E. Covermeter and radar.
Petrochemical plant (30 years)	Condition assessment / lifetime including earthquake damage	Safety	Concrete quality and delamination surveys. Reinforcement cover-thickness.	U.P.E. S.A.S.W. I.E. Covermeter
Harbour structure (30 years)	Condition assessment / lifetime	Visible damage	Cover thickness	Covermeter
Spherical (L.P.G.) tank columns (20 years)	Risk of corrosion to steel columns under concrete fire-proofing	Known risk	Quality and bond of concrete.	S.A.S.W. I.E.
Spherical (L.P.G.) tank columns (30 years)	Risk of corrosion to steel columns under concrete fire-proofing	Known risk	Remaining thickness of steel	H.E.C.R.

Examples of old structures, for which condition assessments have been made. N.D.E has not been specifically required but has been introduced as an important part of the condition assessment.

APPENDIX 3 –End user priorities

Table A.3.1

APPLICATION & PURPOSE	COMMENT	End-user rating	Suited technique		
		%	1	2	3
Measurement of concrete thickness, to obtain as built details	Quantification of capability for measuring concrete thickness for sections > 1.0 m thick (radar, acoustic, radiography).	32	2	4	2
	Enhanced ease and speed of application for measuring section thickness in all structures (radar, radiography, acoustic).	35			4
	Measure section thickness with single sided access with sensitivity of ± 5% section thickness (radar, acoustic).	38			
	Measure section thickness in presence of congested steelwork, with sensitivity of ± 5% section thickness (acoustic).	23			
Mapping / sizing of steel reinforcement and tendons to establish as built details.	Enhanced resolution to measure reinforcement diameter with sensitivity of ± 10% either in thick sections (> 1 m) or in presence of congested reinforcement (individual reinforcement at spacings 150 mm). (Radar, radiography, …).	20	1	3	1
	Resolve multiple layers of reinforcement, identifying individual reinforcement at spacing << 150 mm and depths > 30 mm AND measure reinforcement diameter with sensitivity of ± 10% (radar, radiography, …).	20	1	3	1
	Quantifying existing performance capability for mapping /sizing of steel reinforcement and tendons with section depth (radar, radiography, …)	38	1	3	3
Detection of corrosion in pre-stressing tendons	Quantify performance limits for detection of corrosion by measuring loss of section / hydrogen embrittlement in pre-stressing tendons in heavily reinforced structures (radiography, …)	36	3	3	3
	Detect evidence of corrosion in grouted prestressing tendons by measuring loss of section, pitting or hydrogen embrittlement (radiography, …)	34	3	3	2
Detection of voids & inhomogneity, typically to locate construction flaws.	Quantify void detection threshold in thick sections (variables: size of void, depth). (Radar, acoustic, radiography).	42	2	3	3
	Detection of voids > 20 mm in grouted tendon ducts (radiography, radar).	35	2	3	3
	Detect voids > 20 mm diameter in areas of congested reinforcement/tendons (radiography, radar).	42	2	3	3
Detection and sizing (depth, width, length) of cracks normal to the surface	Combination of techniques may be appropriate: one to detect, one to characterize. Improve variable performance statistics associated with depth measurement of surface cracks, For detection and sizing (depth, width, length) of cracks normal to surface aiming for sensitivity of ± 10% for crack widths > 0.2 mm (acoustic).	42	2	3	3
Detection of delamination of cracks parallel to the surface.	Improve variable performance statistics for detecting large laminar flaws at > 10 mm depth, and > 100 mm in any particular direction (acoustic).	39	2	3	2
	Detection of delamination between prestressing tendons in massive concrete (acoustic).	24	2	2	2
Additional goals	Detection of areal (0,5 m^2) with leaky waterproofing.	-		3	
	Determination of concrete quality as regards compressive strength.	-			

A list of priorities regarding improvements generally according to the end-users in this project is shown in the table above.

APPENDIX 4 – description of Block 2 and more

Block 2 was one of two larger mock-ups constructed specifically for this project. A number of smaller mock-ups have also been used and the results of some of the work on these is also shown below.

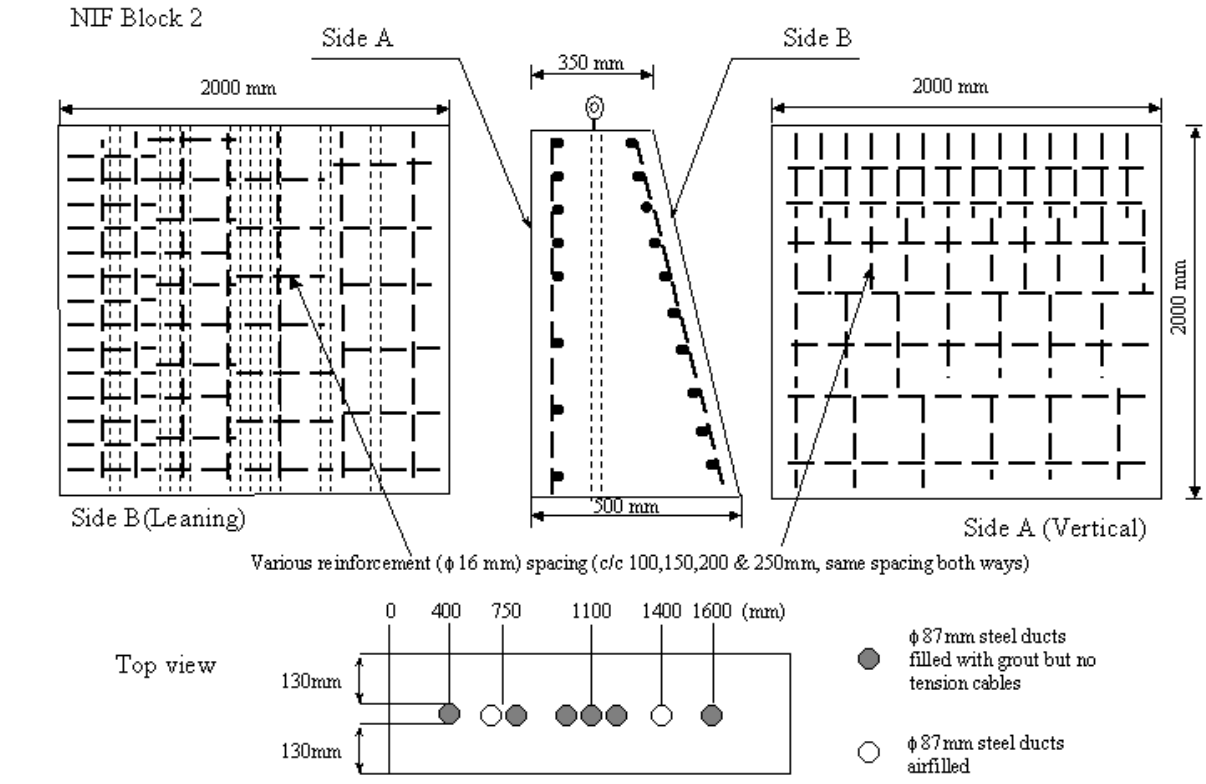

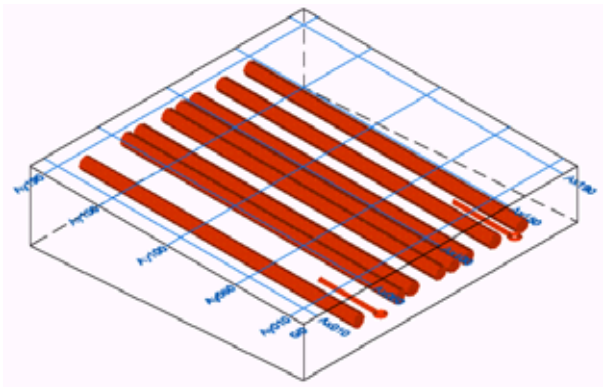

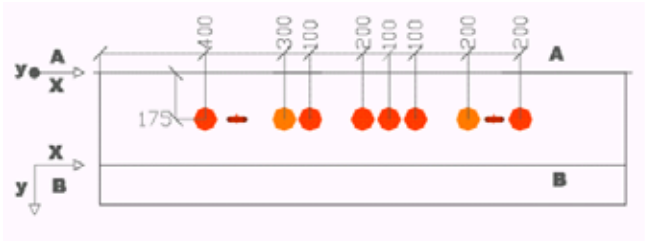

Fig. A.4.1: Block 2. The wedge shape enables tests to be made at gradually increasing thickness. Various rebar spacings are used. The Block contains a number of ϕ 87 mm steel pipes.

The block was constructed with various reinforcement configurations and ducts (pipes) at different depths. It was designed specifically for radar tests, and as the ultrasonic pulse echo became available at the start of the project this was also tried but not so extensively as radar.

The main objective was to determine which ducts could be detected. The effects of different antenna configurations were studied and this resulted in some improvements to the antenna.

Unfortunately the block was built with steel pipes and not ducts. It was felt that exhaustive UPE tests would not be meaningfull, as the respose from a steel pipe contra duct can be expected to be different. The concrete used was a standard mix of class K40 with max aggregate size 32 mm.

GPR Measurements on Block 2

Several different antenna/scan configurations have been tried and it was found that the commonly used "Broadside" and "In-line" methods work well together both in the case of the test block and on site.

The maximum depth at which a duct could be detected, was only 220mm (to top of duct), see Fig. A.4.3. However, it has been found on site that ducts at 450 mm can be detected (reinforcement with c/c spacing 150 mm).

In Fig.A.4.2 below small circles represent reinforcement bars while large circles represent cable ducts (with (x) and without ( ) grout.)

Some important results were found in this data set: In the left-hand part of the processed data the closely spaced reinforcement can be clearly seen. However, if the data set is not migrated (a certain processing step) their apparent position can be well off the actual (Fig. A.4.2)

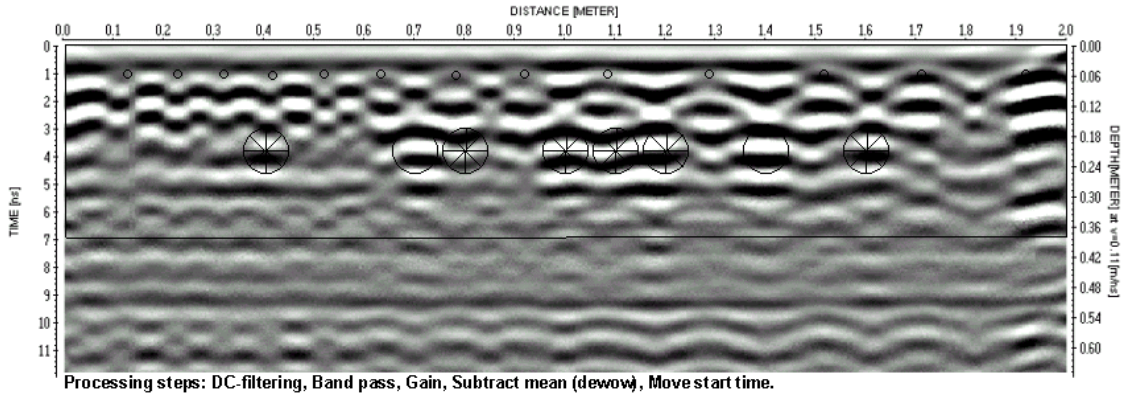

Fig. A.4.2: GPR profile that shows how difficult it can be to acurately position closely spaced reinforcement (in the left part of the profile the spacing is 100 mm). The actual rebar positions are shown as small open circles.

As, seen in Fig. A.4.2 it would be difficult to pinpoint the actual position of the bars in the left part of the radargram. The actual positions are shown as small circles. Migration processing (focusing the energy to its origin) will however correct this.

It was found that a re-bar spacing of 100 mm is about the minimum that will allow a duct to be detected (with the equipment used in this project.)

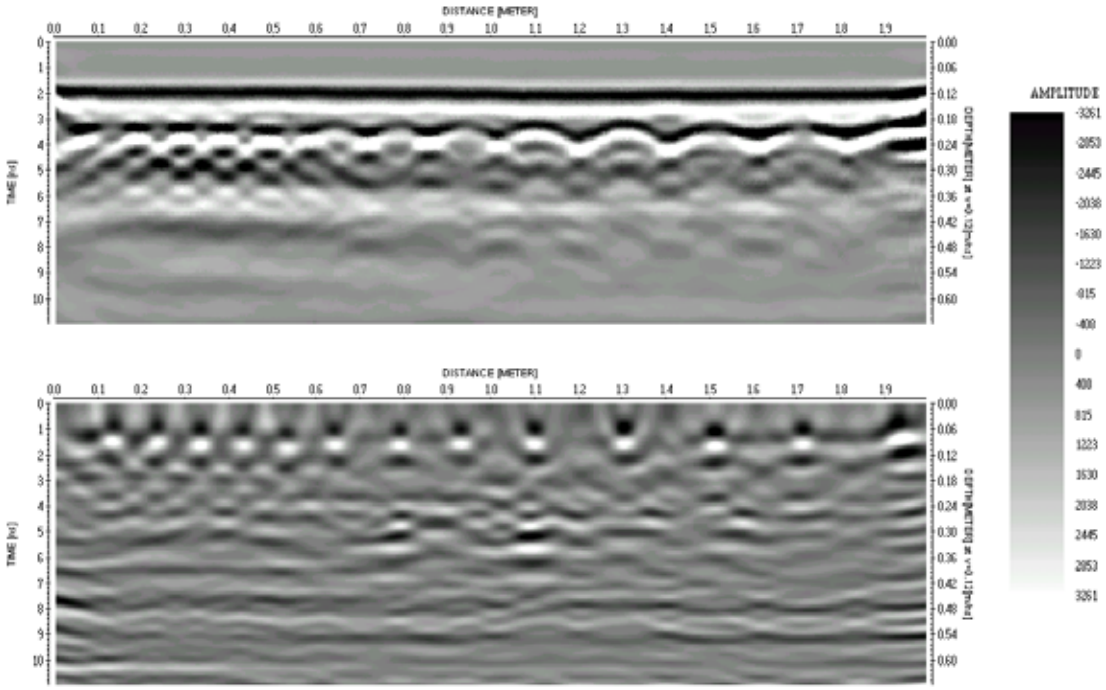

Fig. A.4.3: This is about the maximum depth at which the ducts can be confidently identified (220 mm). This applies to Block 2 and may be very different in other conditions. The raw data is shown in the upper diagram and the processed data in the lower.

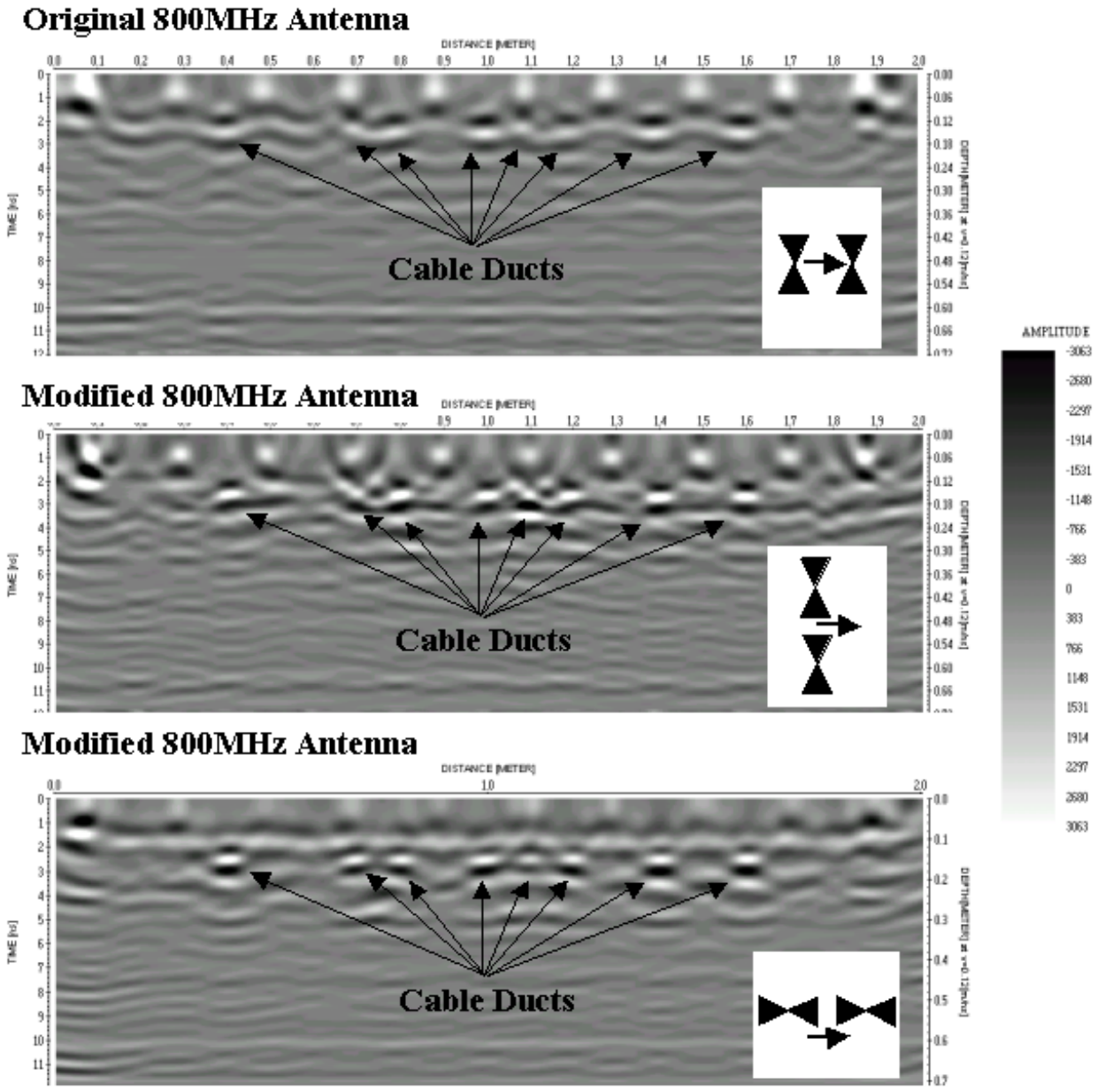

Fig. A.4.4: Comparison of different antennae and survey modes. Notice how the re-bar hyperbolae weaken in the end-fire in-line survey mode (bottom profile) while the ducts become clearer. The antenna configurations used in each case are shown to the right in the figures.

In surveys like these it is important not to be satisfied with (or discouraged by) a single profile. The reinforcement layout above the ducts has a huge influence on the result and should be mapped first in order to try and find a "window" that can be penetrated – in other words find the best position to drag the antenna to minimise interference from reinforcing.

Conclusions from radar tests on BLOCK 2

- Reinforcement spacing should be >100 mm, and preferably at least 150 mm if individual bars are to be accurately mapped and if deeper-lying bars/ducts are to be found.

- A mesh size of about 100 mm can lead to errors in pinpointing the position of the bars.

- A mesh size of about 100 mm will prevent "deeper" investigations with current antenna configurations.

- It is not possible to reliably detect several adjacent ducts. This was found when scanning 3 adjacent ducts – the presence of "something" was established but the individual ducts were not identified.

- The measurements on the block have shown that a flexible antenna configuration is preferable. Flexible means that the operator can change antenna configuration and offset depending on the reinforcement detail and/or the target sought.

- Measurements on Block 2 and other concrete structures have shown that it is very difficult to predict radar performance. Many factors, such as, reinforcement density-size-depth, concrete type and age-dryness, cracks, antenna performance-configuration, processing tools and operator experience, all affect the outcome of the survey.

These conclusions are based on the measurements on this particular Block and experience from other structures. The general conclusion is that results will vary from site to site.

UPE tests on Block 2

A considerable number of profiles have been made across Block 2 with UPE. This was interesting for two reasons – could UPE detect the steel ducts in the concrete and could it distinguish voids in the grout fill inside the ducts? It should be pointed out again that the "ducts" in this case are actually steel pipes, with wall thickness much greater than a standard cable duct. This can be expected to have affected the outcome of the tests. Scanning manually in this way with the UPE-instrument takes considerably longer compared with a radar scan, as each test (A-scan) takes a few seconds and there is no automatic spacing function.

The scans shown below consist of five B-scans each consisting of 40 points. It would take approximately 40 minutes to collect this amount of data.

The UPE instrument emits a shear wave that is perpendicular to the long-axis of the antenna. In the figures below it is possible to compare scans made with the antenna parallel contra perpendicular to the ducts. It seems the former mode is better for detecting the ducts.

The reinforcing and some of the air-filled ducts can be seen, but not the grouted ducts.

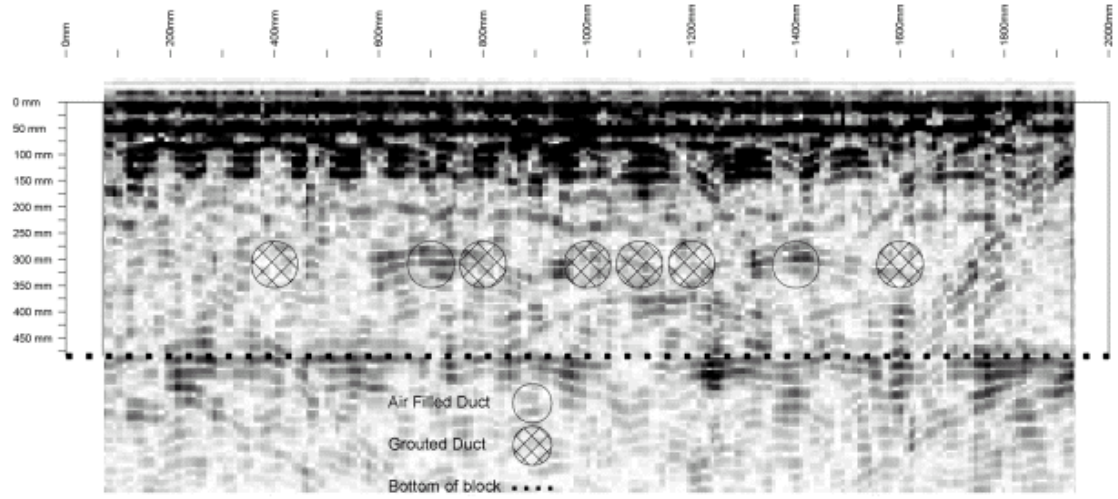

Fig. A.4.5: UPE profile By180 across Block 2. The air-filled ducts can be seen but the grouted ducts cannot. The reinforcing bars appear as dark patches closely spaced in the top part of the diagram. The scan was made with a test intervall of 10 mm and a frequency of 33 K Hz. Antenna orientation parallel. The sloping echoes seen near the end of the scan are thought to have been caused, by reflections from the edges of the block.

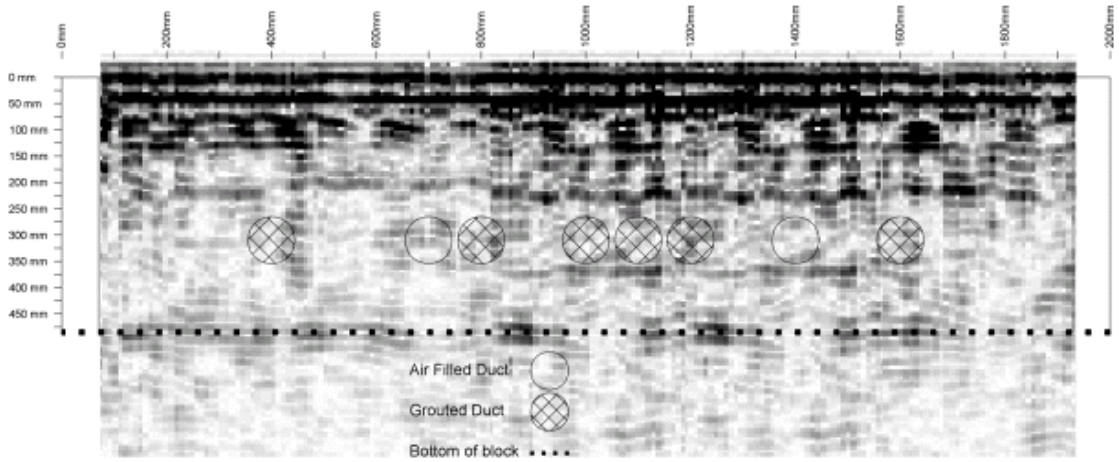

Fig. A.4.6: Same scan as above but with perpendicular antenna orientation. The air-filled ducts and reinforcing bars are not as clear as in the upper diagram.

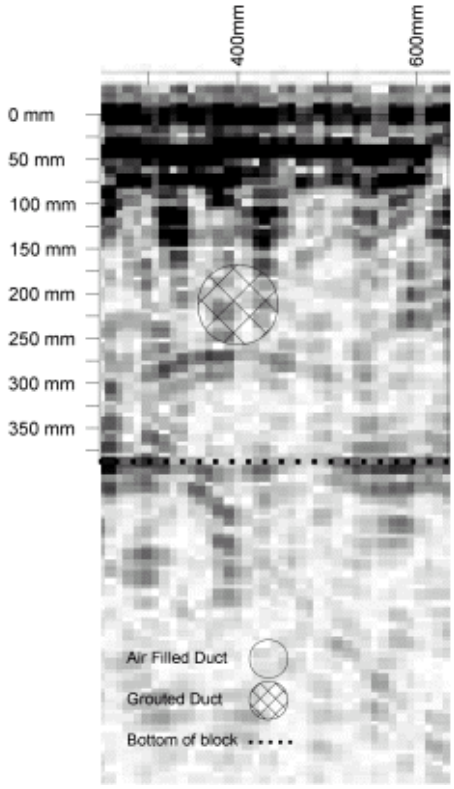

Fig. A.4.7: Grouted duct and hyperbolic reflection that appears *under the duct*.

It was common for hyperbolic reflections to appear *under* the grouted ducts as shown in the figure above. The reason for this is not known.

The air-filled ducts could be detected using UPE to a depth of 265 mm (this was the maximum depth measurements could be made on this block.)

Additional tests with UPE on other test blocks

A number of test blocks were made primarily for radiographic examination. One of these is shown in section 4.3.7 "investigation of voids in cable ducts using HECR". The block in question was carefully made using a concrete with maximum aggregate size 12 mm. The voids inside the ducts are not in contact with the inner surfaces of the duct, except at top and bottom. In the test shown below the path of the ultrasonic waves would be concrete: duct (steel): grout: air: grout: duct (steel): concrete, with reflections at the interfaces.

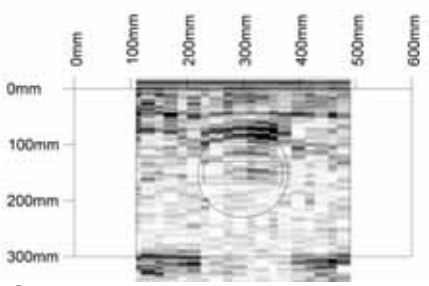

Fig.A.4.8.1: UPE scan across embedded duct with void in grout fill. The duct can be seen quite clearly but the internal void cannot. Scan direction perpendicular to duct long axis.

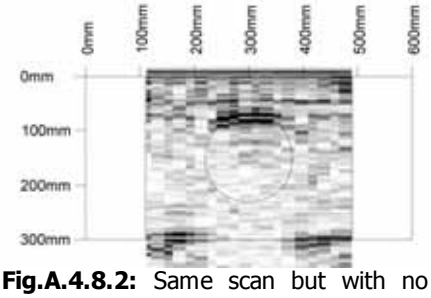

Fig.A.4.8.2: Same scan but with no void inside the grout. The result is similar to the duct with a void. Notice that the back wall echo is blocked in both cases. The scans were made at a frequency of 100 kHz and 20 mm between each point (A-scan). Scan direction perpendicular to duct long axis.

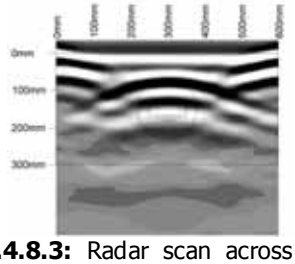

Fig.A.4.8.3: Radar scan across same duct for comparison. Radar will not give any indication of the condition inside the duct. Scan direction perpendicular to duct long axis.

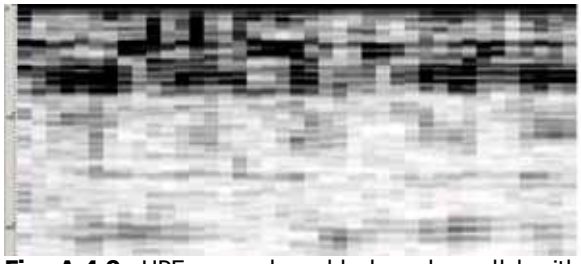

Fig. A.4.9: UPE scan along block and parallel with duct. The depth from the surface to the duct is 75 mm. From left to right it is possible to see the 70, 60, 50, 40 and 30 mm wide voids inside the duct. Weak back-wall reflections can be seen in the intervals between voids.

Note that in this example it was not possible to "see" the void inside the duct when scanning perpendicular to the duct. It is possible to "see" the voids when the scan was made parallel with the duct. The reasons for this can be discussed.

B-scans across Block 1

In the following series of B-scans made with the UPE-instrument across Block 1 it is possible to see the effect of the various voids. The scans were made at 300 mm spacing according to the attached figure. The scan lines are, as can be seen from the figure, not deliberately centred on the voids, so that some indications of the voids are actually obtained with the testing point off-centre.

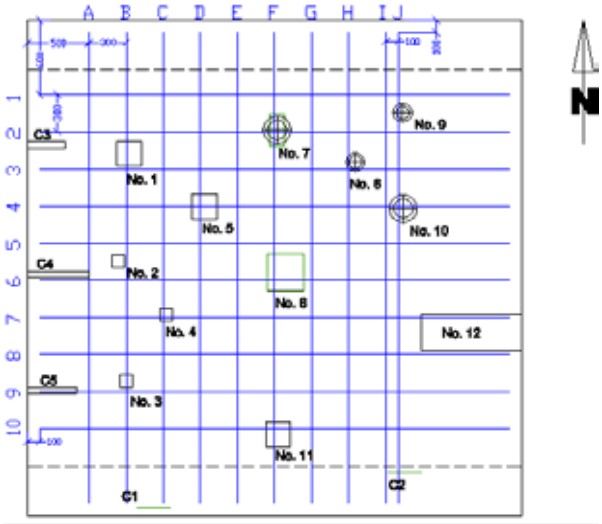

Fig. A.4.10: Block 1 plan showing positions of voids and scan lines A-J. Tests are made (A-scans) at 300 mm centres and at 100 mm along each line.

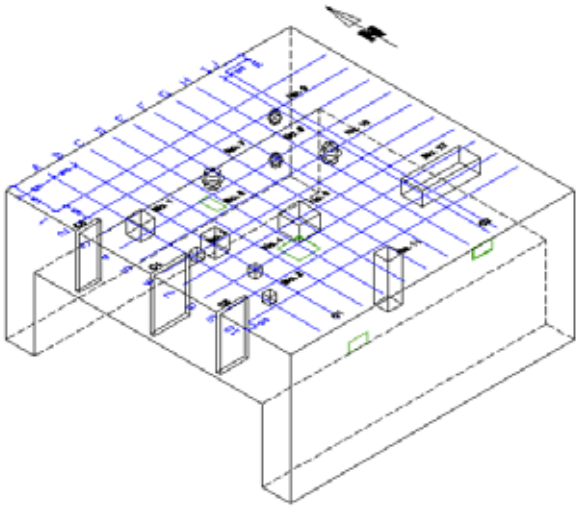

Fig. A.4.11: Block 1 isometric.

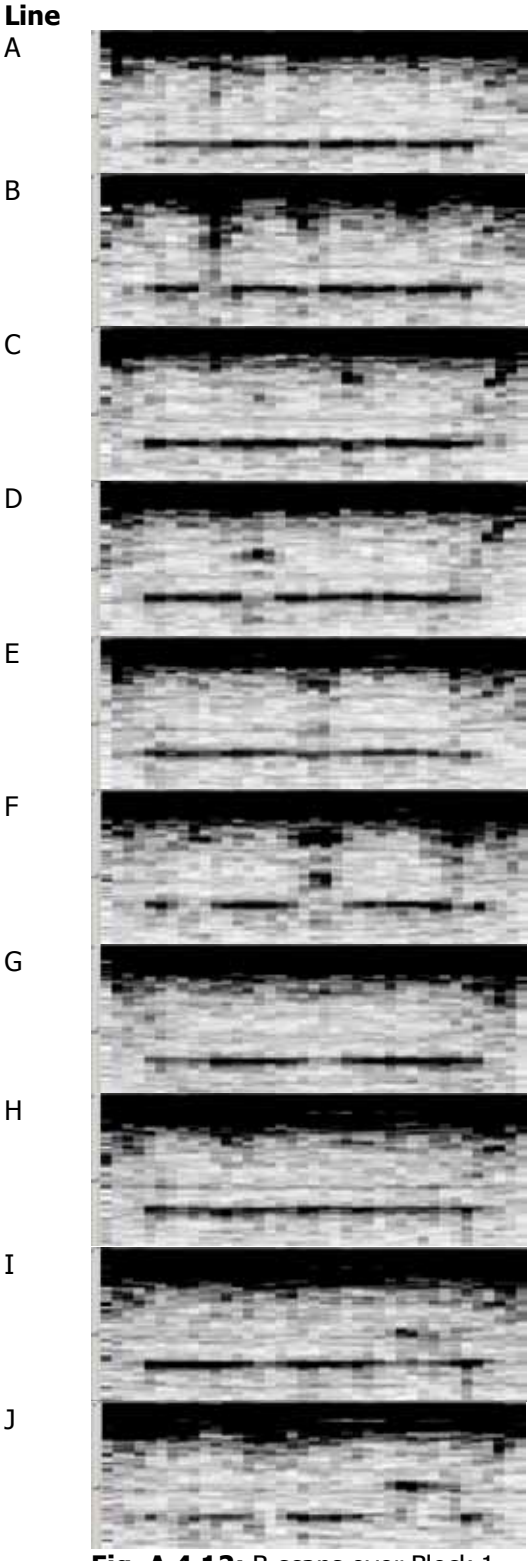

Fig. A.4.12: B-scans over Block 1

Table A.4.1

B-scan line (A-J)	Observation
Line A	A reflection can be seen from Void no.1 although this appears to be a multiple echo. The "cracks" C4 and C5 interrupt the bottom echo.
Line B	A reflection from Void no.1 and multiples of it. This void interrupts the bottom echo. Void no.2 can just be seen and there is a weak interference in the bottom echo. Void no.3 can just be seen but not clearly and there is no bottom echo interference.
Line C	A weak refection from Void no.5 can be seen despite the fact that this 200 mm void is 300 mm off the line centre. A reflection from Void no.4 is quite clear but there is no interference to the bottom echo.
Line D	This line crosses over Void no.5, which can be clearly seen as a reflection and loss of bottom echo.
Line E	Void no.6 can be seen as a reflection despite the fact that the edge of this void is approximately 300 mm off the scan Line. Note the weak linear reflection at about 300 mm above the base, which coincides with the ϕ 20mm tie-rod through the slab.
Line F	Spherical void no.7, cubic void no.6 and 11 can be seen as reflections. The multiple, echo from void no.6 is very clear. All of these interrupt the bottom echo.
Line G	There are no visible reflections. Void no.6 interrupts the bottom echo.
Line H	There are no clear reflections. There may be a weak reflection from Void no.8 but it is not clear, but mixed with other reflections from near surface. Note the linear reflection near the base of the slab, which coincides with the second tie rod (reference to Line E).
Line I	Weak reflections can just be made out from sperical Void no's. 9 and 10. Void no 10 causes some bottom echo interference. At the right hand side it is possible to see a reflection from the steel plate (not shown in the plan above – see photo of Block before casting).
Line J	Void no's 9 and 10 interrupt the bottom echo very clearly. The steel plate can be clearly seen as a reflection and loss of bottom echo.

These scans were made at a frequency of 33 K Hz. There are in total 400 test points (A-scans). The entire test including measurement and data storage was made in less than 1 hour.

The frequency and window was chosen to allow detection of anomalies and not for detailed inspection of individual voids. This is achieved by studying the bottom echo and interference to this. Two examples of detailed scans over Void no's 2 and 5 can be seen in the figures below.

The bottom echo at 800 mm can be clearly seen in Fig. A.4.12.

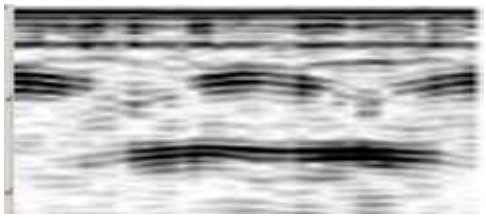

Fig. A.4.13: B-scan across Void no. 1 at a depth of 220 mm. The scan was made at a frequency of 100 KHz and centre-spacing 10 mm (total scan length 400 mm). The time window has been expanded (compare with Fig. A.4.12 (b) above) to make the reflection from the void distinguishable from other reflections. Reflections from the reinforcing bars can also be seen.

Fig. A.4.14: B-scan across Void no. 5 at a depth of 490 mm. The frequency and settings are similar to above. Both the void and reinforcing bars can be clearly seen. (Compare this with Fig. A.4.12 (d)

Reinforcing bar detection with UPE and radar

A block was constructed with reinforcing bars 16 and 20 mm diameter at various depths, as shown in Fig. A.4.15. The block is 300mm thick and made with a concrete containing aggregates up to max. 32 mm.

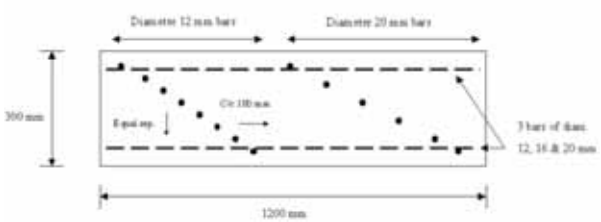

Fig. A.4.15: Section of block showing how the bars were placed at various depths and spacings. On the left side ϕ 16 mm bars and the right side ϕ 20 mm bars.

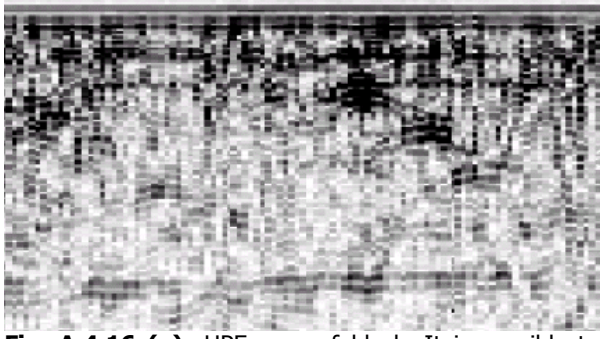

Fig. A.4.16 (a): UPE scan of block. It is possible to distinguish the bars to a depth of 180 mm, but the reflections are not very clear and it would be difficult to confidently locate them without prior knowledge of their position. The 20 mm diameter bars give stronger reflections. The back- side of the block can be seen.

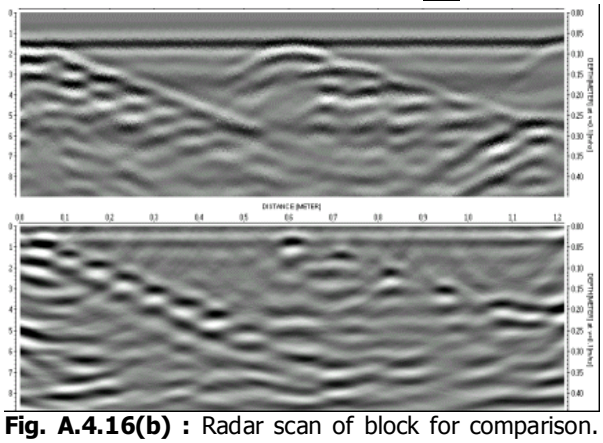

Fig. A.4.16(b) : Radar scan of block for comparison. The upper figure is raw data while the lower is processed. The data is much "cleaner" and almost every bar can be seen. The backside of the block is not visible.

UPE scans of embedded steel plate with voids above

Reflections from a steel plate cast in concrete will not be as strong as those from a void or air-filled crack. This is because the difference in acoustic impedance between concrete and steel is smaller compared to concrete and air. The strength of the reflection will depend on the type of bond between the concrete and steel. Loose bond, i.e. physical contact but no adhesion, may result in reflections similar to a concrete: air interface.

In some situations, it can be interesting to look for air voids around and behind a steel plate cast in concrete. Of course, poor bond or a small air gap between the steel and concrete will have the same effect as a void. UPE cannot distinguish between the two. As can be seen in the following example however, UPE does provide a means of detecting voids behind the steel plate and of measuring their size (parallel to the plate). It could of course be used to determine the type of contact/bond between concrete and steel.

Fig. A.4.17: The steel plate cast in Block 1 (260 mm from the underside). In the left-hand figure the artificial voids can be seen on top of the plate. The steel plate is 8 mm thick. Some semi-spheres made of plastic have been glued to the top of the plate to represent voids inside the concrete adjacent to the (back of) plate. Scans were made along the underside of the slab in line with the two voids nearest the edge (closest to the camera in the photo above).

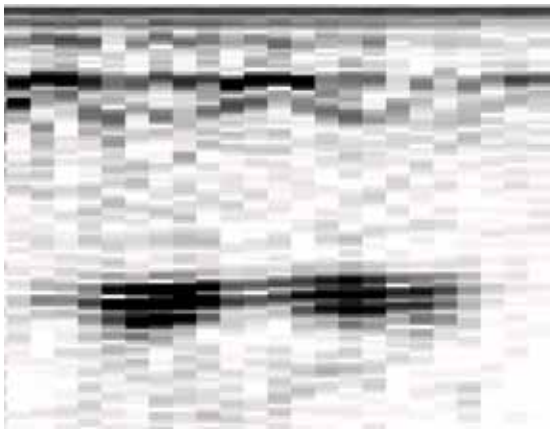

Fig. A.4.17 (a): B-scan across concrete surface with embedded steel plate and voids behind this. This scan was made with c/c separation between A-scans of 10 mm.

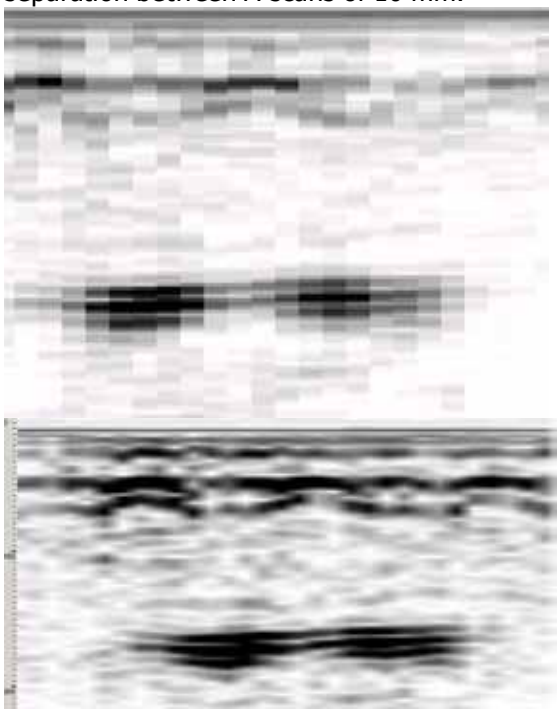

Fig. A.4.17(b): UPE scans through 260 mm concrete showing reflections from the steel plate with the void areas clearly visible. The examples above were produced at various frequencies. The diagrams are "upside down" in the sense that the test was made from the underside of the slab and up-wards, contrary to all other tests shown. The two voids can be distinguished from each other. The maximum reflection amplitude is achieved when the transducer array is centred on the respective voids.

The near-surface hyperbolae are caused, by reinforcing on the slab underside.

Example 2: Holes in steel plate embedded in concrete

In order to test the sensitivity of radiography in detecting holes and reduced section thickness of a steel plate embedded in concrete, an experimental set-up was arranged. An 8 mm steel plate was set, as shown below, between 750 mm and 260 mm thick concrete blocks. Three circular holes of diameter 50, 20 and 10 mm were drilled through the plate, and adjacent to these three similar holes were drilled but only to a depth of 4 mm (half the plate thickness).

The set-up was radiographed using the Betatron.

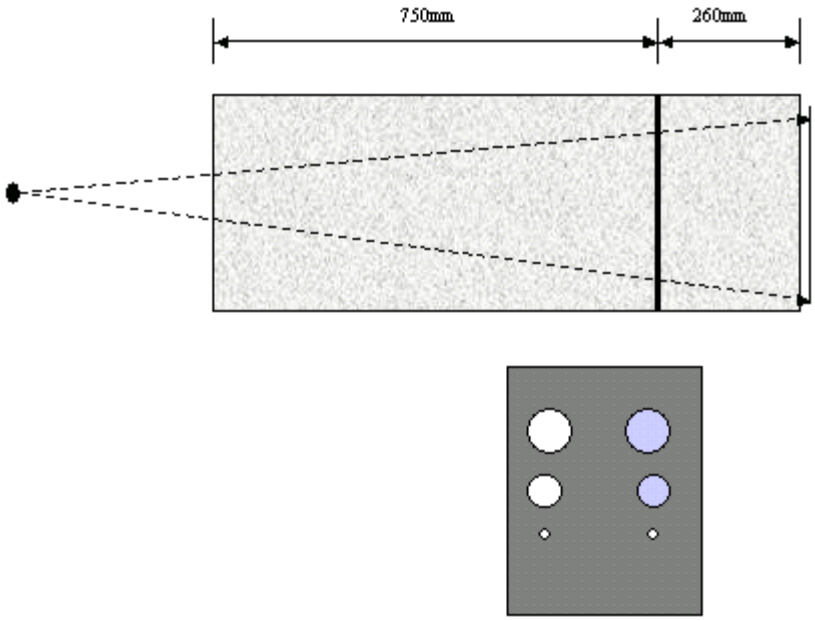

Fig. A.4.18: An 8 mm steel plate has been sandwiched between 750 mm and 260 mm thick concrete. The plate has three holes through it (left in lower figure) and three holes 4 mm deep, i.e. half way through (right in lower figure). The holes have diameter 50, 20 and 10 mm. The mock-up was examined with the Betatron and digital imaging plates (type IPC).

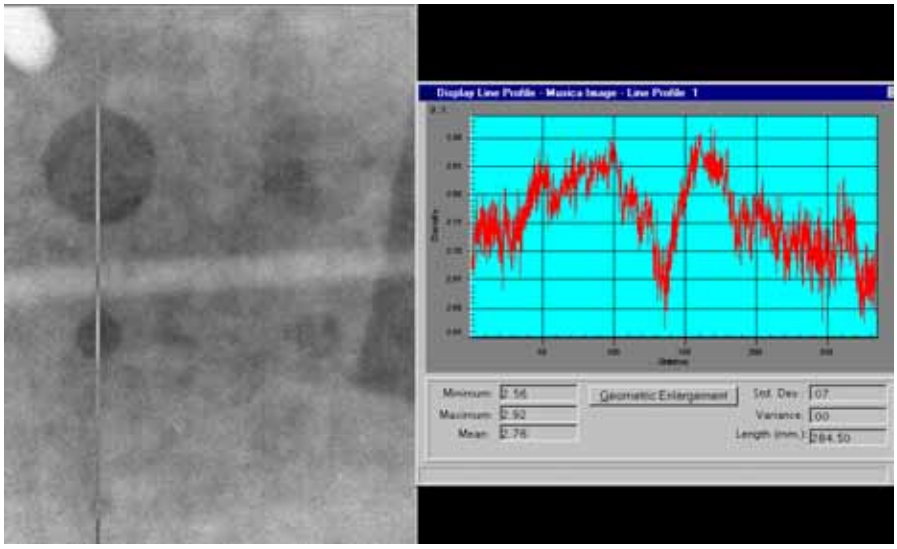

Fig. A.4.18 (a): Radiographic image of the blocks. The three holes that penetrate the steel plate can be clearly seen. The 10 mm hole is not so clear. The density scan shows these quite clearly however. The drop in density, that is, visible in the middle of the scan is caused by a horizontal reinforcing bar.

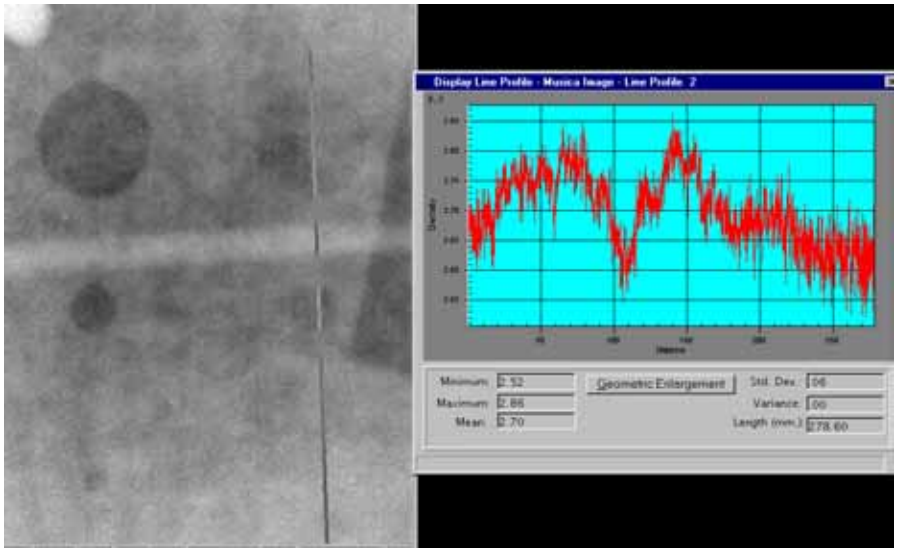

Fig. A.4.18 (b): The three holes that penetrate only half the section of the plate are, as expected not so clear. The two larger holes are quite clear probably because they are perfectly formed. The density scan does indicate their position although the smallest hole is not visible. If these holes had an irregular shape then they may not have been easily recognisable to the eye.

APPENDIX 5

Thickness measurement – a "belt and braces example"

The depth to a casting joint between a concrete floor and an underlying foundation slab to a nuclear containment had to be confirmed prior to drilling cores. According to the drawings the thickness was 200 mm. No reinforcement was to be cut in the process. It was important that the cores were not drilled too deep.

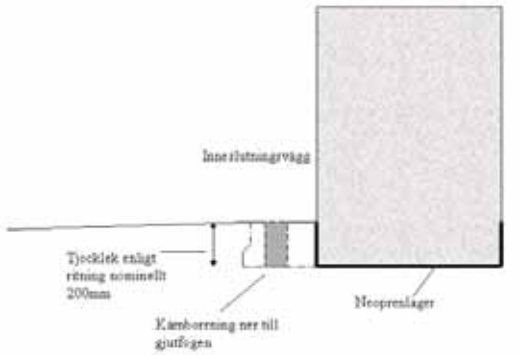

Fig. A.5.1: The depth to the casting joint as shown was 200 mm according to the drawings. The containment wall is shown to the right in the figure.

In this example the following techniques were used: UPV, UPE, Radar, SASW, IE.

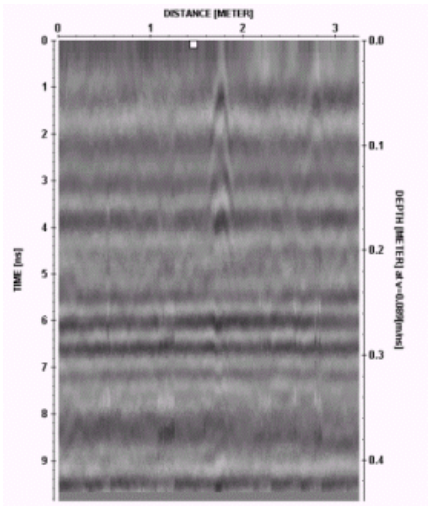

Fig. A.5.2: Radar scan, which shows one indication of a reinforcing bar (probably in the adjacent slab) over a length of 3.3 m. The casting joint can be seen at about 280 mm.

SASW

The confined space between the main floor slab and the wall would not really make conditions ideal for SASW measurement. However, some tests were made.

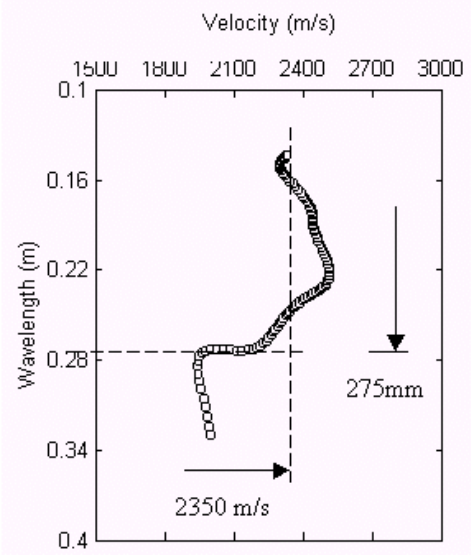

Fig. A.5.3: SASW dispersion curve indicating a Rayleigh wave velocity of 2350 m/s. The curve deviates sharply at 275 mm, which is a typical response if the concrete "changes" or if there is a joint at this depth (thickness).

Note: The impact echo and SASW results have been taken as would be in an infinate medium without correction for geometry. This may have introduced a small error into the calculations.

SASW and UPV

The value of V_r = 2350 m/s is equivalent to a V_p = 4196 m/s and V_s = 2550 m/s. Since conditions were not ideal for SASW tests some indirect velocity measurements were made at the surface with the UK 1440, resulting in an average value of 4100 m/s. Since the measurements were made in the indirect mode at the surface it was thought that the average (full thickness) value of V_P could be higher than this and the value of V_P = 4196 m/s was chosen.

Similar procedures were used at four positions at which cores were to be drilled with V_S values ranging from 2422 to 2675 m/s.

IE

A few IE tests were made also with V_P chosen as 4196 m/s. The lowest peak in the frequency spectrum was 7.6 KHz and the thickness calculated on the basis of this was 285 mm.

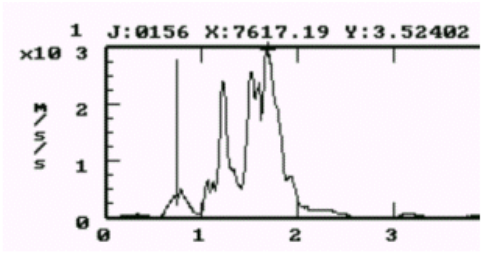

Fig. A.5.4: IE frequency spectrum with lowest peak at 7.6 k Hz and calculated depth 285 mm.

UPE

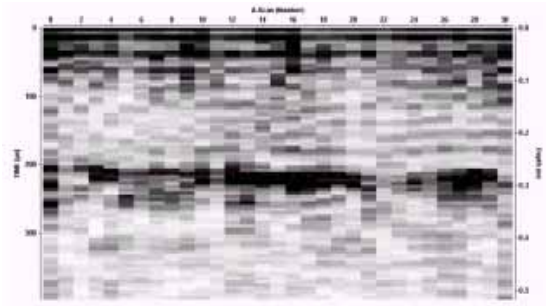

Fig. A.5.5: Example of UPE scan at one position indicating a depth (thickness) of 280 mm. The strength of the echo varies, which is probably due to variations in the bond strength between the layers of concrete.

Result

The depth to the casting joint was given conservatively as 270 mm, although the tests suggested it was 280 mm. On drilling it was found that the joint was formed between two concrete layers with a sloping interface with thickness varying from 275 mm to 285 mm (across a 100 mm diameter core). Four different techniques suggested that this was the thickness of the concrete.

The thickness according to the drawings was 200 mm.

APPENDIX 6

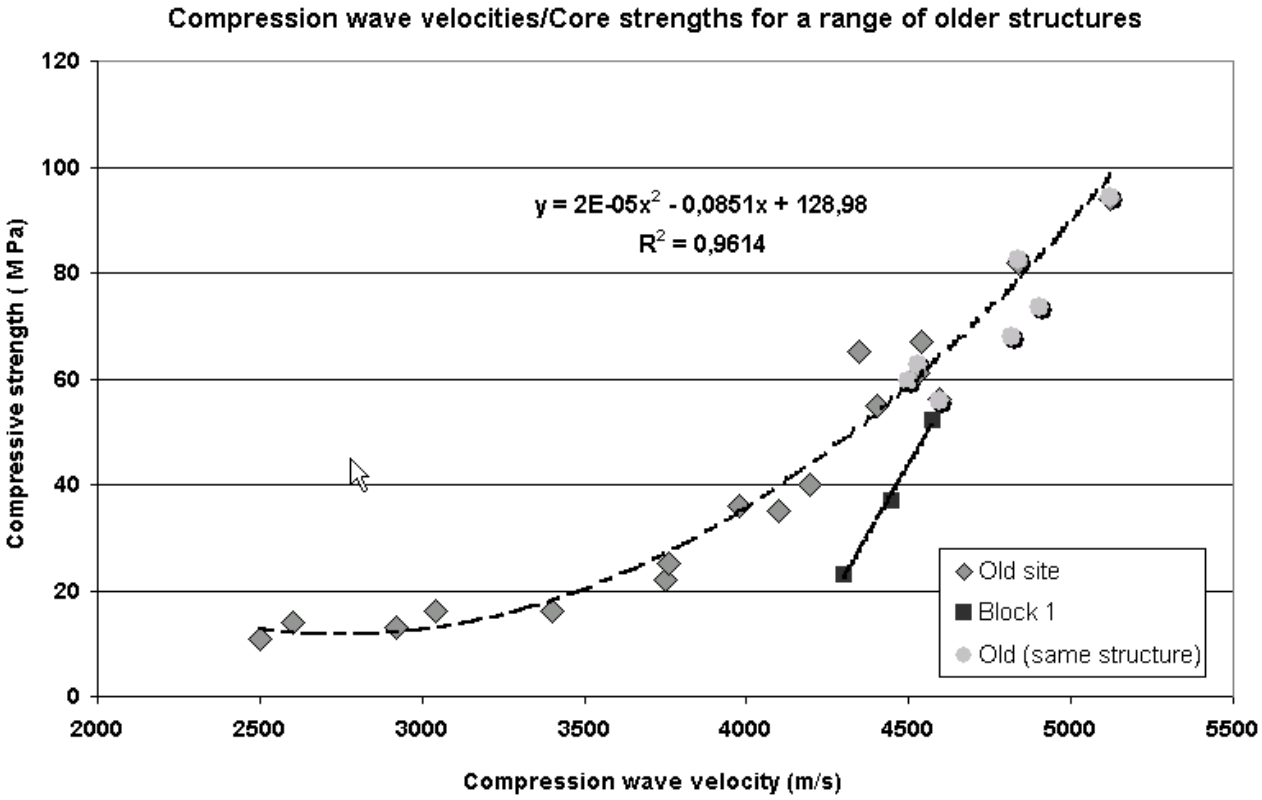

Fig. A.6.1: Examples from site investigations throughout Europe. Compression wave velocities / compressive strength measured in structures and samples taken from these.

References

Foti S. (2000) " Multistation Methods for Geotechnical Characterization using Surface Waves " PhD Degree thesis in Geotechnical Engineering

Rasmussen J. (2003) "Non destructive testing methods for integrity determination of concrete structures" Licenciate Thesis, Luleå University, Department of Environmental Engineering, Division of Applied Geophysics

Neville A.M. (1981) "Properties of Concrete"

CONTECVET – Assessment of Residual Service Life of damaged concrete structures

Lin, Y and Sansalone, M "Transient Response of Thick Circular and Square Bars Subjected to Transverse Elastic Impact" Journal of the Acoustical Society of America, Vol. 91, No.2, February 1992.